Leveraging targeted protein ldegradation for G protein-coupled receptors: the development of CCR2 molecular degraders

Essa, K.; Zacarias, N.V.O.; Roth, S.; Xin, B.T.; Winter, S. de; Horst, C. van der; ... ; Heitman, L.H.

Journal of Medicinal Chemistry

pubs.acs.org/jmc

Article

Leveraging Targeted Protein Degradation for G Protein-Coupled Receptors: The Development of CCR2 Molecular Degraders

Khaled Essa,[#] Natalia V. Ortiz Zacarías,[#] Sascha Roth, Bo-Tao Xin, Sabine de Winter, Cas van der Horst, Bente Bleijs, Richard A. de Heiden, Rodanthi Voulgaraki, Elsa Neubert, Huib Ovaa, Erik H. J. Danen, Monique P. C. Mulder, Kevin Moreau, Daan van der Es,* and Laura H. Heitman*

Cite This: J. Med. Chem. 2025, 68, 26525−26546

Read Online

ACCESS | Metrics & More | Article Recommendations | Supporting Information

ABSTRACT: Targeted protein degradation (TPD) is one of the most prominent and rapidly advancing modalities in drug discovery. However, only few degraders have been reported for the membrane-bound G protein-coupled receptors (GPCRs). Therefore, using CC chemokine receptor 2 (CCR2) as a GPCR model, we synthesized potential CCR2 molecular degraders. The putative proteolysis-targeting chimeras (PROTACs) employed an allosteric intracellular CCR2 ligand tethered to commonly used E3 ligase ligands. Among these compounds, LUF7996 (**8**) demonstrated engagement of both CCR2 and the E3 ligase cereblon and displayed sustained and concentration-dependent degradation of CCR2 over 24 h. Mechanistic studies revealed the reliance of LUF7996 on the lysosomal pathway to induce CCR2 degradation. Finally, LUF7996 (**8**) efficiently inhibited monocyte migration in a transwell assay. Collectively, the developed assessment workflow led to identification of the first CCR2 molecular degraders and has the potential to expand the repertoire of degraders targeting the pharmacologically rich GPCRs.

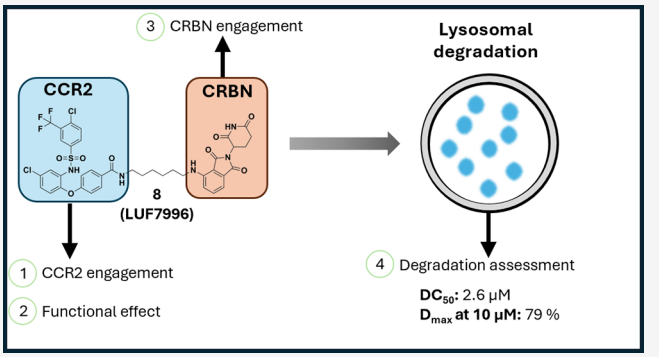

INTRODUCTION

Targeted protein degradation (TPD), via the proteasomal and lysosomal pathways, represents a novel tool to explore cellular pathways, as well as a promising therapeutic approach. Most TPD strategies including proteolysis-targeting chimeras (PROTACs),[1] molecular glues,[2] and SNIPERs[3] primarily utilize the ubiquitin-proteasome system (UPS) and are largely limited to intracellular proteins. In contrast, lysosome-dependent TPD strategies such as LYTACs,[4] MoDE-AS,[5] and AUTOTACs[6] can degrade membrane proteins, extracellular proteins, and protein aggregates, significantly broadening the scope of potential substrates. Among TPD strategies, PROTACs have increasingly gained attention as pharmaceutical modality, as this approach has led to the development of several preclinical and clinical candidates targeting proteins involved in various cancers and immune disorders.[7] PROTACs enable the degradation of a selected protein of interest (POI) by hijacking the UPS. PROTACs employ a POI ligand and an E3 ubiquitin ligase ligand tethered by a linker. Simultaneous binding of the PROTAC to the POI and E3 ligase enables the formation of a ternary complex, which results in polyubiquitination and degradation of the POI by the 26S proteasome.[8] The event-driven and catalytic mode of action of PROTACs coupled with their observed improvement in target selectivity led to the opening of new avenues in drug discovery on certain targets that were once deemed undruggable by conventional antagonists.[9]

To date, ∼6000 PROTACs targeting ∼450 proteins have been developed.[10] Strikingly, only three of these targets are membrane-bound GPCRs, despite the fact that GPCRs are currently targeted by approximately 37% of approved drugs.[11] To effectively degrade GPCRs, a small-molecule PROTAC needs to engage the GPCR from inside the cell to recruit the UPS located in the cytosol and trigger degradation.[12] Thus, ligands binding at the intracellular interface of GPCRs are useful in the design of GPCR PROTACs. In fact, a reported GPCR PROTAC targeting CCR9 utilized an allosteric intracellular CCR9 ligand tethered to a VHL ligand and demonstrated proteasomal degradation of the target receptor,[13] further supporting this approach for GPCRs. Yet, two out of the three GPCR PROTACs (GPER[14] and α-1 AR[15]) employed an extracellular POI ligand; thus, further studies are needed to

Received: October 10, 2025
Revised: November 11, 2025
Accepted: November 14, 2025
Published: December 11, 2025

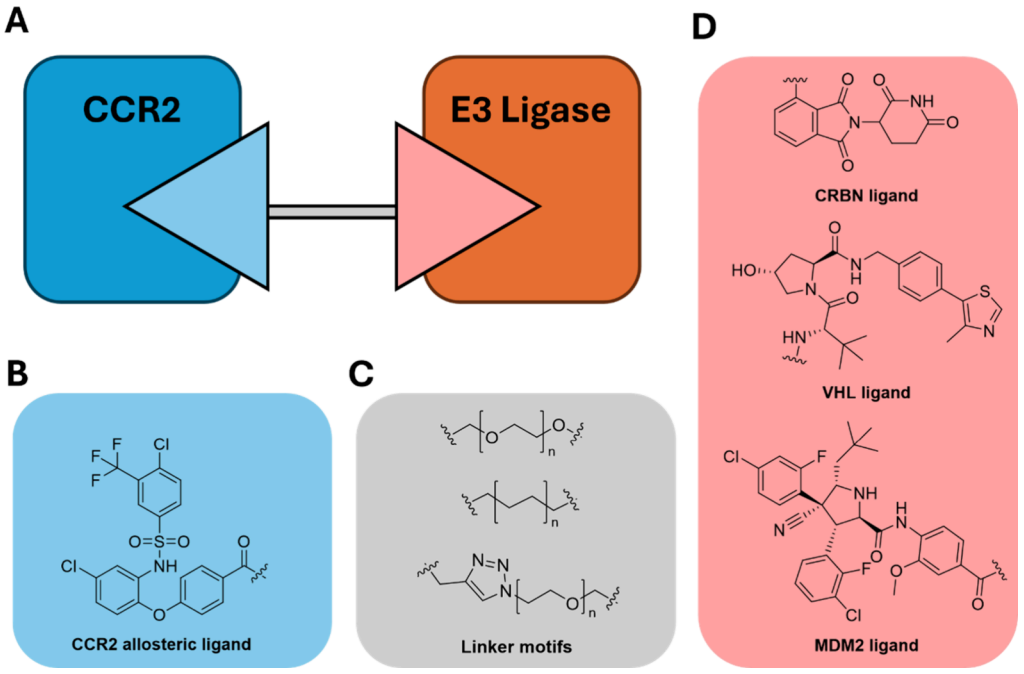

Figure 1. (A) Schematic design of CCR2 molecular degraders. (B) Chemical structure of the CCR2 intracellular allosteric ligand. (C) Chemical structures of linker types used in the study. (D) Chemical structure of employed E3 ligase ligands.

Table 1. Binding Affinities Determined in [^{3}H]CCR2-RA-[*R*] Displacement Assays Using U2OS-CCR2 Membranes

Compound	Linker	E3-recruited[a]	pK_i ± SEM (K_i, nM)[b] or displacement % at 10 μM (%)[c]
1		-	8.2 ± 0.10 (7)
5	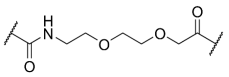	VHL	6.1 ± 0.01 (780)
6	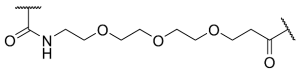	VHL	6.6 ± 0.03 (274)
7 (LUF7995)	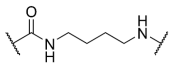	CRBN	6.9 ± 0.07 (138)
8 (LUF7996)	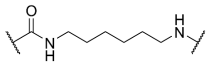	CRBN	6.3 ± 0.11 (560)
9	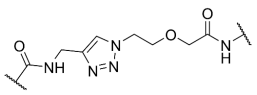	CRBN	6.9 ± 0.03 (130)
10	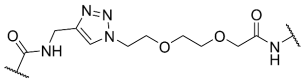	CRBN	6.7 ± 0.10 (219)
11	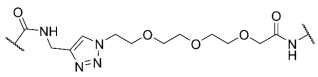	CRBN	6.7 ± 0.05 (203)
12	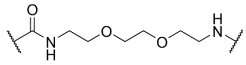	CRBN	6.4 ± 0.03 (417)
13	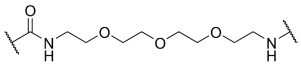	CRBN	6.4 ± 0.09 (474)
14 (LUF8062)	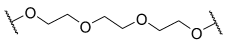	CRBN	6.5 ± 0.10 (339)
15 (LUF8063)	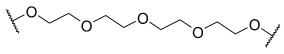	CRBN	6.5 ± 0.09 (344)
16	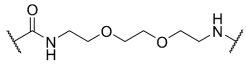	MDM2	18% (18, 17)[c]
17	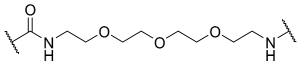	MDM2	14% (12, 17)[c]

[a]Structures of E3 ligase ligands and degraders orientation are shown in Figure 1A,D. [b]Data are presented as mean pK_i ± standard error of the mean (SEM) and mean K_i (in nM) of at least three individual experiments performed in duplicate. [c]For compounds displaying less than 50% displacement, we provide values that represent mean percentage displacement of [^{3}H]CCR2-RA-[*R*] by 10 μM of compound obtained in two individual experiments. Data from individual experiments are shown in brackets.

elucidate how extracellular PROTACs recruit cytosolic E3 ligases to induce proteasomal degradation.

A particular GPCR of our interest is the class A GPCR, CC chemokine receptor 2 (CCR2).[16] Being expressed on

https://doi.org/10.1021/acs.jmedchem.5c02920
J. Med. Chem. 2025, 68, 26525−26546

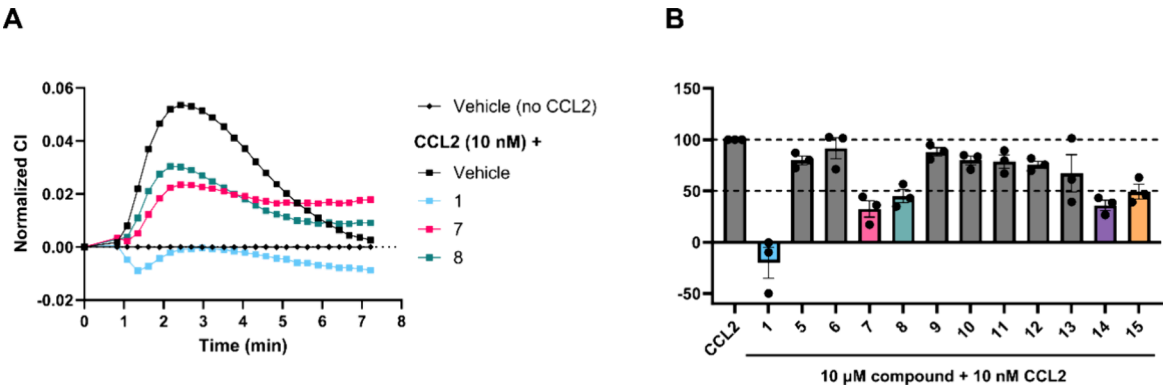

Figure 2. Putative CCR2 degraders **7**, **8**, **14**, and **15** induce functional CCR2 inhibition in a whole-cell, impedance-based assay (xCELLigence), using U2OS cells stably expressing CCR2 (U2OS-CCR2). Before stimulation of U2OS-CCR2 cells with 10 nM CCL2, cells were pretreated for 1 h with 10 μM of CCR2 compounds or vehicle control. (A) Representative vehicle-corrected xCELLigence traces, showing the inhibitory effect of compounds **1**, **7**, and **8** as examples. Representative data show the mean normalized cell index (CI) values of a single experiment performed in duplicate. (B) Inhibition of CCL2-induced cellular response by the indicated compounds (10 μM). Cellular response was derived from peak-height analysis of the vehicle-corrected, normalized CI xCELLigence traces within the first 6 min after stimulation. For comparison, cellular response was normalized to 10 nM CCL2 in the absence of any compound. The dotted line indicates either 100 or 50% CCL2 response. Data are shown as mean ± SEM of three independent experiments performed in duplicate, with the individual values also displayed.

membranes of leukocytes, CCR2 regulates their trafficking to inflammatory sites to maintain immunohomeostasis.[17−21] Leukocyte trafficking occurs as a result of CCR2 activation upon binding of its cognate endogenous chemokines, mainly chemokine ligand 2 (CCL2).[22,23] An aberrant increase in CCL2-CCR2 signaling and/or expression is implicated in the pathophysiology of numerous immunoinflammatory diseases.[23,24] Such pathologies include tumorigenesis and metastasis of several cancers,[24] atherosclerosis,[25] neuropathic pain,[26] hepatic fibrosis,[27] and rheumatoid arthritis.[28] Due to its pharmacological significance, several selective and dual (mostly dual CCR2 and CCR5) antagonists have progressed to clinical trials.[29] However, to date, no clinical candidates have passed phase III trials. Lack of efficacy has been hypothesized to be the main reason for failure to meet clinical end points in the CCR2 clinical trials.[30−32] These clinical failures can be attributed to potential scaffolding functions involving CCR2 that cannot be blocked by conventional antagonists as a result of activation of G protein independent signaling.[33,34] Therefore, developing novel modalities such as degraders can potentially tackle CCR2 functions beyond chemokine-related effects and/or inhibit activation of alternative signaling pathways.

Previous work from our group has identified an intracellular allosteric binding site in CCR2, along with a variety of small molecules binding to this site.[16,35] Additionally, we have previously confirmed that CCR2 is amenable to targeted degradation by demonstrating degradation of a CCR2-HaloTag-HiBiT construct upon treatment with HaloPROTAC3.[36] With this knowledge in hand, we envisioned that designing a small-molecule PROTAC that binds endogenous CCR2 intracellularly can achieve its targeted degradation by engaging cytosolic E3 ligases. Herein, we report the discovery and development of novel CCR2 molecular degraders, starting from a PROTAC discovery approach. Our pharmacology workflow can facilitate the discovery of novel GPCR degraders, by tackling target engagement, functional response and receptor degradation. As a result, we have discovered the first lysosome-dependent CCR2 molecular degraders.

RESULTS AND DISCUSSION

Design and Synthesis of CCR2 Molecular Degraders. The first focus of our workflow was the design of the CCR2 molecular degraders, using a PROTAC approach (Figure 1A). As previously described, a PROTAC must bind CCR2 on the intracellular face of the receptor to enable E3 ligase recruitment and subsequent target degradation. We have previously discovered compound **1** (Figure 1B and Table 1) as a potent allosteric intracellular CCR2 ligand.[37] In a previous study, we examined the binding mode of ligand **1** and observed that the carboxylic acid moiety is solvent-exposed rendering it a suitable exit vector for a PROTAC linker.[35] We selected thalidomide derivative **2**, VHL ligand **3**, and Idasanutlin **4** as recruiters for CRBN,[38] VHL,[39] and MDM2,[40] respectively (Figure 1D). The choice of these E3 ligases is based on their widespread use in current PROTACs,[41] their ubiquitous expression in many cell lines,[41] and the commercial availability of potent, selective small-molecule binders for them. To tether the CCR2 ligand **1** to the E3 ligase ligands, we then focused on linker design, a critical aspect of PROTAC development to ensure sufficient membrane permeability and efficient ternary complex formation.[42] Thus, we introduced variations in linker length, chemical composition, and the functional groups used to attach the linkers to the E3 and POI ligand (Figure 1C and Table 1). Based on the mentioned aspects of PROTAC elements, we designed several putative CCR2 PROTACs composed of CCR2 ligand **1** tethered by various linkers to the mentioned E3 ligase ligands. The designed compounds were synthesized through either linear or modular approaches (Schemes S1−S6).

CCR2 Molecular Degraders Exhibit Reduced yet Sufficient Binding Affinity to CCR2. With the set of putative CCR2 degraders (**5**−**17**) in hand, we then aimed to assess their CCR2 engagement. The binding affinities of the synthesized PROTACs to CCR2 were evaluated in a previously described [^{3}H]CCR2-RA-[*R*] competition binding assay using membranes from U2OS cells stably expressing human CCR2b (U2OS-CCR2).[43] After screening, all putative CCR2 degraders at a single concentration of 10 μM, compounds that displaced >50% of [^{3}H]CCR2-RA-[*R*] binding, were further evaluated using multiple concentrations to determine their binding

https://doi.org/10.1021/acs.jmedchem.5c02920
J. Med. Chem. 2025, 68, 26525−26546

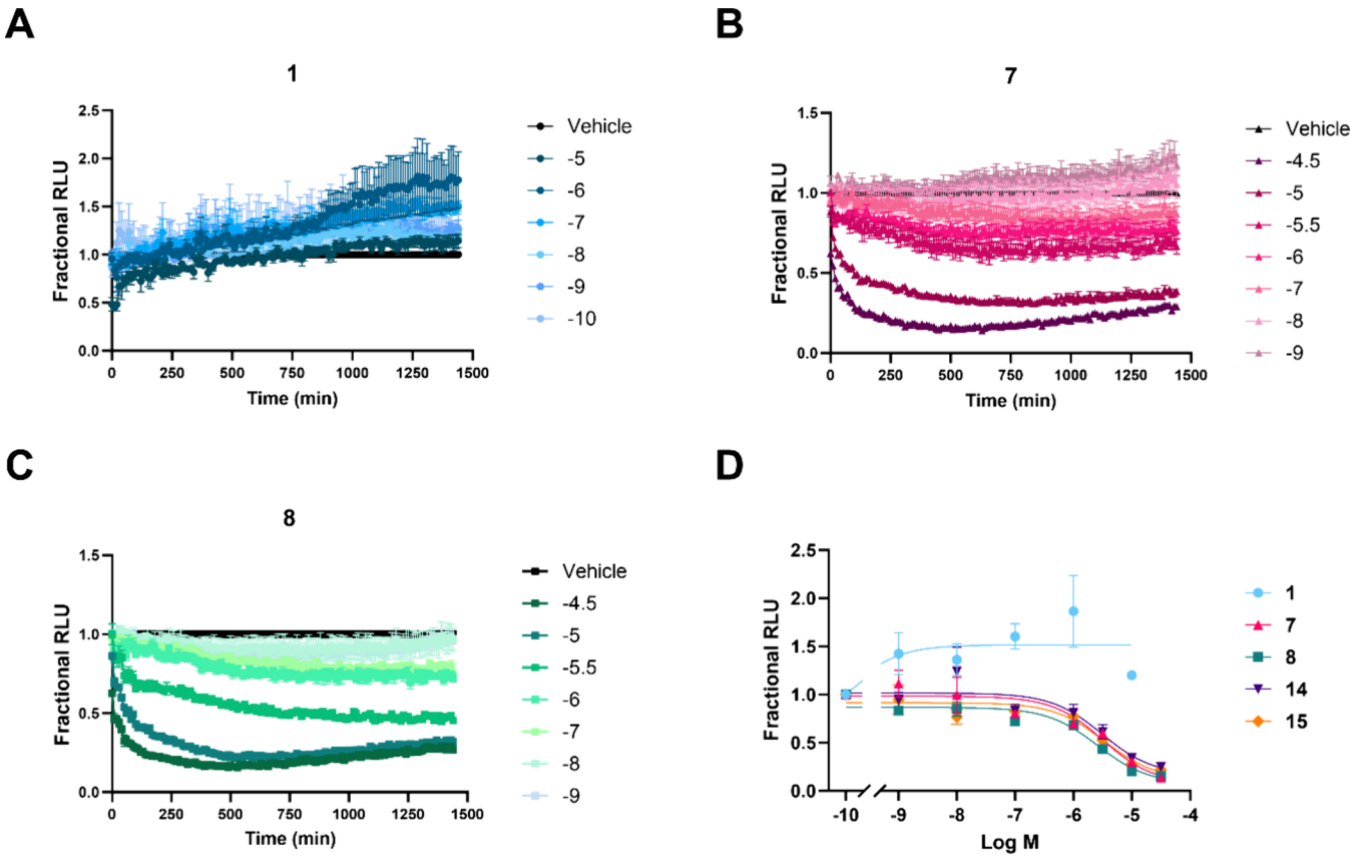

Figure 3. CCR2 molecular degraders induce rapid and sustained degradation of CCR2. (A−D) Kinetic degradation profiles of CCR2-HiBiT after treatment with multiple concentrations of compound **1** (A), **7** (B), or **8** (C). Kinetic profiles were obtained in a real-time HiBiT detection assay, using HEK293-LgBiT cells transiently transfected with 2 μg CCR2-HiBiT. (D) Degradation curves showing the fractional RLU values corresponding to D_{max} (RLU values represent the maximal degradation achieved over 24 h) at each concentration of the indicated compound. D_{max} values were obtained from the real-times traces. Data are shown as mean ± SEM of three independent experiments performed in duplicate (A−D).

affinities (pK_i). The parent ligand **1** displaced [^{3}H]CCR2-RA-[*R*] with a K_i of 7 nM (Table 1), displaying strong affinity to CCR2 as previously shown for a similar compound (−CF_3 moiety is substituted with a −Cl moiety).[35] All VHL- and CRBN-recruiting CCR2 compounds fully displaced [^{3}H]CCR2-RA-[*R*] binding in a concentration-dependent manner. In comparison to **1**, a reduced yet still moderate affinity to CCR2 (K_i range of 130−780 nM, Table 1) was found. In contrast, MDM2-recruiting CCR2 compounds **16** and **17** displayed a complete loss in affinity (<20% displacement at 10 μM, Table 1) to CCR2 despite employing linkers of a similar length/structure to the VHL and CRBN-recruiting compounds. This reduced affinity has been shown before when functionalizing parent ligands into PROTACs; however, such reduction in affinity can often be mitigated through the inherent catalytic activity of PROTACs.[44,36] A potential explanation for the reduced CCR2 affinity observed for the CCR2 bifunctional degraders is the resulting conformation/orientation of the CCR2 ligand when functionalized into a putative PROTAC, which can potentially lead to clashes within the CCR2 binding pocket.[45,46] In this regard, the failure of MDM2-recruiting compounds to engage CCR2 can be attributed to potential intramolecular hydrogen bonding within the compounds. Based on the binding data, we proceeded with further characterization of VHL- and CRBN-recruiting CCR2 compounds, while those recruiting MDM2 were not further evaluated.

Some Putative CCR2 Degraders Display Inhibitory Activity in an Impedance-Based Whole-Cell Assay. As binding affinity of the VHL- and CRBN-recruiting CCR2 compounds was determined in membrane preparations, we next aimed to evaluate their ability to pass through the plasma membrane and induce functional inhibition of CCR2. This was assessed using a label-free, whole-cell assay (xCELLigence) that measures changes in cellular electrical impedance, expressed as cell index (CI), which can be correlated to changes in GPCR signaling within the cells (i.e., activation or inhibition of GPCRs).[47,48] Inhibition of the CCL2-induced CCR2 response by 50% or higher was set as the cutoff point for sufficient inhibition of CCR2. At 10 μM, the parent ligand **1** displayed full inhibition of CCR2 (Figure 2). However, within the evaluated CCR2 degraders, only four CRBN-recruiting compounds (**7**, **8**, **14**, and **15**) displayed >50% inhibition of the CCR2 response, with inhibition percentages ranging from 51 to 67% (Figure 2B). Despite exhibiting binding affinities similar to those of **7**, **8**, **14**, and **15**, all other compounds displayed <50% inhibition in this assay. Since this assay was carried out in whole cells, the observations suggest that the compounds are less able to pass through the cell membrane and bind CCR2 allosterically to induce functional inhibition in contrast to the parent ligand. By examining the structures of the potential degraders, we observed that an increase in overall lipophilicity of the compounds due to linker modification can lead to higher CCR2 inhibition as a potential consequence of improved permeability. Specifically,

https://doi.org/10.1021/acs.jmedchem.5c02920
J. Med. Chem. 2025, 68, 26525−26546

using lipophilic alkyl linkers in **7** and **8** or substituting the amide/amine connecting functionalities with ethers in **14** and **15** resulted in improved CCR2 inhibition in the functional assay. It is important to note that the xCELLigence assay only evaluates the functional CCR2 response and that permeability can only be estimated in comparison to the known affinities of the tested compounds. As only the CRBN-recruiting compounds **7**, **8**, **14**, and **15** displayed sufficient inhibition in this assay, they were selected for further characterization of their CCR2-degradative capacity.

CCR2 Bifunctional Compounds Induce Concentration-Dependent Degradation of CCR2. While Western blotting is considered standard practice in evaluating targeted protein degradation, the use of this technique to evaluate GPCR levels is troublesome. This arises from a relatively low level of protein expression, and a lack of specific and selective GPCR antibodies. Hence, to evaluate the degradative capacity of **7**, **8**, **14**, and **15**, we used a previously described real-time HiBiT detection assay.[36,49] This assay relies on the high-affinity complementation between the 11-amino acid peptide tag HiBiT—appended to CCR2—and the larger subunit LgBiT to generate a luminescent NanoBiT luciferase. Addition of the extended live cell NanoGlo Endurazine substrate generates a bioluminescent signal that is proportional to the level of the HiBiT-tagged protein. Using HEK293 cells stably expressing LgBiT (HEK293-LgBiT) allows the real-time measurement of HiBiT-tagged protein levels, such as CCR2-HiBiT, instead of end-point measurements of degradation as would be achieved by Western blotting.[41] Treatment with the parent ligand **1** did not show any reduction in CCR2 levels throughout the whole incubation period across all concentrations (Figure 3A). On the contrary, an increase in CCR2 levels was observed over time, which may occur due to a potential improvement in translocation of CCR2 from the ER to the plasma membrane (i.e., pharmacochaperone effect).[50] Additionally, antagonist binding can potentially stabilize an inactive conformation of CCR2, thus reducing the constitutive receptor internalization leading to an increase in CCR2 levels.[51] A similar increase was observed with a compound similar to our parent ligand in addition to other CCR2 antagonists in a previous study using a CCR2-HaloTag-HiBiT construct.[36] Compounds **7**, **8**, **14**, and **15** did not display any substantial degradative capacity when tested at concentrations below 1 μM (Figure 3B−D and Figure S1). However, upon treatment with concentrations higher than 1 μM of **7**, **8**, **14**, and **15**, we observed a rapid and concentration-dependent degradation of CCR2, with half maximal degradation (DC_{50}) potencies ranging from 2.6 to 3.8 μM (Figure 3B−D, Figure S1, and Table 2), without indication of a hook effect at these concentrations. Maximal degradation (D_{max}) was achieved between 4 and 8h, with D_{max} values ranging from 66 to 79% at 10 μM (Table 2). Remarkably, the degradative effect of **7**, **8**, **14**, and **15** was sustained over the course of the experiment (24 h) with little-to-no signs of CCR2 recovery to basal levels, highlighting the sustained and possibly catalytic degradative effect of the CCR2 molecular degraders. This observation is remarkable considering the short half-life (1.3 ± 0.019 h) of CCR2-HiBiT (Figure S2), which was determined by treating the cells with the protein synthesis inhibitor cycloheximide prior to evaluating the levels of CCR2-HiBiT in the same assay used for the molecular degraders. Of note, the observed degradative effect of the CCR2 degraders was not a result of cellular toxicity. The CellTiter-Glo viability assay confirmed that the cells did not demonstrate a significant reduction in viability upon treatment with these compounds (Figure S3). Since degrader **8** displayed the highest degradative potency among the CCR2 degraders, we selected it for further assessments.

Table 2. Degradation Potencies of Assessed CCR2 Molecular Degraders[c]

compound	pDC_{50} ± SEM (DC_{50}, μM)[a]	D_{max} (%) at 31.6 μM[b]	D_{max} (%) at 10 μM[b]
7	5.5 ± 0.23 (3.8)	86 ± 0.4	70 ± 1.6
8	5.6 ± 0.04 (2.6)	85 ± 0.6	79 ± 0.6
14	5.5 ± 0.12 (3.2)	75 ± 2.5	66 ± 2.2
15	5.5 ± 0.05 (3.5)	78 ± 0.3	72 ± 2.8
18	5.5 ± 0.04 (3.5)	62 ± 1.7	59 ± 2.0
19	6.2 ± 0.20 (0.8)	50 ± 0.6	48 ± 3.9

[a]Potency of CCR2-HiBiT degradation (DC_{50}) determined in real-time HiBiT assays. [b]Maximal degradation (D_{max}) determined at the specified compound concentration. [c]Data shown represent mean ± SEM of at least three experiments performed in duplicate.

CRBN Mediates Degrader-Induced CCR2 Degradation. After confirming that CCR2 PROTACs can degrade CCR2, we investigated their dependency on CRBN recruitment for degradation. A standard approach in PROTAC validation is to synthesize derivatives that are unable to bind the E3 ligase, helping to confirm the reliance on E3 ligase recruitment for degradation. To this end, we synthesized CRBN-inactive derivatives **18** and **19** (Scheme S7), which are based on **7** and **8**, respectively.[52−54] These negative controls **18** and **19** (Figure 4A) share the same structure as **7** and **8**, except for methylation of the glutarimide moiety of the thalidomide derivative, which significantly reduces CRBN binding, preventing ubiquitination and subsequent degradation.[55,56] As expected, compounds **18** and **19** bound CCR2 (197 and 427 nM, respectively) with similar affinities as **7** and **8** (Table S1). Next, we investigated the CRBN engagement of **7**, **8**, **18**, and **19** in a FRET-based CRBN engagement assay.[48−50] As expected, compounds **7** and **8** exhibited the strongest CRBN engagement (IC_{50}= 41 and 143 nM, respectively), while the negative controls **18** and **19** displayed a significant reduction in binding affinity to CRBN (IC_{50}= 24.8 and 1.8 μM, respectively) (Table S2). When tested in the xCELLigence assay, control **18** induced ∼50% inhibition of CCR2, while control **19** only induced ∼30% inhibition (Figure 4B). Nevertheless, both controls were included in further assessment to allow clear understanding of the role of CRBN in CCR2 degradation. Unexpectedly, **18** and **19** induced a concentration-dependent degradation of CCR2 (Figure 4C,D and Table 2). Interestingly, **19** even displayed the highest degradation potency among all compounds (DC_{50} of 0.8 μM, Table 2). However, the D_{max} values achieved by **18** and **19** (59 and 48% at 10 μM, respectively; Table 2) were lower than those of their counterparts **7** and **8** (D_{max} values of 70 and 79% at 10 μM, respectively; Table 2). Thus, while compounds **18** and **19** retain the ability to induce CCR2 degradation, their lower D_{max} may result from less efficient recruitment of CRBN. To further confirm if the CCR2 degradation is mediated by CRBN, we performed degradation assays in the absence or presence of a CRBN inhibitor (pomalidomide) or a previously described CRBN degrader (CRBN-6-5-5-VHL).[57] Competition for the CRBN binding pocket or elimination of CRBN (Figure 4E,F) led to partial yet significant rescue of CCR2 degradation upon cotreatment with degrader **8**. It is important to note that treatment with pomalidomide or the CRBN degrader alone did not affect CCR2-HiBiT levels (Figure S4A). The observations

https://doi.org/10.1021/acs.jmedchem.5c02920
J. Med. Chem. 2025, 68, 26525−26546

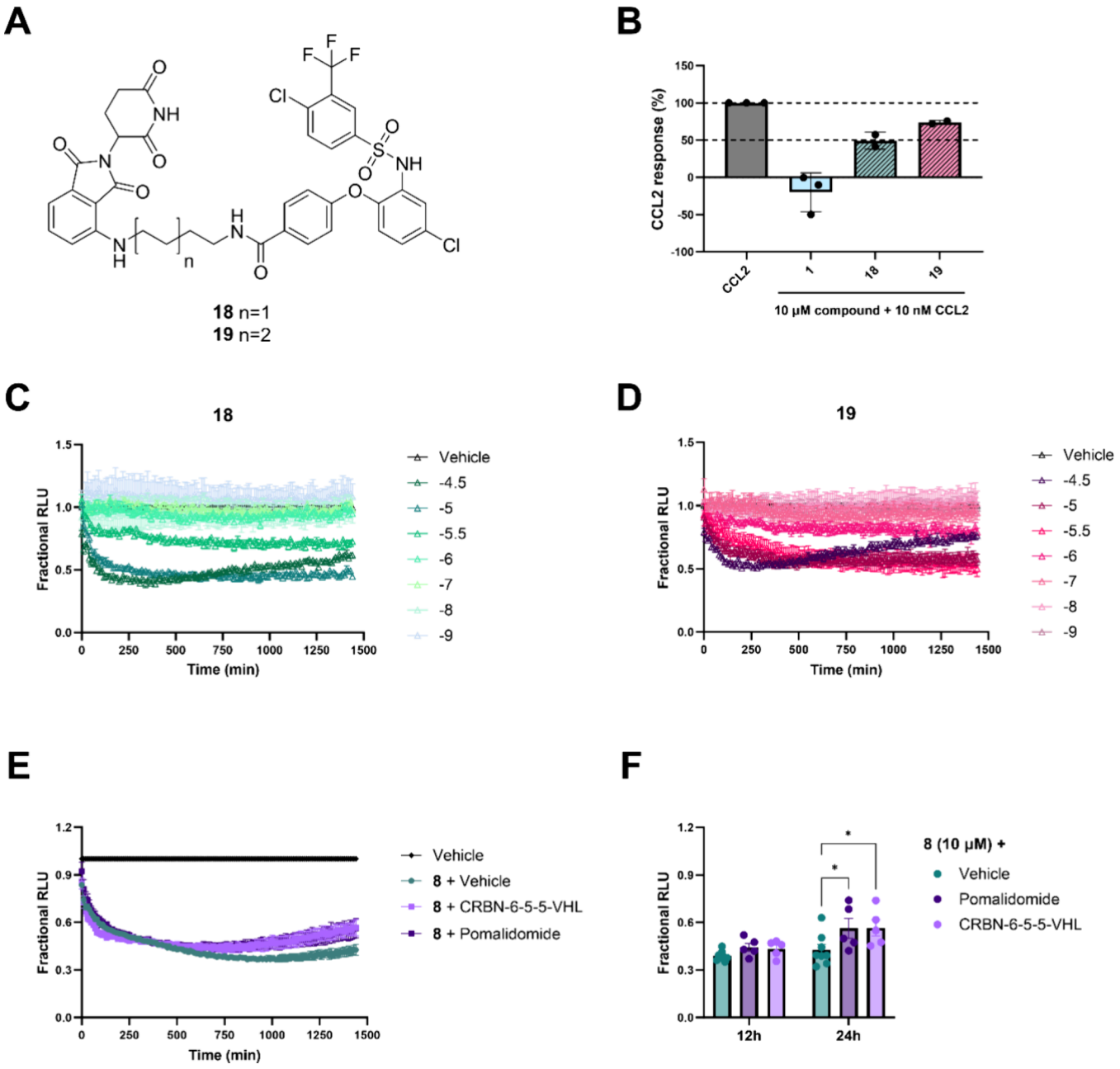

Figure 4. Compounds **18** and **19** developed as a negative control of CCR2 degrader **7** and **8** maintain CCR2 inhibitory activity and degradation capacity. (A) Chemical structures of compounds **18** and **19**. (B) Inhibition of CCL2-induced cellular response by the indicated compounds (10 μM), determined in xCELLigence assays using U2OS-CCR2 cells. Cellular response was derived from peak-height analysis of the vehicle-corrected, normalized CI xCELLigence traces within the first 6 min after stimulation. For comparison, cellular response was normalized to 10 nM CCL2 in the absence of any compound. Data are shown as mean ± SEM of two independent experiments performed in duplicate. (C, D) Kinetic degradation profiles of CCR2-HiBiT after treatment with multiple concentrations of compound **18** (C) or **19** (D). The kinetic profile was obtained in a real-time HiBiT detection assay, using HEK293-LgBiT cells transiently transfected with 2 μg CCR2-HiBiT. (E) Kinetic degradation profiles of CCR2-HiBiT after treatment with compound **8** in the presence of pomalidomide (100 μM) or CRBN-6-5-5-VHL (1 μM). Cells were pretreated for 2 h before addition of compound **8** and measurement of luminescence. Kinetic profiles were obtained in a real-time HiBiT detection assay, using HEK293-LgBiT cells transiently transfected with 2 μg of CCR2-HiBiT plasmid. (F) Bar graph showing the fractional RLU values after 12 or 24 h of measuring luminescence. Fractional RLU values were obtained from the real-times traces shown in panel (E). Dotted lines indicate either 100 or 50% CCL2 response. Data are shown as mean ± SEM of at least three independent experiments performed in duplicate or triplicate. Statistical differences between fractional RLU values of compound **8** in the absence and presence of pomalidomide or CRBN-6-5-5-VHL at different time points were analyzed using a two-way ANOVA with Dunnett's posthoc test: * $p < 0.05$.

obtained from the cotreatment of degrader **8** with pomalidomide or CRBN degrader hint toward a mechanism where CRBN contributes to CCR2 degradation.

As CRBN recruitment is expected to induce ubiquitination of the target protein, we next used a NanoBRET-based assay to evaluate the ubiquitination of CCR2 upon treatment with degrader **8**. Treatment with degrader **8** for 3 h resulted in a significant increase in CCR2 ubiquitination compared with vehicle control or compound **1** (Figure S4B). Therefore, the presented findings suggest that CCR2 degradation proceeds, at

https://doi.org/10.1021/acs.jmedchem.5c02920
J. Med. Chem. 2025, 68, 26525−26546

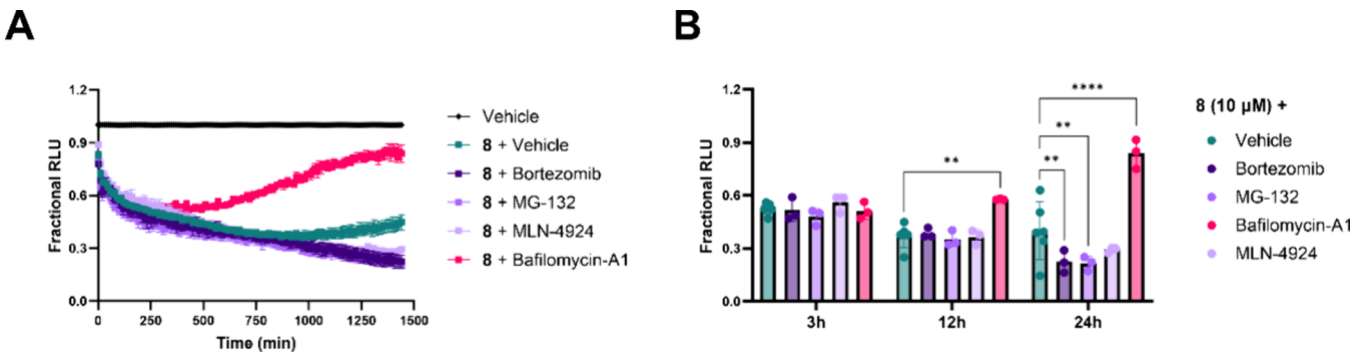

Figure 5. Compound **8** induces CCR2-HiBiT degradation via the lysosomal pathway. (A) Kinetic degradation profiles of CCR2-HiBiT after treatment with compound **8** in the presence of bortezomib (10 μM), MG-132 (10 μM), MLN-4924 (250 nM), or bafilomycin-A1 (100 nM). Cells were pretreated for 2 h with proteasomal or lysosomal inhibitors before addition of compound **8** and measurement of luminescence. Kinetic profiles were obtained in a real-time HiBiT detection assay, using HEK293-LgBiT cells transiently transfected with 2 μg CCR2-HiBiT plasmid. (B) Bar graph showing the fractional RLU values after 3, 12, or 24 h of measuring luminescence. Fractional RLU values were obtained from the real-times traces shown in panel (A). Data are shown as mean ± SEM of three independent experiments performed in triplicate. Statistical differences between fractional RLU values of compound **8** in the absence and presence of proteasomal/lysosomal inhibitors at different time points were analyzed using a two-way ANOVA with Dunnett's posthoc test: ** $p < 0.01$, **** $p < 0.0001$.

least partially through CRBN and ubiquitin-dependent mechanisms. The remaining cellular machinery implicated in targeted degradation of CCR2 and potentially other GPCRs remains to be further investigated.

CCR2 Degrader 8 Degrades CCR2 through the Autophagy-Lysosome Pathway. Next, we set out to unravel the degradation machinery hijacked to achieve the observed CCR2 degradation. It is established that the majority of PROTACs lead to polyubiquitination of the POI followed by its degradation by the 26S proteasome.[9] Accordingly, we investigated the effect of cotreating compound **8** (10 μM) with the proteasome inhibitors bortezomib or MG-132 (10 μM) or the neddylation inhibitor MLN-4924 (250 nM) using the real-time HiBiT assay (Figure 5). Cotreatment of **8** with the proteasomal and neddylation inhibitors did not block CCR2 degradation; instead, it further enhanced CCR2 degradation after 16h (Figure 5A,B), suggesting a proteasome- and neddylation-independent mechanism of action. Notably, treatment with either proteasomal inhibitors alone led to a decrease in CCR2 levels, which returned to baseline after 24 h (Figure S5A). It has been shown that high concentrations of proteasomal inhibitors (such as the 10 μM used in this study) over extended periods (longer than 6h) can cause degrader-independent protein degradation.[58] This effect has been linked to compromised cellular viability, mitochondrial integrity, and tubulin activity due to prolonged exposure to high concentrations of bortezomib or MG-132. Thus, the further increase in degradation may be explained as a combination of the degradative effect of **8** and the cytotoxic effect of the proteasome inhibitors. In contrast, treatment with MLN-4924 alone (Figure S5A) led to a minimal decrease in CCR2-HiBiT levels that was maintained over the course of the experiment. This effect can be attributed to the minimal cytotoxicity associated with MLN-2492.

Although there are some examples where GPCRs are constitutively degraded through the proteasome, most GPCRs are constitutively degraded or recycled through the lysosomal pathway.[57−61] It has been shown that the natural ubiquitination of GPCRs can lead to internalization through clathrin-coated pits followed by either lysosomal degradation or recycling back to the plasma membrane.[59−63] Thus, if a degrader is able to induce ubiquitination of a GPCR, it can potentially induce receptor degradation via the lysosomal pathway. As such, we were curious if the CCR2 degraders exert their activity via hydrolytic degradation in lysosomal vesicles. Therefore, we evaluated the degradative capacity of **8** (10 μM) in the presence of the lysosomal inhibitor bafilomycin-A1 (Baf-A1) at 100 nM (Figure 5A,B). Baf-A1 is a potent V-ATPase inhibitor that specifically blocks the acidification of the lysosome, which prevents the fusion of the autophagosome to lysosomal vesicles, resulting in inhibition of lysosomal mediated protein degradation.[64] Treatment with both **8** and Baf-A1 led to a reduction in degradation with a significantly higher level of CCR2 present after 12 h of cotreatment and full restoration of CCR2 levels toward baseline over 24 h (Figure 5A,B). This full restoration suggests that inhibition of the lysosomal pathway prevents the degradation effect of compound **8**. Cotreatment with another lysosomal inhibitor (chloroquine) also resulted in a decreased degradative effect of degrader **8** (Figure S5B), although the effect was much less pronounced. However, the reduced degradation further supports a role of the lysosomal pathway in degrading CCR2. Of note, treatment with Baf-A1 or chloroquine alone did not induce noticeable reduction in CCR2 levels (Figure S5C). From the reported examples of PROTACs targeting integral membrane proteins, only one protein (EGFR) was found to be targeted for degradation through the autophagy-lysosomal pathway in addition to its proteasomal degradation,[65−67] while the GPCR PROTACs for CCR9, α-1 AR, and GPER have been reported to utilize a proteasome-dependent degradation pathway.[13−15] Thus, according to our knowledge, this is the first evidence of targeting GPCRs for degradation exclusively through the lysosomal pathway by using bifunctional degraders.

CCR2 Molecular Degrader 8 Degrades Endogenous CCR2 and Inhibits Chemotactic Migration of a Monocytic Cell Line. To test the effect of **8** in a more (patho)physiologically relevant cell line where CCR2 is endogenously expressed, we set up a radioligand binding and a chemotaxis assay using the monocytic cell line THP-1.[68] First, to determine degradation of native CCR2 in this cell line, we assessed receptor levels by measuring [^{3}H]CCR2-RA-[R] binding in THP-1 cells treated with compound **1**, **8**, or DMSO control. Cells were treated with equipotent concentrations of each compound (126 nM compound **1** and 10 μM

https://doi.org/10.1021/acs.jmedchem.5c02920
J. Med. Chem. 2025, 68, 26525−26546

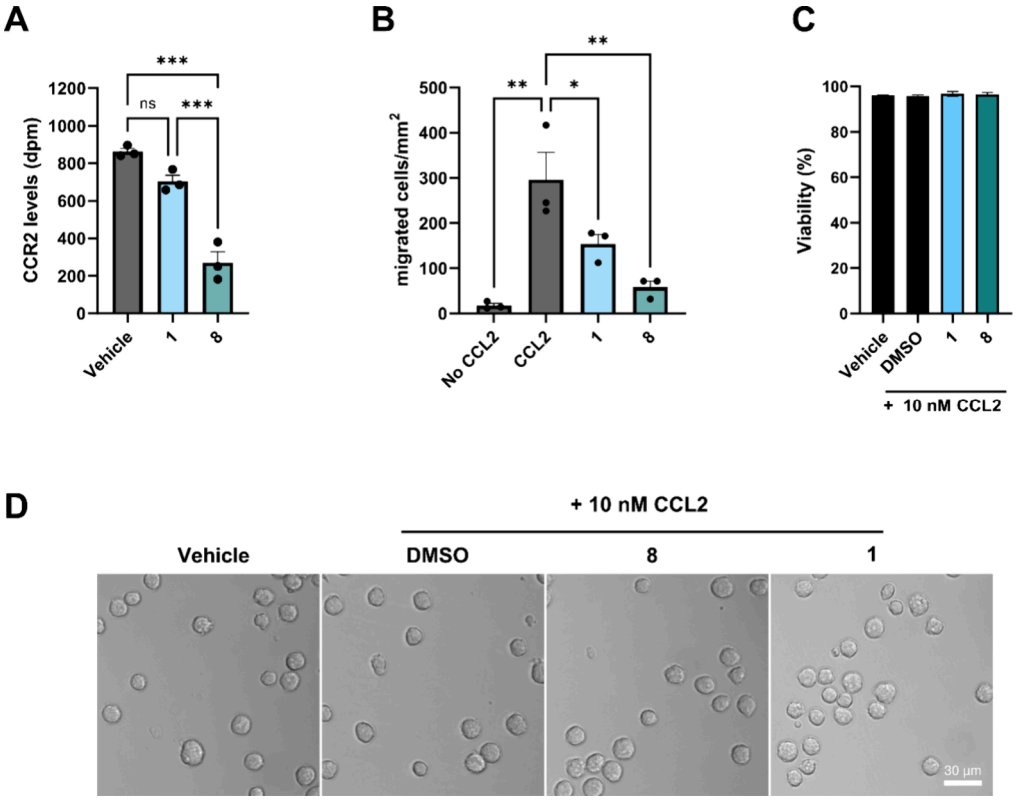

Figure 6. Molecular degrader **8** induces degradation of CCR2 in THP-1 cells and fully inhibits CCL2-induced migration. (A) [^{3}H]CCR2-RA-[*R*] binding, as an indication of CCR2 levels, in THP-1 cells treated for 24 h with equipotent concentrations of compound **1** (126 nM), **8** (10 μM), or DMSO control. (B) Inhibition of CCL2-induced migration of THP-1 cells by the indicated compounds at equipotent concentrations (126 nM compound **1** and 10 μM compound **8**). (C) Cell viability of THP-1 cells is not affected after treatment with vehicle control or CCL2 (10 nM) in the absence or presence of **1** and **8** at 10 μM. (D) Morphology of THP-1 cells is not affected after treatment with vehicle control or CCL2 (10 nM) in the absence or presence of 10 μM compounds **1** and **8**. Data are shown as mean ± SEM of three independent experiments performed in duplicate. Statistical differences between radioligand binding in the different cell treatments were analyzed using a one-way ANOVA with Tukey's posthoc test, while statistical differences between the number of migrated THP-1 cells per mm^2 after treatment with CCL2 in the absence or presence of the indicated compounds were analyzed using a paired, one-way ANOVA with Tukey's posthoc test: * $p < 0.05$, ** $p < 0.01$, *** $p < 0.001$.

compound **8**), based on their binding affinity (Table 1), for 24 h before measuring radioligand binding. Treatment with compound **8** resulted in a significant reduction in [^{3}H]CCR2-RA-[R] binding compared with cells treated with vehicle control (69% reduction in binding, Figure 6A), indicating a reduction of CCR2 levels. In contrast, cells treated with compound **1** did not significantly affect radioligand binding, indicating similar receptor levels compared with vehicle control. These data indicate that compound **8** is able to degrade both the modified CCR2-HiBiT construct and native CCR2.

Previous studies have shown that CCL2 induces migration of THP-1 cells *in vitro*, following a bell-shaped dose−response curve with maximal migration responses at 1−10 nM.[69,70] Thus, we next used 10 nM CCL2 to stimulate cell migration in a transwell migration setup, which led to a clear increase in THP-1 cell migration compared to vehicle control (Figure 6B and Figure S6B). For the inhibition assays, cells were preincubated for 3 h with CCR2 compounds before treatment with 10 nM CCL2 and further coincubation for 1.5 h. The 3 h-preincubation time was selected based on the degradation profile of **8**, as >80% degradation was observed after 3 h treatment with 10 μM (Figure 3C). Treatment with 10 μM of degrader **8** demonstrated potent inhibition of CCL2-induced monocyte migration (Figure S6B). For comparison, we also tested parent ligand **1** and the reference CCR2 antagonists INCB3344 (orthosteric) and CCR2-RA-[R] (allosteric). At 10 μM, migration of THP-1 cells was fully inhibited upon treatment with the CCR2 antagonists to levels similar as vehicle control (Figure S6B). However, when tested at equipotent concentrations, based on their binding affinities (Table 1), compound **1** only inhibited 48% of CCL2-induced migration, compared with 84% inhibition achieved by compound **8** (Figure 6B). It is worth noting that, even though **8** only achieved ∼50% inhibition at 10 μM in the xCELLigence assay (Figure 2B), it was able to fully inhibit the *in vitro* migration of a monocytic cell line. Importantly, treatment of THP-1 cells with CCL2 or the selected CCR2 compounds at 10 μM did not affect cell viability (Figure 6C and Figure S6A) or cell morphology (Figure 6D). Although it has been shown that targeted protein degradation can be impacted by both treatment duration and protein expression levels,[49] these experiments prove that CCR2 degraders, such as **8**, can potently inhibit CCR2 function in a more translational setup.

CONCLUSIONS

In the present study we used a degrader evaluation pipeline that can be applicable for other GPCR TPD programs. The mentioned pipeline was utilized to evaluate our synthesized molecular degraders as a potential therapeutic alternative to traditional CCR2 antagonists. Our pipeline includes POI- and E3 ligase-engagement assays, *in vitro* cellular functional assays, and real-time degradation assays. The degradation assay using a HiBiT-tagged CCR2 provided us with real-time measurements

https://doi.org/10.1021/acs.jmedchem.5c02920
J. Med. Chem. 2025, 68, 26525−26546

of receptor levels and allowed us to overcome the lack of reliable GPCR antibodies for Western blotting or ELISA. Moreover, the real-time luminescence readout mitigates the difficulties that arise when assessing degradation of short-lived proteins (such as CCR2) where the choice of degrader concentration and measurement time point can be very challenging, particularly when using end-point experiments (i.e., Western blotting or ELISA). Furthermore, this degradation assay was used to explore the mechanism of action of the degraders of interest. As a result, compounds **7**, **8**, **14**, and **15** have been identified as the first CCR2 molecular degraders. These shortlisted CRBN-recruiting CCR2 degraders displayed sustained CCR2 degradation through the lysosomal rather than the proteasomal pathway. Further optimization rounds will aim toward improving PROTAC engagement of CCR2 and modifying linker composition to achieve higher degradation potencies. The approach herein presented has the potential to further expand the field of targeted GPCR degradation and thus provide potential GPCR degraders as novel therapeutics.

EXPERIMENTAL SECTION

General Chemistry Methods. All solvents and reagents were purchased from commercial sources and were used without further purification. ^{1}H and ^{13}C spectra were recorded on a Bruker AV 400 MHz liquid, Bruker AV 400 MHz wide bore, Bruker AV 500 MHz, and Bruker AV 600 MHz at room temperature (rt) using $CDCl_3$, MeOD, or DMSO as a solvent. Chemical shifts are reported in ppm relative to internal standard tetramethylsilane (TMS) or solvent resonance. Purity of all final compounds used in biological assays was at least >95% pure by HPLC analysis. Reactions were monitored by TLC using Merck TLC Silica gel 60 F254 aluminum sheets. Compounds were visualized by UV irradiation or by staining with a $KMnO_4$ solution in H_2O. For the flash chromatography, Davisil silica gel (40−63 μm) was used. The automatic flash chromatography was performed on an Isolera One Automatic Flash Chromatography System by Biotage with prepacked flash cartridges (Biotage Sfar D). Automated reverse-phase chromatography was performed using HPLC-grade acetonitrile and demi H_2O, both containing 0.1% TFA as the eluent system. Mass spectra were measured using a Shimadzu Prominence LC-MS-2020 system and a Gemini C18 Phenomenex column (50 × 3 mm, 3 μm) flow rate = 1.3 mL/min, using a gradient of 10−90% MeCN/H_2O (0.1% FA) and measuring UV absorbance at 254 nm.

Synthetic Procedures. *(9H-Fluoren-9-yl)methyl(2S,4R)-4-(tert-butoxy)-2-((4-(4-methylthiazol-5-yl)benzyl)carbam-oyl)pyrrolidine-1-carboxylate (**20**).* (4-(4-Methylthiazol-5-yl)phenyl)methanamine (5.7 g, 28 mmol) and Fmoc-Hyp(tBu)-OH (9.2 g, 22.4 mmol) were dissolved in DCM (120 mL), followed by addition of HCTU (496.5 mg, 22.4 mmol) and DIPEA (11.7 mL, 67.2 mmol). The reaction mixture was stirred for 18 h at rt. Upon reaction completion, the reaction mixture was concentrated in vacuum, redissolved in EtOAc, and washed with 1 M HCl (2 × 100 mL), sat. aq. $NaHCO_3$ (3 × 100 mL), and brine (100 mL). The organic layer was then dried over magnesium sulfate, and the solvent was evaporated under reduced pressure. The crude mixture was purified by flash column chromatography using a gradient of 0−8% EtOAc in *n*-heptane to obtain (9*H*-fluoren-9-yl)methyl(2*S*,4*R*)-4-(*tert*-butoxy)-2-((4-(4-methylthiazol-5-yl)benzyl)carbam-oyl)pyrrolidine-1-carboxylate (2.0 g, 3.4 mmol, yield: 12%). ^{1}H NMR (300 MHz, chloroform-*d*) δ 8.60 (s, 1H), 7.71 (d, J = 7.5 Hz, 2H), 7.51 (t, J = 9.8 Hz, 2H), 7.35 (t, J = 7.7 Hz, 3H), 7.28−7.22 (m, 5H), 4.50−4.15 (m, 7H), 3.66 (dd, J = 10.6, 6.5 Hz, 1H), 3.30 (dd, J = 10.5, 6.1 Hz, 1H), 2.48−2.37 (m, 4H), 1.99 (s, 1H), 1.20 (d, J = 6.5 Hz, 9H). ^{13}C NMR (75 MHz, chloroform-*d*) δ 171.5, 156.1, 148.4, 143.7, 141.3, 138.1, 130.8, 129.4, 127.8, 127.7, 127.1, 125.1, 120.1, 74.1, 69.7, 67.9, 59.2, 53.1, 47.1, 43.0, 36.3, 28.3, 16.0.

*(9H-Fluoren-9-yl)methyl((S)-1-((2S,4R)-4-(tert-butoxy)-2-((4-(4-methylthiazol-5-yl)benzyl)carbamoyl)pyrrolidin-1-yl)-3,3-dimethyl-1-oxobutan-2-yl)carbamate (**21**).* **20** (2.0 g, 3.4 mmol) was dissolved in 50% diethylamine/DCM (30 mL) stirred at rt for 3 h. Upon reaction completion, the reaction mixture was concentrated in vacuum and coevaporated with toluene (3 × 20 mL). The deprotected intermediate and Fmoc-Tle-OH (1.5 g, 4.1 mmol) were dissolved in DCM (40 mL), followed by addition of HCTU (1.7 g, 4.1 mmol) and DIPEA (2.1 mL, 11.9 mmol). The reaction mixture was stirred at rt for 18 h. Upon reaction completion, the reaction mixture was concentrated in vacuo, redissolved in EtOAc (40 mL), and washed with 1 M HCl (2× 0 mL), sat. aq. $NaHCO_3$ (3× 20 mL), and brine (30 mL). The organic layer was then dried over magnesium sulfate, and the solvent was evaporated under reduced pressure. The crude mixture was purified by flash column chromatography using a gradient of 0−8% MeOH/DCM to obtain (9*H*-fluoren-9-yl)methyl((*S*)-1-((2*S*,4*R*)-4-(*tert*-butoxy)-2-((4-(4-methylthiazol-5-yl)benzyl)carbamoyl)pyrrolidin-1-yl)-3,3-dimethyl-1-oxobutan-2-yl)carbamate (1.9 g, 2.7 mmol, yield: 79%). ^{1}H NMR (300 MHz, chloroform-*d*) δ 8.88 (s, 1H), 7.79−7.73 (m, 2H), 7.58 (d, J = 7.4 Hz, 2H), 7.43−7.28 (m, 8H), 5.43 (d, J = 9.7 Hz, 1H), 4.72 (dd, J = 8.3, 3.1 Hz, 1H), 4.60−4.07 (m, 8H), 3.75 (dd, J = 10.0, 6.6 Hz, 1H), 3.64−3.50 (m, 1H), 2.57 (s, 5H), 1.20 (s, 9H), 0.92 (s, 9H). ^{13}C NMR (75 MHz, chloroform-*d*) δ 172.1, 170.9, 156.3, 144.0, 141.5, 138.8, 129.7, 128.5, 127.9, 127.2, 125.3, 125.2, 120.2, 74.4, 70.1, 67.2, 59.0, 58.8, 54.7, 47.4, 43.4, 35.9, 35.1, 28.4, 26.4, 15.2.

*(9H-Fluoren-9-yl)methyl(2-(2-(2-(((S)-1-((2S,4R)-4-(tert-butoxy)-2-((4-(4-methylthiazol-5-yl)benzyl)ncarbamoyl)pyrrolidin-1-yl)-3,3-dimethyl-1-oxobutan-2-yl)amino)-2-oxoethoxy)-ethoxy)ethyl)-carbamate (**22**).* **21** (567 mg, 0.8 mmol) was dissolved in 50% diethylamine/DCM (10 mL) and stirred at rt for 3 h. Upon reaction completion, the reaction mixture was concentrated in vacuum and coevaporated with toluene (3 × 10 mL). The deprotected intermediate and Fmoc-PEG_2-CH_2COOH (385 mg, 1.0 mmol) were dissolved in DCM (10 mL), followed by addition of HCTU (431 mg, 1.0 mmol) and DIPEA (0.5 mL, 2.8 mmol). The reaction mixture was stirred at rt for 18 h. Upon reaction completion, the reaction mixture was concentrated in vacuo, redissolved in EtOAc (20 mL), and washed with 1 M HCl (2 × 10 mL), sat. aq. $NaHCO_3$ (3 × 10 mL), and brine (15 mL). The organic layer was then dried over magnesium sulfate, and the solvent was evaporated under reduced pressure. The crude mixture was purified by flash column chromatography using a gradient of 0−8% MeOH/DCM to obtain (9*H*-fluoren-9-yl)methyl (2-(2-(2-(((*S*)-1-((2*S*,4*R*)-4-(*tert*-butoxy)-2-((4-(4-methylthiazol-5-yl)benzyl)-carbamoyl)pyrrolidin-1-yl)-3,3-dimethyl-1-oxobutan-2-yl)amino)-2-oxoethoxy)-ethoxy)ethyl)carbamate (572 mg, 0.67 mmol, yield: 84%). ^{1}H NMR (300 MHz, chloroform-*d*) δ 8.67 (d, J = 1.7 Hz, 1H), 7.76 (d, J = 7.5 Hz, 2H), 7.56 (ddt, J = 25.5, 15.2, 7.8 Hz, 3H), 7.44−7.35 (m, 2H), 7.34−7.16 (m, 5H), 4.83−4.57 (m, 3H), 4.46−4.00 (m, 6H), 3.97−3.76 (m, 2H), 3.76−3.19 (m, 8H), 3.18−2.82 (m, 1H), 2.47 (d, J = 18.5 Hz, 2H), 2.40−1.90 (m, 2H), 1.21 (d, J = 3.6 Hz, 9H), 0.96 (d, J = 17.1 Hz, 8H). LC-MS (ESI) m/z $[M + H]^+$ Calcd for $C_{47}H_{59}N_5O_8S$: 854.4163; found 854.4133.

*(9H-Fluoren-9-yl)methyl((S)-14-((2S,4R)-4-(tert-butoxy)-2-((4-(4-methylthiazol-5-yl)benzyl)carbamoyl)pyrrolidine-1-carbonyl)-15,15-dimethyl-12-oxo-3,6,9-trioxa-13-azahexadecyl)carbamate (**23**).* **21** (567 mg, 0.8 mmol) was dissolved in 50% diethylamine/DCM (10 mL) and stirred at rt for 3 h. Upon reaction completion, the reaction mixture was concentrated in vacuum and coevaporated with toluene (3 × 10 mL). The deprotected intermediate and Fmoc-PEG_3-COOH (443 mg, 1.0 mmol) were dissolved in DCM (10 mL), followed by addition of HCTU (443 mg, 1.0 mmol) and DIPEA (0.5 mL, 2.8 mmol). The reaction mixture was tirred at rt for 18 h. Upon reaction completion, the reaction mixture was concentrated in vacuo, redissolved in EtOAc (20 mL), and washed with 1 M HCl (2 × 10 mL), sat. aq. $NaHCO_3$ (3 × 10 mL), and brine (15 mL). The organic layer was then dried over magnesium sulfate, and the solvent was evaporated under reduced pressure. The crude mixture was purified by flash column chromatography using a gradient of 0−8% MeOH/DCM to obtain (9*H*-fluoren-9-yl)methyl((*S*)-14-((2*S*,4*R*)-4-(*tert*-butoxy)-2-((4-(4-methylthiazol-5-yl)benzyl)carbamoyl)pyrrolidine-1-carbonyl)-15,15-dimethyl-12-oxo-3,6,9-trioxa-13-azahexadecyl)carbamate (624 mg, 0.69 mmol, yield: 86%). ^{1}H NMR (300 MHz, chloroform-*d*) δ 8.59 (s, 1H), 7.67 (dt, J = 7.5, 1.0 Hz, 2H), 7.51 (d, J = 7.5 Hz, 2H),

https://doi.org/10.1021/acs.jmedchem.5c02920
J. Med. Chem. 2025, 68, 26525−26546

7.35−7.17 (m, 9H), 6.79 (d, J = 9.2 Hz, 1H), 5.53 (t, J = 5.9 Hz, 1H), 4.64−4.51 (m, 2H), 4.51−4.37 (m, 2H), 4.37−4.02 (m, 4H), 3.74−3.38 (m, 14H), 3.29 (q, J = 5.3 Hz, 3H), 2.42 (s, 5H), 1.78 (dt, J = 12.4, 8.1 Hz, 1H), 1.11 (s, 9H), 0.83 (s, 9H). ^{13}C NMR (75 MHz, chloroform-d) δ 171.7, 170.9, 156.6, 144.0, 141.3, 138.1, 129.5, 128.2, 127.7, 127.1, 125.1, 120.0, 74.2, 70.5, 70.3, 70.1, 70.0, 67.4, 66.6, 58.7, 56.6, 54.6, 47.3, 43.1, 41.0, 37.0, 35.7, 35.3, 28.3, 26.4, 16.1. LC-MS (ESI) m/z [M + H]$^+$ Calcd for $C_{50}H_{65}N_5O_9S$: 912.4581; found 912.4591.

*(2S,4R)-1-((S)-12-(tert-Butyl)-1-(4-(4-chloro-2-((4-chloro-3-(trifluoromethyl)phenyl)sulfonamido)phenoxy)phenyl)-1,10-dioxo-5,8-dioxa-2,11-diazatridecan-13-oyl)-4-hydroxy-N-(4-(4-methylthiazol-5-yl)benzyl)pyrrolidine-2-carboxamide (**5**).* **22** (20 mg, 25 μmol) was dissolved in 50% diethylamine/ACN (3 mL) and stirred at rt for 3 h. Upon reaction completion, the reaction mixture was concentrated in vacuum. The deprotected intermediate and 4-(4-chloro-2-((4-chloro-3-(trifluoromethyl)phenyl)sulfonamido)-phenoxy)benzoic acid (12 mg, 0.023 mmol) were dissolved in DMF (1 mL), followed by addition of PyBOP (16 mg, 1.2 mmol) and DIPEA (0.5 M), and the reaction mixture was stirred at rt for 18 h. The reaction mixture was concentrated in vacuo and coevaporated with toluene (3 × 5 mL). After treatment with TFA, HPLC purification was followed to yield (2*S*,4*R*)-1-((*S*)-12-(*tert*-butyl)-1-(4-(4-chloro-2-((4-chloro-3-(trifluoromethyl)phenyl)sulfonamido)phenoxy)phenyl)-1,10-dioxo-5,8-dioxa-2,11-diazatridecan-13-oyl)-4-hydroxy-*N*-(4-(4-methylthiazol-5-yl)benzyl)pyrrolidine-2-carboxamide (10.21 mg, 10.8 μmol, yield: 43%). ^{1}H NMR (300 MHz, DMSO-d6) δ 9.07 (s, 1H), 7.99 (d, J = 2.2 Hz, 1H), 7.80 (dd, J = 8.5, 2.1 Hz, 1H), 7.73−7.64 (m, 2H), 7.60 (dd, J = 2.5, 1.5 Hz, 1H), 7.53 (d, J = 8.5 Hz, 1H), 7.48−7.32 (m, 4H), 7.17 (dd, J = 8.7, 2.5 Hz, 1H), 6.79 (dd, J = 8.8, 1.5 Hz, 1H), 6.56 (d, J = 9.1 Hz, 2H), 4.70 (s, 1H), 4.62−4.39 (m, 3H), 4.29 (d, J = 15.7 Hz, 1H), 4.09−3.93 (m, 2H), 3.87−3.48 (m, 10H), 2.47 (s, 3H), 2.28−1.99 (m, 2H), 1.00 (s, 9H). ^{13}C NMR (75 MHz, DMSO-d6) δ 174.2, 172.2, 171.8, 168.9, 160.3, 148.9, 141.0, 140.6, 133.8, 132.9, 130.5, 130.4, 129.0, 128.5, 128.2, 122.1, 118.1, 72.4, 71.2, 71.0, 70.9, 70.8, 60.9, 58.2, 58.2, 43.7, 41.0, 39.0, 37.3, 27.0, 15.2. LC-MS (ESI) m/z [M + H]$^+$ Calcd for $C_{48}H_{51}Cl_2F_3N_6O_{10}S_2$:1063.2516; found 1063.2585.

*(2S,4R)-1-((S)-16-(tert-Butyl)-1-(4-(4-chloro-2-((4-chloro-3-(trifluoromethyl)phenyl)sulfonamido)phenoxy)phenyl)-1,14-dioxo-5,8,11-trioxa-2,15-diazaheptadecan-17-oyl)-4-hydroxy-N-(4-(4-methylthiazol-5-yl)benzyl)pyrrolidine-2-carboxamide (**6**).* **23** (22.8 mg, 25 μmol) was dissolved in 50% diethylamine/ACN (3 mL) and stirred at rt for 3 h. Upon reaction completion, the reaction mixture was concentrated in vacuum. The deprotected intermediate and 4-(4-chloro-2-((4-chloro-3-(trifluoromethyl)phenyl)sulfonamido)-phenoxy)benzoic acid (12 mg, 0.023 mmol) were dissolved in DMF (1 mL), followed by addition of PyBOP (16 mg, 1.2 mmol) and DIPEA (0.5 M), and the reaction mixture was stirred at rt for 18 h. The reaction mixture was concentrated in vacuo and coevaporated with toluene (3 × 5 mL). After treatment with TFA, HPLC purification was followed to yield (2*S*,4*R*)-1-((*S*)-16-(*tert*-butyl)-1-(4-(4-chloro-2-((4-chloro-3-(trifluoromethyl)phenyl)sulfonamido)phenoxy)phenyl)-1,14-dioxo-5,8,11-trioxa-2,15-diazaheptadecan-17-oyl)-4-hydroxy-*N*-(4-(4-methylthiazol-5-yl)benzyl)pyrrolidine-2-carboxamide (8.38 mg, 9.4 μmol, yield: 38%). ^{1}H NMR (300 MHz, methanol-d_4) δ 9.09 (d, J = 8.3 Hz, 1H), 7.97 (d, J = 8.9 Hz, 1H), 7.87−7.32 (m, 9H), 7.16 (t, J = 8.9 Hz, 1H), 6.81 (d, J = 9.4 Hz, 1H), 6.56 (d, J = 8.9 Hz, 2H), 4.68−4.23 (m, 5H), 3.93−3.43 (m, 16H), 2.59−2.39 (m, 5H), 2.26−1.92 (m, 2H), 0.98 (d, J = 8.9 Hz, 9H). ^{13}C NMR (75 MHz, methanol-d_4) δ 174.5, 173.9, 172.1, 168.9, 160.3, 148.9, 141.0, 140.8, 133.8, 132.9, 130.6, 130.4, 130.4, 129.1, 128.5, 128.3, 127.4, 127.3, 122.1, 118.0, 71.6, 71.6, 71.5, 71.4, 71.3, 71.1, 70.6, 68.3, 60.8, 58.9, 58.0, 43.7, 41.0, 38.9, 37.3, 36.8, 27.0, 15.2. LC-MS (ESI) m/z [M + H]$^+$ Calcd for $C_{51}H_{57}Cl_2F_3N_6O_{11}S_2$: 1121.2935; found 1121.2938.

*tert-Butyl (4-((2-(2,6-Dioxopiperidin-3-yl)-1,3-dioxoisoindolin-4-yl)amino)butyl)carbamate (**24**).* In a round-bottom flask, 2-(2,6-dioxopiperidin-3-yl)-4-fluoroisoindoline-1,3-dione (150 mg, 0.54 mmol) and *tert*-butyl (4-aminobutyl)carbamate (113 mg, 0.60 mmol) were dissolved in DMF (7.5 mL). Subsequently, DIPEA (0.19 mL, 1.09 mmol) was added. The mixture was allowed to stir at 90 °C overnight. Upon completion, the reaction mixture was concentrated in vacuo, redissolved in EtOAc (10 mL), and poured into H_2O (50 mL). The product was extracted with EtOAc (4 × 50 mL). The combined organic layers were washed with H_2O (3 × 10 mL) and brine (1 × 50 mL), dried over magnesium sulfate, filtered, and concentrated in vacuo. The crude was purified by silica gel column chromatography (1−3% MeOH/DCM) to yield *tert*-butyl (4-((2-(2,6-dioxopiperidin-3-yl)-1,3-dioxoisoindolin-4-yl)amino)butyl)carbamate as a bright green oil. (46 mg, 0.10 mmol, yield: 19%). ^{1}H NMR (400 MHz, MeOD) δ 7.96 (s, 1H), 7.51 (dd, J = 8.5, 7.2 Hz, 1H), 7.01 (dd, J = 7.8, 4.7 Hz, 2H), 6.62 (t, 1H), 6.42 (t, J = 5.8 Hz, 1H), 5.04 (dd, J = 12.5, 5.4 Hz, 1H), 3.35−3.30 (m, J = 4.2, 3.0 Hz, 2H), 3.12−3.01 (m, J = 12.4, 5.7 Hz, 2H), 2.90−2.61 (m, 3H), 2.16−2.03 (m, 1H), 1.70−1.50 (m, 4H), 1.41 (s, 9H); LC-MS (ESI) m/z [M + Na]$^+$ Calcd for $C_{22}H_{28}N_4O_6$: 467.20; found: 467.10.

*tert-Butyl (6-((2-(2,6-Dioxopiperidin-3-yl)-1,3-dioxoisoindolin-4-yl)amino)hexyl)carbamate (**25**).* In a round-bottom flask, 2-(2,6-dioxopiperidin-3-yl)-4-fluoroisoindoline-1,3-dione (150 mg, 0.54 mmol) and *tert*-butyl (6-aminohexyl)carbamate (130 mg, 0.60 mmol) were dissolved in DMF (7.5 mL). Subsequently, DIPEA (0.14 mL, 0.60 mmol) was added. The mixture was allowed to stir at 90 °C overnight. Upon completion, the reaction mixture concentrated in vacuo, redissolved in EtOAc (10 mL), and poured into H_2O (50 mL). The product was extracted with EtOAc (4 × 50 mL). The combined organic layers were washed with H_2O (3 × 10 mL) and brine (50 mL), dried over magnesium sulfate, filtered, and concentrated in vacuo. The crude was used in the next step without further purification.

*4-((4-Aminobutyl)amino)-2-(2,6-dioxopiperidin-3-yl)isoindoline-1,3-dione (**26**).* In a round-bottom flask, **24** (46 mg, 0.10 mmol) was dissolved in TFA (3 mL). The mixture was allowed to stir at RT for 1 h. Upon completion, the reaction mixture was diluted with DCM (6 mL) and concentrated in vacuo to obtain the 4-((4-aminobutyl)amino)-2-(2,6-dioxopiperidin-3-yl)isoindoline-1,3-dione compound as a TFA salt. The crude product was used in the next step without further purification.

*4-((6-Aminohexyl)amino)-2-(2,6-dioxopiperidin-3-yl)isoindoline-1,3-dione (**27**).* In a round-bottom flask, **25** (139 mg, 0.29 mmol) was dissolved in TFA (10 mL). The mixture was allowed to stir at RT for 1 h. Upon completion, the reaction mixture was diluted with DCM (20 mL) and concentrated in vacuo. The crude was purified by silica gel column chromatography (15−18% MeOH/DCM) to obtain *tert*-butyl (6-((2-(2,6-dioxopiperidin-3-yl)-1,3-dioxoisoindolin-4-yl)amino)-hexyl)carbamate (104 mg, 0.28 mmol, yield: 46% over two steps) as a green oil. ^{1}H NMR (400 MHz, MeOD) δ 7.54 (t, J = 7.8 Hz, 1H), 7.04 (d, J = 2.4 Hz, 1H), 7.02 (s, 1H), 5.05 (dd, J = 12.5, 5.4 Hz, 1H), 3.36−3.32 (m, 2H), 2.92 (t, 2H), 2.89−2.62 (m, 3H), 2.16−2.06 (m, 1H), 1.73−1.63 (m, 4H), 1.45 (dd, J = 15.2, 12.1 Hz, 4H); LC-MS (ESI) m/z [M + H]$^+$ Calcd for $C_{19}H_{24}N_4O_4$: 373.18; found: 373.05.

*4-(4-Chloro-2-((4-chloro-3-(trifluoromethyl)phenyl)-sulfonamido)phenoxy)-N-(4-((2-(2,6-dioxopiperidin-3-yl)-1,3-dioxoisoindolin-4-yl)amino)butyl)benzamide (**7**).* In a round-bottom flask, **26** (34 mg, 0.10 mmol) was in dissolved in DMF (10 mL) followed by addition of HATU (45 mg, 0.15 mmol), DIPEA (0.05 mL, 0.30 mmol), and 4-(4-chloro-2-((4-chloro-3-(trifluoromethyl)-phenyl)sulfonamido)phenoxy)benzoic acid (76 mg, 0.15 mmol) (dissolved in 10 mL DMF). The mixture was allowed to stir at RT for 2 h. Upon completion, the reaction mixture was concentrated in vacuo, redissolved in EtOAc (20 mL), and poured into H_2O (100 mL) and the product was extracted with EtOAc (4 × 20 mL). The combined organic layers were washed with H_2O (5 × 20 mL) and brine (100 mL), dried over magnesium sulfate, filtered, and concentrated in vacuo. The crude was purified by silica gel column chromatography (1−6% MeOH/DCM) to obtain 4-(4-chloro-2-((4-chloro-3-(trifluoromethyl)phenyl)sulfonamido)phenoxy)-*N*-(4-((2-(2,6-dioxopiperidin-3-yl)-1,3-dioxoisoindolin-4-yl)amino)butyl)benzamide (84.7 mg, 0.10 mmol, Yield over 2 steps: 100%) as a green oil. ^{1}H NMR (500 MHz, $CDCl_3$) δ 8.63 (s, 1H), 8.11 (d, J = 2.1 Hz, 1H), 7.85 (dd, J = 8.4, 2.2 Hz, 1H), 7.69 (d, J = 2.5 Hz, 1H), 7.64 (dt, J = 8.7 Hz, 2H), 7.53 (d, J = 8.4 Hz, 1H), 7.48 (dd, J = 8.3, 7.3 Hz, 1H), 7.09 (dd, J = 7.1, 3.6 Hz, 1H), 7.06 (d, J = 7.1 Hz, 1H), 6.89 (d, J = 8.6 Hz, 1H), 6.73 (d, J

https://doi.org/10.1021/acs.jmedchem.5c02920
J. Med. Chem. 2025, 68, 26525−26546

= 8.7 Hz, 1H), 6.62 (dt, *J* = 8.8 Hz, 2H), 6.48 (t, *J* = 5.8 Hz, 1H), 6.25 (t, *J* = 5.6 Hz, 1H), 4.98−4.88 (m, 1H), 3.50 (q, *J* = 5.8 Hz, 2H), 3.33 (q, *J* = 5.6 Hz, 2H), 2.91−2.68 (m, 3H), 2.16−2.09 (m, 1H), 1.80−1.72 (m, *J* = 2.8 Hz, 4H), ^{13}C NMR (101 MHz, $CDCl_3$) δ 171.8, 169.6, 169.1, 167.7, 166.6, 158.3, 146.8, 145.6, 138.3, 137.7, 136.2, 132.4, 132.3, 131.4, 130.1, 130.1, 129.5, 129.1, 128.6, 126.7, 126.5, 123.9, 123.2, 120.5, 120.2, 117.1, 116.8, 111.6, 109.8, 48.8, 42.1, 39.6, 31.3, 29.7, 27.0, 26.5, 22.7; LC-MS (ESI) *m*/*z* $[M + H]^+$ Calcd for $C_{37}H_{30}Cl_2F_3N_5O_8S$: 830.12; found: 830.10.

*4-(4-Chloro-2-((4-chloro-3-(trifluoromethyl)phenyl)-sulfonamido)phenoxy)-N-(6-((2-(2,6-dioxopiperidin-3-yl)-1,3-dioxoisoindolin-4-yl)amino)hexyl)benzamide (**8**).* In a round-bottom flask, **27** (34 mg, 0.09 mmol) was dissolved in DMF (10 mL) followed by the addition of HATU (51 mg, 0.18 mmol), DIPEA (0.05 mL, 0.27 mmol), and 4-(4-chloro-2-((4-chloro-3-(trifluoromethyl)phenyl)-sulfonamido)phenoxy)benzoic acid (51 mg, 0.18 mmol) (dissolved in 10 mL DMF). The mixture was allowed to stir at RT for 2 h. Upon completion, the reaction mixture was concentrated in vacuo, redissolved in EtOAc (20 mL), and poured into H_2O (100 mL) and the product was extracted with EtOAc (4 × 20 mL). The combined organic layers were washed with H_2O (5 × 20 mL) and brine (100 mL), dried over magnesium sulfate, filtered, and concentrated in vacuo. The crude was purified by silica gel column chromatography (0−6% MeOH/DCM) to obtain 4-(4-chloro-2-((4-chloro-3-(trifluoromethyl)phenyl)sulfonamido)phenoxy)-*N*-(6-((2-(2,6-dioxopiperidin-3-yl)-1,3-dioxoisoindolin-4-yl)amino)hexyl)benzamide (39.5 mg, 0.05 mmol, yield: 51%) as a green oil. ^{1}H NMR (500 MHz, $CDCl_3$) δ 8.38 (s, 1H), 8.08 (d, *J* = 2.1 Hz, 1H), 7.82 (dd, *J* = 8.4, 2.2 Hz, 1H), 7.69 (d, *J* = 5.6 Hz, 1H), 7.63 (dt, 2H), 7.55 (s, 1H), 7.53−7.46 (m, 2H), 7.11−7.02 (m, 2H), 6.87 (d, *J* = 8.6 Hz, 1H), 6.71 (d, *J* = 8.0 Hz, 1H), 6.61 (dt, 2H), 6.23 (t, *J* = 4.9 Hz, 2H), 4.95−4.84 (m, 1H), 3.44 (q, *J* = 13.4, 6.5 Hz, 2H), 3.27 (q, *J* = 12.5, 6.7 Hz, 2H), 2.90−2.67 (m, 3H), 2.15−2.08 (m, *J* = 7.8, 6.4, 4.0 Hz, 1H), 1.71 (s, 2H), 1.70−1.59 (m, *J* = 24.5, 14.1, 7.0 Hz, 4H), 1.52−1.40 (m, 4H), ^{13}C NMR (101 MHz, $CDCl_3$) δ 171.3, 169.6, 168.7, 167.6, 166.4, 158.2, 147.0, 145.5, 138.2, 137.7, 136.2, 132.4, 132.4, 131.4, 130.5, 130.1, 129.5, 129.0, 128.5, 126.8, 126.5, 123.8, 123.2, 120.4, 120.2, 117.2, 116.7, 111.5, 109.8, 48.9, 42.5, 40.0, 38.6, 36.5, 31.4, 29.5, 29.0, 26.6, 22.8; LC-MS (ESI) *m*/*z* $[M + H]^+$ Calcd for $C_{39}H_{34}Cl_2F_3N_5O_8S$: 860.15; found: 860.10.

*4-(4-Chloro-2-((4-chloro-3-(trifluoromethyl)phenyl)-sulfonamido)phenoxy)-N-(prop-2-yn-1-yl)benzamide (**28**).* To a mixture of **1** (304 mg, 0.6 mmol), HOBt (101 mg, 0.658 mmol), EDC (126 mg, 0.658 mmol) in anhydrous DMF (15 mL) was added dropwise propargylamine (0.046 mL, 0.718 mmol), and the mixture was stirred at rt for 0.5 h, then DIPEA (0.314 mL, 1.795 mmol) was added at 0 °C, and the mixture was stirred at the same temperature for 0.5 h. The mixture was allowed to warm to rt, and the stirring was continued for additional 18 h. H_2O (36 mL) was added, and the resulting mixture was extracted with EtOAc (3 × 60 mL). The combined organic layers were washed with H_2O (150 mL) and brine (150 mL). The organic layers were combined, dried over magnesium sulfate, and concentrated under vacuum. The organic layer was evaporated under reduced pressure to give 4-(4-chloro-2-((4-chloro-3-(trifluoromethyl)phenyl)sulfonamido)phenoxy)-*N*-(prop-2-yn-1-yl)-benzamide (300 mg, 0.552 mmol, yield: 92%) as a brown oil. ^{1}H NMR (400 MHz, MeOD) δ 8.01 (d, *J* = 2.2 Hz, 1H), 7.80 (dd, *J* = 8.4, 2.2 Hz, 1H), 7.76−7.66 (m, 2H), 7.62 (d, *J* = 2.6 Hz, 1H), 7.52 (d, *J* = 8.4 Hz, 1H), 7.14 (dd, *J* = 8.7, 2.6 Hz, 1H), 6.84 (d, *J* = 8.7 Hz, 1H), 6.64−6.55 (m, 2H), 4.15 (d, *J* = 2.5 Hz, 2H), 2.60 (t, *J* = 2.5 Hz, 1H). LC-MS (ESI) *m*/*z* $[M + H]^+$ Calcd for $C_{23}H_{15}Cl_2F_3N_2O_4S$: 543.00; found: 542.95.

*2-(2-Hydroxyethoxy)ethyl 4-Methylbenzenesulfonate (**29**).* 2,2′-Oxybis(ethan-1-ol) (53.1 g, 500 mmol) was dissolved in DCM (60 mL) under a nitrogen atmosphere. The solution was cooled to 0 °C with an ice bath, and triethylamine (10.45 mL, 75 mmol) was added. Subsequently, 4-methylbenzenesulfonyl chloride (9.53 g, 50 mmol) was added in portions to the cooled reaction mixture. After complete addition, the solution was allowed to warm to room temperature and was stirred for 18 h. The mixture was washed with H_2O (3 × 100 mL), the aqueous fractions were re-extracted with DCM (3 × 300 mL), and the combined organic layers were washed with 5% citric acid (2 × 500 mL), dried over magnesium sulfate, filtered, and concentrated under reduced pressure. The crude product was purified by column chromatography using a gradient of 2.5−10% MeOH in EtOAc to obtain 2-(2-hydroxyethoxy)ethyl 4-methylbenzenesulfonate (9.50 g, 36.5 mmol, yield: 73%) as a clear oil. ^{1}H NMR (400 MHz, $CDCl_3$) δ 7.86−7.79 (m, 2H), 7.37 (d, *J* = 8.1 Hz, 2H), 4.25−4.18 (m, 2H), 3.75−3.66 (m, 4H), 3.59−3.52 (m, 2H), 2.47 (s, 3H). LC-MS (ESI) *m*/*z* $[M + H]^+$ Calcd for $C_{11}H_{16}O_5S$: 261.07; found: 261.00.

*2-(2-(2-Hydroxyethoxy)ethoxy)ethyl 4-Methylbenzenesulfonate (**30**).* 2,2′-(Ethane-1,2-diylbis(oxy))bis(ethan-1-ol) (15.02 g, 100 mmol) was dissolved in DCM (15 mL) under a nitrogen atmosphere. The solution was cooled to 0 °C with an ice bath, and triethylamine (2.091 mL, 15.00 mmol) was added. Subsequently, 4-methylbenzenesulfonyl chloride (1.906 g, 10 mmol) was added in portions to the cooled reaction mixture. After complete addition, the solution was allowed to warm to room temperature and was stirred for 18 h. The mixture was washed with H_2O (3 × 25 mL), the aqueous fractions were re-extracted with DCM, and the combined organic layers were washed with 5% citric acid (3 × 15 mL), dried over magnesium sulfate, filtered, and concentrated under reduced pressure. The crude mixture was purified by flash column chromatography using a gradient of 0−20% acetone in DCM to obtain 2-(2-(2-hydroxyethoxy)ethoxy)ethyl 4-methylbenzenesulfonate (2.53 g, 8.30 mmol, yield: 83%) as a clear oil. ^{1}H NMR (400 MHz, $CDCl_3$) δ 7.82 (d, *J* = 8.4 Hz, 2H), 7.36 (d, *J* = 8.1 Hz, 2H), 4.22−4.15 (t, *J* = 6 Hz 2H), 3.72 (q, *J* = 4.6 Hz, 4H), 3.61 (m, 6H), 2.46 (s, 3H). LC-MS (ESI) *m*/*z* $[M + H]^+$ Calcd for $C_{13}H_{20}O_6S$: 305.10; found: 305.00

*2-(2-(2-(2-Hydroxyethoxy)ethoxy)ethoxy)ethyl 4-Methylbenzenesulfonate (**31**).* 2,2′-((Oxybis(ethane-2,1-diyl))bis(oxy))bis(ethan-1-ol) (97 g, 500 mmol) was dissolved in DCM (60 mL) under a nitrogen atmosphere. The solution was cooled to 0 °C with an ice bath, and triethylamine (10.45 mL, 75 mmol) was added. Subsequently, 4-methylbenzenesulfonyl chloride (9.53 g, 50 mmol) was added in portions to the cooled reaction mixture. After complete addition, the solution was allowed to warm to room temperature and was stirred for 18 h. The mixture was washed with H_2O (3 × 100 mL), the aqueous fractions were re-extracted with DCM (3 × 300 mL), and the combined organic layers were washed with 5% citric acid (2 × 500 mL), dried over magnesium sulfate, filtered, and concentrated under reduced pressure. The crude product was purified by column chromatography using a gradient of 2.5−10% MeOH in EtOAc to obtain 2-(2-(2-(2-hydroxyethoxy)ethoxy)ethoxy)ethyl 4-methylbenzenesulfonate (14.81 g, 42.5 mmol, yield: 85%) as a clear oil. ^{1}H NMR (400 MHz, $CDCl_3$) δ 7.79 (d, *J* = 8.4 Hz, 2H), 7.37−7.29 (d, *J* = 8.1 Hz, 2H), 4.19−4.12 (m, 2H), 3.75−3.56 (m, 14H), 2.44 (s, 3H). LC-MS (ESI) *m*/*z* $[M + H]^+$ Calcd for $C_{15}H_{24}O_7S$: 349.12; found: 349.00.

*1-(2-(2-Hydroxyethoxy)ethyl)triaza-1,2-dien-2-ium (**32**).* Sodium azide (2.013 g, 31.0 mmol) was added to a solution of **29** (3.12 g, 12.00 mmol) in acetonitrile (50 mL), and the mixture was refluxed for 8 h. Upon reaction completion, the solution was allowed to cool down to room temperature and H_2O (50 mL) was added to the solution. The aqueous phase was extracted with DCM (3 × 50 mL), and the combined organic portions were dried over magnesium sulfate, filtered, and concentrated under reduced pressure. The crude was purified by flash chromatography using a gradient of 40−100% EtOAc in PE to yield 1-(2-(2-hydroxyethoxy)ethyl)triaza-1,2-dien-2-ium (1.316 g, 9.96 mmol, yield: 83%) as a clear oil. ^{1}H NMR (400 MHz, $CDCl_3$) δ 3.80−3.74 (m, 2H), 3.71 (dd, *J* = 5.5, 4.4 Hz, 2H), 3.66−3.59 (m, 2H), 3.42 (t, 2H).

*1-(2-(2-(2-Hydroxyethoxy)ethoxy)ethyl)triaza-1,2-dien-2-ium (**33**).* Sodium azide (2.210 g, 34 mmol) was added to a solution of **30** (5.17 g, 17.00 mmol) in acetonitrile (50 mL), and the mixture was refluxed overnight. Upon reaction completion, the solution was allowed to cool down to room temperature and H_2O (50 mL) was added to the solution. The aqueous phase was extracted with DCM (3 × 50 mL), and the combined organic portions were dried over magnesium sulfate, filtered, and concentrated under reduced pressure. The crude was purified by flash chromatography using a gradient of 40−100% EtOAc

https://doi.org/10.1021/acs.jmedchem.5c02920
J. Med. Chem. 2025, 68, 26525−26546

in PE to obtain 1-(2-(2-(2-hydroxyethoxy)ethoxy)ethyl)triaza-1,2-dien-2-ium (2.097 g, 11.90 mmol, yield: 70%) as a clear oil. ^{1}H NMR (400 MHz, $CDCl_3$) δ 3.80−3.67 (m, 8H), 3.67−3.61 (m, 2H), 3.43 (dd, J = 5.5, 4.4 Hz, 2H). LC-MS (ESI) m/z $[M + H]^+$ Calcd for $C_6H_{14}N_3O_3^+$: 176.10; found: 176.85.

*1-(2-(2-(2-(2-Hydroxyethoxy)ethoxy)ethoxy)ethyl)triaza-1,2-dien-2-ium (**34**).* Sodium azide (0.949 g, 14.59 mmol) was added to a solution of **31** (3.18 g, 9.12 mmol) in acetonitrile (20 mL), and the mixture was heated to reflux and stirred for 8 h. Upon reaction completion, the solution was allowed to cool down to room temperature and H_2O (20 mL) was added to the solution. The aqueous phase was extracted with DCM (3 × 20 mL), and the combined organic portions were dried over magnesium sulfate, filtered, and concentrated under reduced pressure. The crude mixture was purified by flash column chromatography using an eluent gradient of 60−100% EtOAc/PE to obtain 1-(2-(2-(2-(2-hydroxyethoxy)ethoxy)-ethoxy)ethyl)triaza-1,2-dien-2-ium (1.667 g, 7.57 mmol, yield: 83%) as a clear oil. ^{1}H NMR (400 MHz, $CDCl_3$) δ 3.79−3.60 (m, 14H), 3.42 (t, J = 5.0 Hz, 2H). LC-MS (ESI) m/z $[M + H]^+$ Calcd for $C_8H_{18}N_3O_4^+$: 221.13; found: 220.05.

*2-(2-Azidoethoxy)acetic Acid (**35**).* A solution of chromium trioxide Jones reagent (1792 mg, 17.92 mmol) in 1.5 M H_2SO_4 in H_2O (31 mL) was added dropwise to a solution of **32** (740 mg, 5.6 mmol) in acetone (55 mL) at 0 °C by an additional funnel. The reaction was allowed to stir at room temperature overnight. Reaction progress was monitored by TLC (DCM:MeOH, 9:1). The reaction was quenched by addition of isopropanol (30 mL). The reaction mixture was then concentrated under vacuum, and the residue was extracted by DCM (50 mL × 4). The organic layers were combined, dried over magnesium sulfate, and concentrated under vacuum. The crude product was purified by silica flash chromatography using a gradient of 1−5% MeOH in DCM to obtain 2-(2-azidoethoxy)acetic acid (332 mg, 2.288 mmol, yield: 41%) as a clear oil. ^{1}H NMR (400 MHz, $CDCl_3$) δ 7.26 (s, 2H), 6.81 (dd, J = 5.5, 4.5 Hz, 2H), 6.53 (t, J = 5.5, 4.4 Hz, 2H). LC-MS (ESI) m/z $[M - H]^-$ Calcd for $C_4H_7N_3O_3^+$: 144.05; found: 144.05.

*2-(2-(2-Azidoethoxy)ethoxy)acetic Acid (**36**).* A solution of chromium trioxide Jones reagent (1792 mg, 17.92 mmol) in 1.5 M H_2SO_4 (31 mL) was added dropwise to a solution of **33** (987 mg, 5.6 mmol) in acetone (55 mL) at 0 °C by an additional funnel. The reaction was allowed to stir at room temperature overnight. Reaction progress was monitored by TLC (DCM:MeOH, 9:1). The reaction was quenched by addition of isopropanol (30 mL). The reaction mixture was then concentrated under vacuum, and the residue was extracted by DCM (4 × 50 mL). The organic layers were combined, dried over magnesium sulfate, and concentrated under vacuum. The crude product was purified by silica flash chromatography using a gradient of 2−5% MeOH in DCM to obtain 2-(2-(2-azidoethoxy)ethoxy)acetic acid (540 mg, 2.85 mmol, yield: 51%) as a clear oil. ^{1}H NMR (400 MHz, $CDCl_3$) δ 4.20 (s, 2H), 3.82−3.74 (m, 2H), 3.78−3.65 (m, 4H), 3.43 (t, J = 5.6, 4.5 Hz, 2H). LC-MS (ESI) m/z $[M - H]^-$ Calcd for $C_6H_{11}N_3O_4^+$: 188.08; found: 188.05.

*2-(2-(2-(2-Azidoethoxy)ethoxy)ethoxy)acetic Acid (**37**).* A solution of chromium trioxide Jones reagent (1.510 g, 15.10 mmol) in 1.5 M H_2SO_4 (31 mL) was added dropwise to a solution of **34** (1.040 g, 4.72 mmol) in acetone (55 mL) at 0 °C by an additional funnel. The reaction was allowed to stir at room temperature overnight. Reaction progress was monitored by TLC (DCM:MeOH, 9:1). The reaction was quenched by addition of isopropanol (30 mL). The reaction mixture was then concentrated under vacuum, and the residue was extracted by DCM (4 × 50 mL). The organic layers were combined, dried over magnesium sulfate, and concentrated under vacuum. The crude product was purified by silica flash chromatography using a gradient of 2.5−10% MeOH in DCM to obtain 2-(2(2-(2-azidoethoxy)ethoxy)-ethoxy)acetic acid (0.760 g, 3.26 mmol, yield: 69%) as a clear oil. ^{1}H NMR (400 MHz, $CDCl_3$) δ 4.21 (s, 2H), 3.83−3.67 (m, 10H), 3.43 (t, J = 5.5, 4.5 Hz, 2H). LC-MS (ESI) m/z $[M - H]^-$ Calcd for $C_8H_{15}N_3O_5^+$: 232.10; found: 231.95.

*2-(2-Azidoethoxy)-N-(2-(2,6-dioxopiperidin-3-yl)-1,3-dioxoisoindolin-4-yl)acetamide (**38**).* **35** (154 mg, 1.06 mmol) was dissolved in thionyl chloride (7 mL, 96 mmol) and heated at 65 °C 1 h. After reaction completion, thionyl chloride was evaporated under reduced pressure. The reaction mixture was then dissolved in dry THF (11 mL). To this solution was added pomalidomide (290 mg, 1.06 mmol). The resulting mixture was refluxed for 18 h. Upon reaction completion, the reaction was diluted with H_2O (10 mL) and extracted with EtOAc (2 × 50 mL). The combined organic layers were washed with H_2O (30 mL) and brine (30 mL). The organic layers were combined, dried over magnesium sulfate, and concentrated under vacuum. The crude mixture was purified by flash column chromatography using an isocratic elution of 2% MeOH in DCM to obtain 2-(2-azidoethoxy)-*N*-(2-(2,6-dioxopiperidin-3-yl)-1,3-dioxoisoindolin-4-yl)acetamide (264 mg, 0.659 mmol, yield: 62%) as an off-white solid. ^{1}H NMR (400 MHz, DLC-MSO) δ 11.16 (s, 1H), 10.35 (s, 1H), 8.71 (d, J = 8.4 Hz, 1H), 7.87 (dd, J = 8.5, 7.3 Hz, 1H), 7.64 (d, J = 7.3 Hz, 1H), 5.17 (dd, J = 13.0, 5.4 Hz, 1H), 4.25 (s, 2H), 3.81 (t, J = 4.9 Hz, 2H), 3.58 (t, J = 4.9 Hz, 2H), 2.97−2.83 (m, 1H), 2.65−2.54 (m, 2H), 2.14−2.01 (m, 1H). LC-MS (ESI) m/z $[M + H]^+$ Calcd for $C_{17}H_{16}N_6O_6^+$: 401.11; found: 401.00.

*1-(2-(2-(2-((2-(2,6-Dioxopiperidin-3-yl)-1,3-dioxoisoindolin-4-yl)-amino)-2-oxoethoxy)ethoxy)ethyl)triaza-1,2-dien-2-ium (**39**).* **36** (228 mg, 1.200 mmol) was dissolved in thionyl chloride (7 mL, 96 mmol) and heated at 65 °C 1 h. After reaction completion, thionyl chloride was evaporated under reduced pressure. The crude mixture was then dissolved in dry THF (10 mL). To this solution was added pomalidomide (219 mg, 0.8 mmol). The resulting mixture was refluxed for 18 h. Upon reaction completion, the reaction was diluted with H_2O (10 mL) and extracted with EtOAc (2 × 50 mL). The combined organic layers were washed with H_2O (30 mL) and brine (30 mL). The organic layers were combined, dried over magnesium sulfate, and concentrated under vacuum. The crude mixture was purified using an isocratic elution of 3% MeOH in DCM to obtain 1-(2-(2-(2-((2-(2,6-dioxopiperidin-3-yl)-1,3-dioxoisoindolin-4-yl)amino)-2-oxoethoxy)-ethoxy)ethyl)triaza-1,2-dien-2-ium (307 mg, 0.689 mmol, yield: 86%) as a slightly yellow solid. ^{1}H NMR (400 MHz, $CDCl_3$) δ 10.47 (s, 1H), 8.88 (dd, J = 8.5, 0.8 Hz, 1H), 8.02 (s, 1H), 7.74 (dd, J = 8.5, 7.3, 0.5 Hz, 1H), 7.59 (dd, J = 7.4, 0.8 Hz, 1H), 5.01−4.92 (m, 1H), 4.22 (s, 2H), 3.88−3.79 (m, 4H), 3.73 (dd, J = 5.6, 4.7 Hz, 2H), 3.43−3.36 (m, 2H), 2.98−2.70 (m, 3H), 2.23−2.13 (m, 1H). LC-MS (ESI) m/z $[M + Na]^+$ Calcd for $C_{19}H_{21}N_6O_7^+$: 467.98; found: 467.00.

*2-(2-(2-(2-Azidoethoxy)ethoxy)ethoxy)-N-(2-(2,6-dioxopiperidin-3-yl)-1,3-dioxoisoindolin-4-yl)acetamide (**40**).* **37** (0.247 g, 1.06 mmol) was dissolved in thionyl chloride (10 mL, 137 mmol) and heated at 65 °C for 1 h. After reaction completion, the mixture was evaporated under reduced pressure and redissolved in dry THF (15 mL). To this solution pomalidomide (0.290 g, 1.060 mmol) was added, and the resulting mixture was refluxed for 8 h. After cooling to room temperature, the reaction mixture was filtered through celite. The reaction mixture was diluted with H_2O (10 mL) and extracted with EtOAc (2 × 50 mL). The combined organic layers were washed with H_2O (30 mL) and brine (30 mL). The organic layers were combined, dried over magnesium sulfate, and concentrated under vacuum. The crude mixture was purified by silica gel column chromatography using a gradient of 5−10% MeOH in DCM to obtain 2-(2-(2-(2-azidoethoxy)-ethoxy)ethoxy)-*N*-(2-(2,6-dioxopiperidin-3-yl)-1,3-dioxoisoindolin-4-yl)acetamide (0.264 g, 0.541 mmol, yield: 51%) as a yellow solid. ^{1}H NMR (400 MHz, MeOD) δ 8.81 (dd, J = 8.5, 0.9 Hz, 1H), 7.82 (dd, J = 8.5, 7.4 Hz, 1H), 7.62 (dd, J = 7.4, 0.8 Hz, 1H), 5.17 (dd, J = 12.6, 5.4 Hz, 1H), 4.25 (s, 2H), 3.85 (m, 4H), 3.73−3.70 (m, 2H), 3.68−3.62 (m, 4H), 3.34 (t, J = 3.3, 1.6 Hz, 2H), 2.97−2.86 (m, 1H), 2.84−2.70 (m, 2H), 2.24−2.16 (m, 1H). LC-MS (ESI) m/z $[M + H]^+$ Calcd for $C_{21}H_{24}N_6O_8^+$: 489.16; found: 489.18.

*4-(4-Chloro-2-((4-chloro-3-(trifluoromethyl)phenyl)-sulfonamido)phenoxy)-N-((1-(2-(2-((2-(2,6-dioxopiperidin-3-yl)-1,3-dioxoisoindolin-4-yl)amino)-2-oxoethoxy)ethyl)-1H-1,2,3-triazol-4-yl)methyl)benzamide (**9**).* **38** (0.032 g, 0.080 mmol), **28** (0.043 g, 0.080 mmol), (+)-sodium L-ascorbate (3.17 mg, 0.016 mmol), and copper(II) sulfate pentahydrate (3.98 mg, 0.016 mmol) were dissolved in THF (0.799 mL) and two drops of H_2O. The reaction mixture was stirred at rt for 20 h. Upon reaction completion, H_2O (10 mL) was added to the mixture and extracted with DCM (3 × 20 mL). The

https://doi.org/10.1021/acs.jmedchem.5c02920
J. Med. Chem. 2025, 68, 26525−26546

combined organic layers were washed with saturated aqueous sodium bicarbonate (60 mL). The organic layers were combined, dried over magnesium sulfate, and concentrated under vacuum. The crude mixture was purified by flash column chromatography using a gradient elution of 1−5% MeOH in DCM to obtain 4-(4-chloro-2-((4-chloro-3-(trifluoromethyl)phenyl)sulfonamido)phenoxy)-*N*-((1-(2-(2-((2-(2,6-dioxopiperidin-3-yl)-1,3-dioxoisoindolin-4-yl)amino)-2-oxoethoxy)ethoxy)ethyl)-1*H*-1,2,3-triazol-4-yl)methyl) benzamide (37 mg, 0.039 mmol, yield: 49%) as an off-white solid. ^{1}H NMR (400 MHz, MeOD) δ 8.72 (d, J = 8.4 Hz, 1H), 8.22 (s, 1H), 7.96 (d, J = 2.2 Hz, 1H), 7.81−7.71 (m, 2H), 7.63 (d, J = 2.6 Hz, 1H), 7.60−7.52 (m, 3H), 7.48 (d, J = 8.3 Hz, 1H), 7.22 (dd, J = 8.8, 2.6 Hz, 1H), 6.86 (d, J = 8.8 Hz, 1H), 6.45 (d, J = 8.5 Hz, 2H), 5.23 (dd, J = 12.7, 5.4 Hz, 1H), 4.76 (t, J = 4.8 Hz, 2H), 4.67−4.53 (m, 2H), 4.15 (s, 2H), 4.05 (t, J = 4.9 Hz, 2H), 2.97−2.83 (m, 1H), 2.81−2.66 (m, 2H), 2.23−2.13 (m, 1H). LC-MS (ESI) m/z [M + H]$^+$ Calcd for $C_{40}H_{31}Cl_2F_3N_8O_{10}S$: 943.12; found: 943.10.

*4-(4-Chloro-2-((4-chloro-3-(trifluoromethyl)phenyl)-sulfonamido)phenoxy)-N-((1-(2-(2-(2-((2-(2,6-dioxopiperidin-3-yl)-1,3-dioxoisoindolin-4-yl)amino)-2-oxoethoxy)ethoxy)ethyl)-1H-1,2,3-triazol-4-yl)methyl)benzamide (**10**).* **39** (39.0 mg, 0.088 mmol), **28** (52.3 mg, 0.096 mmol), (+)-sodium L-ascorbate (52.0 mg, 0.263 mmol), and copper(II) sulfate pentahydrate (21.80 mg, 0.088 mmol) were dissolved in H_2O (0.600 mL), *tert*-butanol (3 mL), and DCM (2.2 mL) at rt for 1 h. Upon reaction completion, H_2O (10 mL) was added to the mixture and extracted with DCM (3 × 20 mL). The combined organic layers were washed with saturated aqueous sodium bicarbonate (60 mL). The organic layers were combined, dried over magnesium sulfate, and concentrated under vacuum. The crude mixture was purified by flash column chromatography using a gradient elution of 1−10% MeOH in DCM to obtain 4-(4-chloro-2-((4-chloro-3-(trifluoromethyl)phenyl)sulfonamido)phenoxy)-*N*-((1-(2-(2-(2-((2-(2,6-dioxopiperidin-3-yl)-1,3-dioxoisoindolin-4-yl)amino)-2-oxoethoxy)ethoxy)ethyl)-1*H*-1,2,3-triazol-4-yl)methyl)benzamide (40 mg, 0.040 mmol, yield: 46% yield) as an off-white solid. ^{1}H NMR (400 MHz, $CDCl_3$) δ 10.33 (s, 1H), 9.74 (s, 1H), 8.79 (d, J = 8.4 Hz, 1H), 8.43 (s, 1H), 8.13 (d, J = 2.1 Hz, 1H), 7.84 (d, J = 7.9 Hz, 1H), 7.73−7.66 (m, 2H), 7.64 (d, J = 2.5 Hz, 2H), 7.52 (dd, J = 13.9, 7.8 Hz, 2H), 7.06 (dd, J = 8.8, 2.5 Hz, 1H), 6.70 (d, J = 8.7 Hz, 1H), 6.47 (d, J = 7.4 Hz, 2H), 4.99 (d, J = 14.2 Hz, 1H), 4.53 (d, J = 40.7 Hz, 4H), 4.11−3.96 (m, 2H), 3.92 (s, 2H), 3.70 (s, 4H), 2.93−2.65 (m, 3H), 2.15 (s, 1H). LC-MS (ESI) m/z [M + H]$^+$ Calcd for $C_{42}H_{35}Cl_2F_3N_8O_{11}S$: 987.15; found: 987.10.

*4-(4-Chloro-2-((4-chloro-3-(trifluoromethyl)phenyl)-sulfonamido)phenoxy)-N-((1-(2-(2-(2-(2-((2-(2,6-dioxopiperidin-3-yl)-1,3-dioxoisoindolin-4-yl)amino)-2-oxoethoxy)ethoxy)ethoxy)-ethyl)-1H-1,2,3-triazol-4-yl)methyl)benzamide (**11**).* **40** (40.0 mg, 0.082 mmol), **28** (66.7 mg, 0.123 mmol), (+)-sodium L-ascorbate (97 mg, 0.491 mmol), and copper(II) sulfate pentahydrate (61.2 mg, 0.246 mmol) were dissolved in H_2O (1,6 mL) and *tert*-butanol (6.4 mL) and stirred at rt for 20 h. Upon reaction completion, H_2O (10 mL) was added to the mixture and extracted with DCM (3 × 20 mL). The combined organic layers were washed with saturated aqueous sodium bicarbonate (60 mL). The organic layers were combined, dried over magnesium sulfate, and concentrated under vacuum. The crude mixture was purified by flash column chromatography using a gradient elution of 1−5% MeOH in DCM to obtain 4-(4-chloro-2-((4-chloro-3-(trifluoromethyl)phenyl)sulfonamido)phenoxy)-*N*-((1-(2-(2-(2-(2-((2-(2,6-dioxopiperidin-3-yl)-1,3-dioxoisoindolin-4-yl)amino)-2-oxoethoxy)ethoxy)ethoxy)ethyl)-1*H*-1,2,3-triazol-4-yl)methyl)-benzamide (45 mg, 0.044 mmol, yield: 53%) as a slightly green solid. ^{1}H NMR (400 MHz, $CDCl_3$) δ 10.33 (s, 1H), 9.79 (s, 1H), 8.79 (d, J = 8.4 Hz, 1H), 8.35 (s, 1H), 8.14 (d, J = 2.1 Hz, 1H), 7.85 (dd, J = 8.3, 2.2 Hz, 1H), 7.76−7.61 (m, 4H), 7.53 (dd, J = 14.7, 7.8 Hz, 2H), 7.03 (dd, J = 8.8, 2.5 Hz, 1H), 6.66 (d, J = 8.7 Hz, 1H), 6.48 (d, J = 7.7 Hz, 2H), 4.97 (dd, J = 12.2, 5.5 Hz, 1H), 4.64 (s, 2H), 4.48 (s, 2H), 4.22−3.97 (m, 2H), 3.85 (s, 2H), 3.71−3.52 (m, 8H), 2.80 (ddt, 3H), 2.15 (d, J = 4.9 Hz, 1H). LC-MS (ESI) m/z [M + H]$^+$ Calcd for $C_{44}H_{39}Cl_2F_3N_8O_{12}S$: 1031.17; found: 1031.15.

*tert-Butyl (2-(2-(2-Aminoethoxy)ethoxy)ethyl)carbamate (**41**).* To a solution of 2,2′-(ethane-1,2-diylbis(oxy))bis(ethan-1-amine) (8.76 mL, 60 mmol) in DCM (70 mL), Boc-anhydride (2.090 mL, 9.00 mmol) in DCM (70 mL) was added dropwise at 0 °C using a syringe pump over 2 h. The reaction was stirred at 0 °C for 4 h and then 18 h at rt. The organic phase was then washed with H_2O (5 × 60 mL). The organic layers were dried over magnesium sulfate and concentrated under vacuum to afford *tert*-butyl (2-(2-(2-aminoethoxy)ethoxy)-ethyl)carbamate (1.1 g, 4.43 mmol, yield: 49%) as a slightly yellow oil. ^{1}H NMR (400 MHz, $CDCl_3$) δ 5.15 (s, 2H), 3.62 (d, J = 1.5 Hz, 4H), 3.53 (dtd, J = 10.3, 5.6, 1.5 Hz, 4H), 3.32 (q, J = 5.5 Hz, 2H), 2.92−2.85 (m, 2H), 1.44 (d, J = 1.6 Hz, 11H). LC-MS (ESI) m/z [M + H]$^+$ Calcd for $C_{11}H_{24}N_2O_4$: 249.17; found: 249.05.

*tert-Butyl (2-(2-(2-(2-Aminoethoxy)ethoxy)ethoxy)ethyl)-carbamate (**42**).* To a solution of 2,2′-((oxybis(ethane-2,1-diyl))bis-(oxy))bis(ethan-1-amine) (0.584 mL, 3.12 mmol) in DCM (20 mL), Boc-anhydride (0.109 mL, 0.468 mmol) in DCM (20 mL) was added dropwise at 0 °C using a syringe pump over 2 h. The reaction was stirred at 0 °C for 4 h and then 18 h at rt. The organic phase was then washed with H_2O (5 × 20 mL). The organic layers were dried over magnesium sulfate and concentrated under vacuum to afford *tert*-butyl (2-(2-(2-(2-aminoethoxy)ethoxy)ethoxy)ethyl)carbamate (87 mg, 0.298 mmol, yield: 64%) as a clear oil without purification. ^{1}H NMR (400 MHz, $CDCl_3$) δ 5.42 (s, 1H), 3.70−3.59 (m, 8H), 3.54 (q, J = 5.4 Hz, 4H), 3.31 (q, J = 5.4 Hz, 2H), 2.91 (s, 1H), 1.77 (s, 2H), 1.44 (s, 9H). LC-MS (ESI) m/z [M + H]$^+$ Calcd for $C_{13}H_{28}N_2O_5$: 293.20; found: 293.10.

*tert-Butyl (2-(2-(2-(4-(4-Chloro-2-((4-chloro-3-(trifluoromethyl)-phenyl)sulfonamido)phenoxy)benzamido)ethoxy)ethoxy)ethyl)-carbamate (**43**).* To a solution of **1** (245 mg, 0.483 mmol) in DMF (2 mL) was added dropwise **41** (100 mg, 0.403 mmol) (diluted in 0.25 mL DMF) followed by addition of 1-((dimethylamino)(dimethyliminio)-methyl)-1*H*-[1,2,3]triazolo[4,5-*b*]pyridine 3-oxide (142 mg, 0.604 mmol) and *N*-ethyl-*N*-isopropylpropan-2-amine (0.246 mL, 1.409 mmol). The reaction was left to stir at rt for 4 h. Upon reaction completion, the mixture was diluted with H_2O (10 mL) and extracted with EtOAc (3 × 10 mL). The organic layer was dried over magnesium sulfate and then concentrated under reduced pressure. The residue was purified by silica column chromatography using a gradient eluent system of 60−100% EtOAc in petroleum ether to yield *tert*-butyl(2-(2-(2-(4-(5-chloro-2-((4-chloro-3-(trifluoromethyl)phenyl)-sulfonamido)phenoxy)benzamido)ethoxy)ethoxy)ethyl)carbamate (100 mg, 0.136 mmol, yield: 34%). ^{1}H NMR (400 MHz, MeOD) δ 8.02 (d, J = 2.2 Hz, 1H), 7.81 (dd, 1H), 7.72 (d, 2H), 7.64 (d, J = 2.6 Hz, 1H), 7.56 (d, J = 8.4 Hz, 1H), 7.20 (dd, J = 8.8, 2.6 Hz, 1H), 6.85 (d, J = 8.8 Hz, 1H), 6.60 (d, 2H), 3.68−3.61 (m, 6H), 3.58 (t, 2H), 3.51 (t, 2H), 3.23−3.18 (m, 2H), 1.42 (s, 9H). LC-MS (ESI) m/z [M + H]$^+$ Calcd for $C_{31}H_{34}Cl_2F_3N_3O_8S$: 735.14; found: 736.05.

*tert-Butyl (1-(4-(4-Chloro-2-((4-chloro-3-(trifluoromethyl)-phenyl)sulfonamido)phenoxy)phenyl)-1-oxo-5,8,11-trioxa-2-aza-tridecan-13-yl)carbamate (**44**).* To a solution of **1** (208 mg, 0.410 mmol) in DMF (2 mL) was added dropwise **42** (100 mg, 0.342 mmol) (diluted in 0.25 mL DMF) followed by addition of 1-((dimethylamino)(dimethyliminio)methyl)-1*H*-[1,2,3]triazolo[4,5-*b*]pyridine 3-oxide (121 mg, 0.513 mmol) and *N*-ethyl-*N*-isopropyl-propan-2-amine (0.209 mL, 1.197 mmol). The reaction was left to stir at rt for 4 h. Upon reaction completion, the mixture was diluted with H_2O (10 mL) and extracted with EtOAc (3 × 10 mL). The organic layer was dried over magnesium sulfate and then concentrated under reduced pressure. The residue was purified by silica column chromatography using a gradient eluent system of 60−100% EtOAc in petroleum ether to yield *tert*-butyl (1-(4-(5-chloro-2-((4-chloro-3-(trifluoromethyl)phenyl)sulfonamido)phenoxy)phenyl)-1-oxo-5,8,11-trioxa-2-azatridecan-13-yl)carbamate (200 mg, 0.256 mmol, yield: 75%). ^{1}H NMR (400 MHz, MeOD) δ 8.02 (d, J = 2.2 Hz, 1H), 7.83 (dd, J = 8.5, 2.3 Hz, 1H), 7.72 (d, J = 8.8 Hz, 2H), 7.64 (d, J = 2.6 Hz, 1H), 7.56 (d, J = 8.4 Hz, 1H), 7.21 (dd, J = 8.8, 2.6 Hz, 1H), 6.85 (d, J = 8.8 Hz, 1H), 6.59 (d, J = 8.9 Hz, 2H), 3.69−3.54 (m, 12H), 3.51−3.44 (m, 2H), 3.22−3.16 (m, 2H), 1.42 (s, 9H). LC-MS (ESI) m/z [M + H]$^+$ Calcd for $C_{33}H_{38}Cl_2F_3N_3O_9S$: 780.63; found: 780.15.

https://doi.org/10.1021/acs.jmedchem.5c02920
J. Med. Chem. 2025, 68, 26525−26546

*N-(2-(2-(2-Aminoethoxy)ethoxy)ethyl)-4-(4-chloro-2-((4-chloro-3-(trifluoromethyl)phenyl)sulfonamido)phenoxy)benzamide (**45**).* To **43** (100 mg, 0.136 mmol) dissolved in DCM (3 mL) was added TFA (1.25 mL, 0.136 mmol), and the reaction was stirred at rt for 30 min. Upon reaction completion, the solvents were evaporated under reduced pressure to yield *N*-(2-(2-(2-aminoethoxy)ethoxy)ethyl)-4-(4-chloro-2-((4-chloro-3-(trifluoromethyl)phenyl)sulfonamido)-phenoxy) benzamide N-(2-(2-(2-aminoethoxy)ethoxy)ethyl)-4-(5-chloro-2-((4-chloro-3-(trifluoromethyl)phenyl)sulfonamido)-phenoxy)benzamide (85 mg, 0.134 mmol, yield: 98%). ^{1}H NMR (400 MHz, MeOD) δ 8.03 (d, J = 2.2 Hz, 1H), 7.84 (dd, J = 8.4, 2.3 Hz, 1H), 7.72 (d, J = 8.9 Hz, 2H), 7.65 (d, J = 2.6 Hz, 1H), 7.57 (d, J = 8.4 Hz, 1H), 7.23 (dd, J = 8.8, 2.6 Hz, 1H), 6.85 (d, J = 8.8 Hz, 1H), 6.60 (d, J = 8.9 Hz, 2H), 3.72−3.65 (m, 8H), 3.58 (t, J = 5.6 Hz, 2H), 3.11 (t, J = 5.0 Hz, 2H). LC-MS (ESI) m/z $[M + H]^+$ Calcd for $C_{26}H_{26}Cl_2F_3N_3O_6S$: 636.09; found: 636.10.

*N-(2-(2-(2-(2-Aminoethoxy)ethoxy)ethoxy)ethyl)-4-(4-chloro-2-((4-chloro-3-(trifluoromethyl)phenyl)sulfonamido)phenoxy)-benzamide (**46**).* To **44** (200 mg, 0.256 mmol) dissolved in DCM (6 mL) was added TFA (0.020 mL, 0.256 mmol), and the reaction was left to stir at rt for 30 min. Upon reaction completion, the solvents were evaporated under reduced pressure to yield *N*-(2-(2-(2-(2-aminoethoxy)ethoxy)ethoxy)ethyl)-4-(5-chloro-2-((4-chloro-3-(trifluoromethyl)phenyl)sulfonamido)phenoxy)benzamide (170 mg, 0.250 mmol, yield: 98%). ^{1}H NMR (400 MHz, MeOD) δ 8.02 (d, 1H), 7.84 (dd, J = 8.4, 2.3 Hz, 1H), 7.72 (dd, J = 8.9 Hz, 2H), 7.65 (d, J = 2.6 Hz, 1H), 7.57 (d, J = 8.4 Hz, 1H), 7.23 (dd, J = 8.8, 2.6 Hz, 1H), 6.86 (d, J = 8.8 Hz, 1H), 6.60 (d, J = 8.9 Hz, 2H), 3.75−3.61 (m, 12H), 3.60−3.56 (m, 2H), 3.14−3.10 (m, 2H). LC-MS (ESI) m/z $[M + H]^+$ Calcd for $C_{28}H_{30}Cl_2F_3N_3O_7S$: 680.11; found: 680.10.

*4-(4-Chloro-2-((4-chloro-3-(trifluoromethyl)phenyl)-sulfonamido)phenoxy)-N-(2-(2-(2-((2-(2,6-dioxopiperidin-3-yl)-1,3-dioxoisoindolin-4-yl)amino)ethoxy)ethoxy)ethyl)benzamide (**12**).* To a solution of **45** (40 mg, 0.063 mmol) and 2-(2,6-dioxopiperidin-3-yl)-4-fluoroisoindoline-1,3-dione (14.47 mg, 0.052 mmol) in DMSO (2 mL) was added *N*-ethyl-*N*-isopropylpropan-2-amine (20.31 mg, 0.157 mmol). The reaction was stirred at 120 °C overnight. Upon reaction completion, the mixture was diluted with H_2O (10 mL) and extracted with EtOAc (3 × 10 mL). The organic layers were then combined, washed with H_2O (2 × 10 mL) and brine (1 × 10 mL), dried over magnesium sulfate, and then concentrated under reduced pressure. The crude was purified by reverse-phase flash column chromatography using a gradient elution of 10−90% MeCN/H_2O to yield (5-chloro-2-((4-chloro-3-(trifluoromethyl)phenyl)sulfonamido)-phenoxy)-*N*-(2-(2-(2-((2-(2,6-dioxopiperidin-3-yl)-1,3-dioxoisoindolin-4-yl)amino)ethoxy)ethoxy)ethyl)benzamide (3 mg, 3.36 μmol, yield: 6%). ^{1}H NMR (400 MHz, MeOD) δ 8.00 (d, J = 2.2 Hz, 1H), 7.81 (dd, J = 8.3, 2.2, 0.5 Hz, 1H), 7.69−7.65 (m, 1H), 7.63 (d, J = 2.5 Hz, 1H), 7.55−7.50 (m, 1H), 7.20 (dd, J = 8.8, 2.6 Hz, 1H), 7.07−7.01 (m, 2H), 6.81 (d, J = 8.8 Hz, 1H), 6.52 (d, J = 9.0 Hz, 2H), 5.05−4.99 (m, 1H), 3.74 (t, J = 5.7, 4.8 Hz, 2H), 3.71−3.63 (m, 6H), 3.57 (t, J = 5.4 Hz, 2H), 3.47 (dd, J = 5.7, 4.9 Hz, 2H), 2.88−2.78 (m, 1H), 2.75−2.61 (m, 2H), 2.10−2.03 (m, 1H). LC-MS (ESI) m/z $[M + H]^+$ Calcd for $C_{39}H_{34}Cl_2F_3N_5O_{10}S$: 892.13; found: 892.00.

*4-(5-Chloro-2-((4-chloro-3-(trifluoromethyl)phenyl)-sulfonamido)phenoxy)-N-(2-(2-(2-(2-((2-(2,6-dioxopiperidin-3-yl)-1,3-dioxoisoindolin-4-yl)amino)ethoxy)ethoxy)ethyl)-benzamide (**13**).* To a solution of **46** (170 mg, 0.250 mmol) and 2-(2,6-dioxopiperidin-3-yl)-4-fluoroisoindoline-1,3-dione (57.5 mg, 0.208 mmol) in DMSO (5 mL) was added *N*-ethyl-*N*-isopropylpropan-2-amine (0.109 mL, 0.625 mmol). The reaction was stirred at 90 °C for 3 h. Upon reaction completion, the mixture was diluted with H_2O (10 mL), extracted with EtOAc (3 × 10 mL), and then washed with H_2O (2 × 10 mL) and brine (1 × 10 mL). The organic layer was dried with magnesium sulfate and concentrated under reduced pressure. The crude mixture was purified by reverse-phase flash column chromatography using a gradient elution of 10−90% MeCN/H_2O to yield 4-(5-chloro-2-((4-chloro-3-(trifluoromethyl)phenyl)sulfonamido)-phenoxy)-*N*-(2-(2-(2-(2-((2-(2,6-dioxopiperidin-3-yl)-1,3-dioxoisoindolin-4-yl)amino)ethoxy)ethoxy)ethoxy)ethyl)benzamide (3 mg, 3.20 μmol, yield: 2%). ^{1}H NMR (600 MHz, MeOD) δ 8.01 (d, J = 2.2 Hz, 1H), 7.82 (dd, J = 8.4, 2.2 Hz, 1H), 7.70 (d, J = 8.8 Hz, 2H), 7.63 (d, J = 2.6 Hz, 1H), 7.57−7.51 (m, 2H), 7.19 (dd, J = 8.8, 2.6 Hz, 1H), 7.07−7.02 (m, 2H), 6.82 (d, J = 8.7 Hz, 1H), 6.57 (d, J = 8.8 Hz, 2H), 5.05−5.02 (m, 1H), 3.69 (t, J = 5.3 Hz, 2H), 3.68−3.65 (m, 4H), 3.65−3.62 (m, 6H), 3.55 (t, J = 5.5 Hz, 2H), 3.47 (t, J = 5.3 Hz, 2H), 2.88−2.82 (m, 1H), 2.76−2.66 (m, 2H), 2.12−2.07 (m, 1H). LC-MS (ESI) m/z $[M + H]^+$ Calcd for $C_{41}H_{38}Cl_2F_3N_5O_{11}S$: 936.16; found: 936.10.

*4-(4-Chloro-2-nitrophenoxy)phenol (**47**).* In a 500 mL flask hydroquinone (6.27 g, 57.0 mmol), 4-chloro-1-fluoro-2-nitrobenzene (1.342 mL, 11.39 mmol) and potassium carbonate (3.15 g, 22.79 mmol) were dissolved in DMF (150 mL) and stirred at 110 °C for 2 h. Upon reaction completion, the reaction mixture was diluted in H_2O (100 mL) and washed with diethyl ether (3 × 250 mL) and brine (500 mL). The organic layer was dried over magnesium sulfate and then concentrated under reduced pressure. The crude mixture was purified by flash column chromatography using a gradient elution of 20−50% EtOAc/petroleum ether to obtain 4-(4-chloro-2-nitrophenoxy)phenol (2.597 g, 9.78 mmol, yield: 86%) as a yellow solid. ^{1}H NMR (400 MHz, $CDCl_3$) δ 7.92 (d, J = 2.6 Hz, 1H), 7.41 (dd, J = 9.0, 2.6 Hz, 1H), 7.01−6.92 (m, 2H), 6.91−6.82 (m, 3H), 4.89 (s, 1H). LC-MS (ESI) m/z $[M - H]^-$ Calcd for $C_{12}H_8ClNO$: 264.01; found: 263.90.

*2-(2-(2-(4-(4-Chloro-2-nitrophenoxy)phenoxy)ethoxy)ethoxy)-ethan-1-ol (**48**).* In a 50 mL flask, **47** (768 mg, 2.89 mmol), potassium iodide (43.6 mg, 0.263 mmol), and potassium carbonate (1090 mg, 7.89 mmol) were dissolved in DMF (20 mL). The reaction mixture was heated for 1 h at 60 °C followed by dropwise addition of **30** (800 mg, 2.63 mmol) (dissolved in 5 mL DMF). The reaction mixture was stirred at 60 °C for 24 h. Upon reaction completion, H_2O (200 mL) was added, the mixture was extracted with diethyl ether (3 × 100 mL), and the combined organic layers were washed with brine (2 × 300 mL). The organic layer was then dried over magnesium sulfate, and the solvent was evaporated under reduced pressure. The crude mixture was purified by flash column chromatography using a gradient elution of 20−100% EtOAc/petroleum ether to obtain 2-(2-(2-(4-(4-chloro-2-nitrophenoxy)phenoxy)ethoxy)ethoxy)ethan-1-ol (776 mg, 1.951 mmol, yield: 74%) as a yellow oil. ^{1}H NMR (400 MHz, $CDCl_3$) δ 7.92 (d, J = 2.6 Hz, 1H), 7.41 (dd, J = 9.0, 2.6 Hz, 1H), 7.07−6.90 (m, 4H), 6.87 (d, J = 9.0 Hz, 1H), 4.17−4.10 (m, 2H), 3.91−3.85 (m, 2H), 3.79−3.68 (m, 7H), 3.68−3.60 (m, 2H), 2.38 (d, J = 6.8 Hz, 1H). LC-MS (ESI) m/z $[M + H]^+$ Calcd for $C_{18}H_{20}ClNO_7$: 398.09; found: 398.00.

*2-(2-(2-(2-(4-(4-Chloro-2-nitrophenoxy)phenoxy)ethoxy)ethoxy)-ethoxy)ethan-1-ol (**49**).* In a 50 mL flask, **47** (755 mg, 2.84 mmol), potassium iodide (42.9 mg, 0.258 mmol), and potassium carbonate (1071 mg, 7.75 mmol) were dissolved in DMF (20 mL). The reaction mixture was heated for 1 h at 60 °C followed by dropwise addition of **31** (900 mg, 2.58 mmol) (dissolved in 5 mL DMF). The reaction mixture was stirred at 60 °C for 24 h. Upon reaction completion, H_2O (200 mL) was added, the mixture was extracted with diethyl ether (5 × 100 mL), and the combined organic layers were washed with brine (1 × 500 mL). The organic layer was then dried over magnesium sulfate, and the solvent was evaporated under reduced pressure. The crude mixture was purified by flash column chromatography using a gradient elution of 1−10% MeOH/DCM ether to obtain 2-(2-(2-(2-(4-(4-chloro-2-nitrophenoxy)phenoxy)ethoxy)ethoxy)ethoxy)ethan-1-ol (500 mg, 1.132 mmol, yield: 44%) as a yellow oil. ^{1}H NMR (400 MHz, $CDCl_3$) δ 7.92 (d, J = 2.6 Hz, 1H), 7.41 (dd, J = 9.0, 2.6 Hz, 1H), 7.04−6.90 (m, 4H), 6.86 (d, J = 9.0 Hz, 1H), 4.19−4.10 (m, 2H), 3.89−3.82 (m, 2H), 3.78−3.66 (m, 11H), 3.65−3.58 (m, 3H). LC-MS (ESI) m/z $[M + H]^+$ Calcd for $C_{20}H_{24}ClNO_8$: 442.12; found: 442.05.

*2-(2-(2-(4-(4-Chloro-2-nitrophenoxy)phenoxy)ethoxy)ethoxy)-ethyl 4-Methylbenzenesulfonate (**50**).* In a 50 mL flask, **48** (415 mg, 1.043 mmol), triethylamine (0.291 mL, 2.086 mmol), and DMAP (12.75 mg, 0.104 mmol) were dissolved in DCM (10 mL). Tosyl-Cl (298 mg, 1.565 mmol) was then added to the reaction mixture, and the reaction was stirred at rt for 2 h. Upon reaction completion, the mixture was diluted with H_2O (60 mL) and washed with DCM (3 × 100 mL). The combined organic layers were washed with 5% citric acid (1 × 150 mL), dried over magnesium sulfate, and then concentrated under reduced pressure. The crude mixture was purified by flash column

https://doi.org/10.1021/acs.jmedchem.5c02920
J. Med. Chem. 2025, 68, 26525−26546

chromatography using a gradient elution of 40−100% EtOAc in petroleum ether to obtain 2-(2-(2-(4-(4-chloro-2-nitrophenoxy)-phenoxy)ethoxy)ethoxy)ethyl 4-methylbenzenesulfonate (495 mg, 0.897 mmol, yield: 86%) as a yellow oil. ^{1}H NMR (400 MHz, $CDCl_3$) δ 7.92 (d, J = 2.6 Hz, 1H), 7.80 (d, J = 8.4 Hz, 2H), 7.40 (dd, J = 9.0, 2.6 Hz, 1H), 7.36−7.32 (m, 2H), 7.00 (d, J = 9.2 Hz, 2H), 6.93 (d, J = 9.2 Hz, 2H), 6.87 (d, J = 9.0 Hz, 1H), 4.20−4.14 (m, 2H), 4.14−4.09 (m, 2H), 3.87−3.82 (m, 2H), 3.74−3.66 (m, 4H), 3.65−3.61 (m, 2H), 2.44 (s, 3H). LC-MS (ESI) m/z $[M + H]^+$ Calcd for $C_{25}H_{26}ClNO_9S$: 552.10; found: 552.00.

*2-(2-(2-(2-(4-(4-Chloro-2-nitrophenoxy)phenoxy)ethoxy)ethoxy)-ethoxy)ethyl 4-Methylbenzenesulfonate (**51**).* In a 50 mL flask, **49** (308 mg, 0.697 mmol), triethylamine (0.194 mL, 1.394 mmol), and DMAP (8.52 mg, 0.070 mmol) were dissolved in DCM (6.5 mL). Tosyl-Cl (199 mg, 1.046 mmol) was then added to the reaction mixture, and the reaction was stirred at rt for 2 h. Upon reaction completion, the mixture was diluted with H_2O (30 mL) and washed with DCM (3 × 50 mL). The combined organic layers were washed with 5% citric acid (1 × 70 mL), dried over magnesium sulfate, and then concentrated under reduced pressure. The crude mixture was purified by flash column chromatography using a gradient elution of 60−100% EtOAc in petroleum ether to obtain 2-(2-(2-(2-(4-(4-chloro-2-nitrophenoxy)phenoxy)ethoxy)ethoxy)ethoxy)ethyl 4-methylbenzenesulfonate (228 mg, 0.383 mmol, yield: 55%) as a yellow oil. ^{1}H NMR (400 MHz, $CDCl_3$) δ 7.92 (d, J = 2.6 Hz, 1H), 7.79 (d, J = 8.4 Hz, 2H), 7.40 (dd, J = 9.0, 2.6 Hz, 1H), 7.38−7.31 (m, 2H), 7.02−6.97 (m, 2H), 6.96−6.92 (m, 2H), 6.86 (d, J = 8.9 Hz, 1H), 4.21−4.09 (m, 4H), 3.92−3.83 (m, 2H), 3.76−3.63 (m, 6H), 3.60 (d, J = 1.1 Hz, 4H), 2.44 (s, 3H). LC-MS (ESI) m/z $[M + H]^+$ Calcd for $C_{27}H_{30}ClNO_{10}S$: 596.13; found: 596.05.

*4-(2-(2-(2-(4-(4-Chloro-2-nitrophenoxy)phenoxy)ethoxy)ethoxy)-ethoxy)-2-(2,6-dioxopiperidin-3-yl)isoindoline-1,3-dione (**52**).* In a 10 mL flask, 2-(2,6-dioxopiperidin-3-yl)-4-hydroxyisoindoline-1,3-dione (49.7 mg, 0.181 mmol) and potassium carbonate (37.6 mg, 0.272 mmol) were dissolved in DMF (1 mL). The reaction mixture was heated for 30 min at 40 °C followed by dropwise addition of **50** (100 mg, 0.181 mmol) (dissolved in 0.8 mL DMF). The reaction mixture was stirred at 60 °C for 18 h. Upon reaction completion, H_2O (20 mL) was added and the mixture was extracted with diethyl ether (3 × 15 mL). The combined organic layers were washed with brine (1 × 30 mL). The organic layer was then dried over magnesium sulfate, and the solvent was evaporated under reduced pressure. The crude mixture was purified by reverse-phase flash column chromatography using a gradient elution of 10−100% MeCN/H_2O to obtain 4-(2-(2-(2-(4-(4-chloro-2-nitrophenoxy)phenoxy)ethoxy)ethoxy)ethoxy)-2-(2,6-dioxopiperidin-3-yl)isoindoline-1,3-dione (37 mg, 0.057 mmol, yield: 31%) as a brown solid. ^{1}H NMR (400 MHz, $CDCl_3$) δ 8.37 (s, 1H), 7.91 (d, J = 2.6 Hz, 1H), 7.67 (dd, J = 8.5, 7.3 Hz, 1H), 7.51−7.37 (m, 2H), 7.30−7.16 (m, 1H), 7.05−6.89 (m, 4H), 6.86 (d, J = 9.0 Hz, 1H), 4.94 (dd, J = 12.0, 5.3 Hz, 1H), 4.41−4.30 (m, 2H), 4.11 (dd, J = 5.6, 3.9 Hz, 2H), 4.02−3.94 (m, 2H), 3.91−3.79 (m, 4H), 3.80−3.74 (m, 2H), 2.94−2.68 (m, 3H), 2.16−2.08 (m, 1H). LC-MS (ESI) m/z $[M + H]^+$ Calcd for $C_{31}H_{28}ClN_3O_{11}$: 654.14; found: 654.10.

*4-(2-(2-(2-(2-(4-(4-Chloro-2-nitrophenoxy)phenoxy)ethoxy)-ethoxy)ethoxy)-2-(2,6-dioxopiperidin-3-yl)isoindoline-1,3-dione (**53**).* In a 10 mL flask, 2-(2,6-dioxopiperidin-3-yl)-4-hydroxyisoindoline-1,3-dione (100 mg, 0.364 mmol) and potassium carbonate (76 mg, 0.546 mmol) were dissolved in DMF (2.5 mL). The reaction mixture was heated for 30 min at 40 °C followed by dropwise addition of **51** (228 mg, 0.383 mmol) (dissolved in 1 mL DMF). The reaction mixture was stirred at 60 °C for 18 h. Upon reaction completion, H_2O (20 mL) was added and the mixture was extracted with diethyl ether (3 × 15 mL). The combined organic layers were washed with brine (1 × 30 mL). The organic layer was then dried over magnesium sulfate, and the solvent was evaporated under reduced pressure. The crude mixture was purified by reverse-phase flash column chromatography using a gradient elution of 10−100% MeCN/H_2O to obtain 4-(2-(2-(2-(2-(4-(4-chloro-2-nitrophenoxy)phenoxy)ethoxy)ethoxy)ethoxy)ethoxy)-2-(2,6-dioxopiperidin-3-yl)isoindoline-1,3-dione (111 mg, 0.159 mmol, yield: 44%) as a yellow oil. ^{1}H NMR (400 MHz, $CDCl_3$) δ 8.10 (s, 1H), 7.92 (d, J = 2.7 Hz, 1H), 7.68 (dd, J = 8.5, 7.3 Hz, 1H), 7.47 (dd, J = 7.3, 0.7 Hz, 1H), 7.43−7.38 (m, 1H), 7.26 (d, J = 4.1 Hz, 1H), 7.02−6.96 (m, 2H), 6.95−6.91 (m, 2H), 6.86 (d, J = 9.0 Hz, 1H), 4.95 (dd, J = 12.3, 5.3 Hz, 1H), 4.37−4.31 (m, 2H), 4.12 (dd, J = 5.7, 3.8 Hz, 2H), 3.98−3.89 (m, 2H), 3.91−3.82 (m, 2H), 3.83−3.77 (m, 2H), 3.76−3.72 (m, 2H), 3.71−3.66 (m, 4H), 2.98−2.66 (m, 3H), 2.17−2.09 (m, 1H). LC-MS (ESI) m/z $[M + H]^+$ Calcd for $C_{33}H_{32}ClN_3O_{12}$: 698.17; found: 698.15.

*4-(2-(2-(2-(4-(2-Amino-4-chlorophenoxy)phenoxy)ethoxy)-ethoxy)ethoxy)-2-(2,6-dioxopiperidin-3-yl)isoindoline-1,3-dione (**54**).* In a 10 mL flask, **52** (37.0 mg, 0.057 mmol) and tin(II) chloride dihydrate (63.8 mg, 0.283 mmol) were dissolved in EtOAc (1 mL). The reaction mixture was stirred at 40 °C for 18 h. Upon reaction completion, 5 mL of 3 M NaOH solution was added, and the mixture was stirred at rt for 10 min. The reaction mixture was then diluted with H_2O (5 mL) and extracted with EtOAc (3 × 25 mL). The combined organic layers were washed with brine (1 × 60 mL). The organic layer was then dried over magnesium sulfate, and the solvent was evaporated under reduced pressure to obtain crude 4-(2-(2-(2-(4-(2-amino-4-chlorophenoxy)phenoxy)ethoxy)ethoxy)ethoxy)-2-(2,6-dioxopiperidin-3-yl)isoindoline-1,3-dione as a yellow oil. The crude was used in the next step without further purification.

*4-(2-(2-(2-(2-(4-(2-Amino-4-chlorophenoxy)phenoxy)ethoxy)-ethoxy)ethoxy)ethoxy)-2-(2,6-dioxopiperidin-3-yl)isoindoline-1,3-dione (**55**).* In a 10 mL flask, **53** (111 mg, 0.159 mmol) and tin(II) chloride dihydrate (179 mg, 0.795 mmol) were dissolved in EtOAc (3 mL). The reaction mixture was stirred at 40 °C for 18 h. Upon reaction completion, 15 mL of 3 M NaOH solution was added, and the mixture was stirred at rt for 10 min. The reaction mixture was then diluted with H_2O (15 mL) and extracted with EtOAc (3 × 75 mL). The combined organic layers were washed with brine (1 × 150 mL). The organic layer was then dried over magnesium sulfate, and the solvent was evaporated under reduced pressure to obtain crude 4-(2-(2-(2-(2-(4-(2-amino-4-chlorophenoxy)phenoxy)ethoxy)ethoxy)ethoxy)ethoxy)-2-(2,6-dioxopiperidin-3-yl)isoindoline-1,3-dione as a yellow oil. The crude was used in the next step without further purification.

*4-Chloro-N-(5-chloro-2-(4-(2-(2-(2-((2-(2,6-dioxopiperidin-3-yl)-1,3-dioxoisoindolin-4-yl)oxy)ethoxy)ethoxy)ethoxy)phenoxy)-phenyl)-3-(trifluoromethyl)benzenesulfonamide (**14**).* A 10 mL flask was charged with **54** (37.0 mg, 0.059 mmol), 4-chloro-3-(trifluoromethyl)benzenesulfonyl chloride (16.55 mg, 0.059 mmol), DMAP (0.724 mg, 5.93 μmol), and pyridine (0.6 mL). The reaction mixture was stirred at rt for 2 h. Upon reaction completion, pyridine was evaporated under reduced pressure, and the residue was taken up in EtOAc (20 mL) and washed with 1 M HCl (3 × 20 mL). The organic layer was dried over magnesium sulfate and then concentrated under reduced pressure. The crude mixture was purified by reverse-phase flash column chromatography using a gradient elution of 10−100% MeCN/H_2O to obtain 4-chloro-*N*-(5-chloro-2-(4-(2-(2-(2-((2-(2,6-dioxopiperidin-3-yl)-1,3-dioxoisoindolin-4-yl)oxy)ethoxy)ethoxy)ethoxy)-phenoxy)phenyl)-3-(trifluoromethyl)benzenesulfonamide (19 mg, 0.022 mmol, yield: 37% over two steps) as a pink solid. ^{1}H NMR (400 MHz, $CDCl_3$) δ 8.29 (s, 1H), 8.12 (d, J = 2.2 Hz, 1H), 7.86 (dd, J = 8.4, 2.3 Hz, 1H), 7.73−7.62 (m, 2H), 7.57 (d, J = 8.4 Hz, 1H), 7.46 (d, J = 7.3 Hz, 2H), 7.27 (d, J = 6.3 Hz, 1H), 6.99 (dd, J = 8.8, 2.5 Hz, 1H), 6.8−6.73 (m, 2H), 6.63−6.43 (m, 3H), 4.91 (dd, J = 12.3, 5.3 Hz, 1H), 4.36 (t, J = 4.7 Hz, 2H), 4.08 (dd, J = 5.7, 3.8 Hz, 2H), 4.04−3.94 (m, 2H), 3.89−3.85 (m, 2H), 3.85−3.82 (m, 2H), 3.80−3.75 (m, 2H), 3.04−2.61 (m, 3H), 2.21−2.05 (m, 1H). ^{13}C NMR (101 MHz, CDCl3) δ 171.3, 168.3, 167.0, 165.8, 156.4, 155.8, 148.5, 147.7, 138.2, 137.8, 136.7, 133.7, 132.4, 131.6, 129.7, 128.4, 127.2, 126.7, 126.6, 126.6, 126.5, 123.1, 120.5, 119.9, 119.4, 117.6, 117.2, 116.3, 115.9, 71.1, 70.8, 69.7, 69.4, 69.1, 67.9, 49.1, 31.4, 22.6. LC-MS (ESI) m/z $[M + H]^+$ Calcd for $C_{38}H_{32}Cl_2F_3N_3O_{11}S$: 866.11; found: 866.05.

*4-Chloro-N-(5-chloro-2-(4-(2-(2-(2-(2-((2-(2,6-dioxopiperidin-3-yl)-1,3-dioxoisoindolin-4-yl)oxy)ethoxy)ethoxy)ethoxy)ethoxy)-phenoxy)phenyl)-3-(trifluoromethyl)benzenesulfonamide (**15**).* A 10 mL flask was charged with **55** (81 mg, 0.121 mmol) and DMAP (1.481 mg, 0.012 mmol) dissolved in pyridine (0.8 mL). 4-Chloro-3-(trifluoromethyl)benzenesulfonyl chloride (33.8 mg, 0.121 mmol) dissolved in pyridine (0.4 mL) was added dropwise at rt. The reaction

https://doi.org/10.1021/acs.jmedchem.5c02920
J. Med. Chem. 2025, 68, 26525−26546

mixture was stirred at rt for 2 h. Upon reaction completion, pyridine was evaporated under reduced pressure, and the residue was taken up in EtOAc (40 mL) and washed with 1 M HCl (3× 40 mL). The organic layer was dried over magnesium sulfate and then concentrated under reduced pressure. The crude mixture was purified by reverse-phase flash column chromatography using a gradient elution of 10−100% MeCN/H_2O to obtain 4-chloro-*N*-(5-chloro-2-(4-(2-(2-(2-(2-((2-(2,6-dioxopiperidin-3-yl)-1,3-dioxoisoindolin4yl)oxy)ethoxy)ethoxy)ethoxy)-ethoxy)phenoxy)phenyl)-3-(trifluoromethyl)benzenesulfonamide (44 mg, 0.048 mmol, yield: 30% over two steps) as a white solid. ^{1}H NMR (400 MHz, $CDCl_3$) δ 8.41 (s, 1H), 8.10 (d, J = 2.2 Hz, 1H), 7.86 (dd, J = 8.4, 2.3 Hz, 1H), 7.67 (dd, J = 8.5, 7.3 Hz, 1H), 7.64 (d, J = 2.5 Hz, 1H), 7.57 (d, J = 8.4 Hz, 1H), 7.48−7.39 (m, 2H), 7.27 (d, J = 8.4 Hz, 1H), 6.99 (dd, J = 8.8, 2.5 Hz, 1H), 6.82−6.75 (m, 2H), 6.55−6.47 (m, 3H), 4.95 (dd, J = 12.2, 5.3 Hz, 1H), 4.35 (t, J = 4.7 Hz, 2H), 4.08 (dd, J = 5.7, 3.7 Hz, 2H), 3.96 (dd, J = 5.6, 3.7 Hz, 2H), 3.86 (dd, J = 5.7, 3.7 Hz, 2H), 3.83−3.79 (m, 2H), 3.77−3.68 (m, 6H), 3.01−2.64 (m, 3H), 2.27−2.01 (m, 1H). ^{13}C NMR (101 MHz, $CDCl_3$) δ 171.4, 168.4, 167.0, 165.8, 156.4, 155.7, 148.4, 147.7, 138.1, 137.8, 136.7, 133.7, 132.4, 131.6, 128.3, 127.1, 126.7, 126.7, 126.6, 126.5, 123.2, 120.5, 119.9, 119.5, 117.5, 117.2, 116.3, 115.9, 71.1, 70.8, 70.6, 70.5, 69.7, 69.4, 69.2, 67.8, 49.1, 31.4, 22.6, 22.5. LC-MS (ESI) m/z $[M + H]^+$ Calcd for $C_{40}H_{36}Cl_2F_3N_3O_{12}S$: 910.13; found: 910.10.

*(2R,3S,4R,5S)-N-(4-((2-(2-(2-(4-(4-Chloro-2-((4-chloro-3-(trifluoromethyl)phenyl)sulfonamido)phenoxy)benzamido)-ethoxy)ethoxy)ethyl)carbamoyl)-2-methoxyphenyl)-3-(3-chloro-2-fluorophenyl)-4-(4-chloro-2-fluorophenyl)-4-cyano-5-neopentyl-pyrrolidine-2-carboxamide (**16**).* **45** (0.066 g, 0.104 mmol) and 4-((2*R*,3*S*,4*R*,5*S*)-3-(3-chloro-2-fluorophenyl)-4-(4-chloro-2-fluorophenyl)-4-cyano-5-neopentylpyrrolidine-2-carboxamido)-3-methoxybenzoic acid (0.061 g, 0.099 mmol) were added to a round-bottom flask. HATU (0.045 g, 0.119 mmol), DMF (1 mL), and DIPEA (0.034 mL, 0.198 mmol) were then added, and the reaction was stirred at room temperature for 1 h. Upon reaction completion, 10 mL of H_2O was added, and the reaction mixture was washed with EtOAc (3 × 20 mL). The combined organic layers were washed with H_2O (2 × 20 mL) and brine (1 × 30 mL). The organic layers were dried over magnesium sulfate and concentrated under vacuum. The crude mixture was purified by automated flash column chromatography using a gradient of 2−5% MeOH in DCM to obtain (2*R*,3*S*,4*R*,5*S*)-*N*-(4-((2-(2-(2-(4-(4-chloro-2-((4-chloro-3-(trifluoromethyl)phenyl)sulfonamido)phenoxy)-benzamido)ethoxy)ethoxy)ethyl)carbamoyl)-2-methoxyphenyl)-3-(3-chloro-2-fluorophenyl)-4-(4-chloro-2-fluorophenyl)-4-cyano-5-neopentylpyrrolidine-2-carboxamide (55 mg, 0.045 mmol, yield: 45%) as a white solid. ^{1}H NMR (400 MHz, $CDCl_3$) δ 10.46 (s, 1H), 8.47 (s, 1H), 8.16 (d, J = 8.3 Hz, 1H), 8.01 (d, J = 2.2 Hz, 1H), 7.72 (dd, J = 8.4, 2.3 Hz, 1H), 7.63 (d, J = 2.5 Hz, 2H), 7.62 (d, J = 2.1 Hz, 1H), 7.60−7.55 (m, 2H), 7.37 (d, J = 8.4 Hz, 1H), 7.26−7.08 (m, 6H), 7.06 (dd, J = 8.7, 2.5 Hz, 1H), 6.96 (t, J = 5.4 Hz, 1H), 6.77 (t, J = 5.3 Hz, 1H), 6.70 (d, J = 8.7 Hz, 1H), 6.56−6.48 (m, 2H), 4.75 (dd, J = 8.7, 1.4 Hz, 1H), 4.63 (t, J = 9.0 Hz, 1H), 4.14−4.04 (m, 1H), 3.93 (s, 3H), 3.69−3.62 (m, 10H), 3.56 (t, J = 7.0, 5.3, 2.3 Hz, 2H), 2.92−2.82 (m, 1H), 1.60 (dd, J = 14.5, 9.8 Hz, 1H), 1.39 (dd, J = 14.5, 1.5 Hz, 1H), 1.02 (s, 9H). ^{13}C NMR (101 MHz, $CDCl_3$) δ 171.0, 166.9, 166.7, 161.0, 158.8, 158.5, 157.8, 155.3, 148.4, 145.4, 138.6, 137.3, 136.3, 136.2, 132.2, 131.3, 130.2, 130.1, 129.8, 129.3, 129.0, 128.9, 127.6, 126.6, 126.3, 125.3, 124.6, 124.4, 124.1, 123.2, 121.3, 121.1, 120.8, 120.4, 118.7, 118.0, 117.8, 117.7, 117.7, 116.8, 109.9, 70.4, 70.2, 69.9, 69.6, 65.1, 65.0, 64.3, 63.1, 63.0, 55.7, 50.0, 44.9, 40.0, 39.7, 30.4, 29.8. LC-MS (ESI) m/z $[M + H]^+$ Calcd for $C_{57}H_{53}Cl_4F_5N_6O_9S$: 1233.23; found: 1233.15.

*(2R,3S,4R,5S)-N-(4-((1-(4-(4-Chloro-2-((4-chloro-3-(trifluoromethyl)phenyl)sulfonamido)phenoxy)phenyl)-1-oxo-5,8,11-trioxa-2-azatridecan-13-yl)carbamoyl)-2-methoxyphenyl)-3-(3-chloro-2-fluorophenyl)-4-(4-chloro-2-fluorophenyl)-4-cyano-5-neopentylpyrrolidine-2-carboxamide (**17**).* **46** (59.9 mg, 0.088 mmol) and 4-((2*R*,3*S*,4*R*,5*S*)-3-(3-chloro-2-fluorophenyl)-4-(4-chloro-2-fluorophenyl)-4-cyano-5-neopentylpyrrolidine-2-carboxamido)-3-methoxybenzoic acid (54.3 mg, 0.088 mmol) were added to a 10 mL round-bottom flask. HATU (40.2 mg, 0.106 mmol), DMF (1 mL), and DIPEA (0.031 mL, 0.176 mmol) were then added, and the reaction was stirred at room temperature for 1 h. Upon reaction completion, 10 mL of H_2O was added, and the reaction mixture was washed with EtOAc (3 × 20 mL). The combined organic layers were washed with H_2O (2 × 20 mL) and brine (1 × 30 mL). The organic layers were combined, dried over magnesium sulfate, and concentrated under vacuum. The crude mixture was purified by automated flash column chromatography using a gradient of 2−5% MeOH in DCM to obtain (2*R*,3*S*,4*R*,5*S*)-*N*-(4-((1-(4-(4-chloro-2-((4-chloro-3-(trifluoromethyl)phenyl)sulfonamido)phenoxy)phenyl)-1-oxo-5,8,11-trioxa-2-azatridecan-13-yl)carbamoyl)-2-methoxyphenyl)-3-(3-chloro-2-fluorophenyl)-4-(4-chloro-2-fluorophenyl)-4-cyano-5-neopentylpyrrolidine-2-carboxamide (53 mg, 0.041 mmol, yield: 47%) as a white solid. ^{1}H NMR (400 MHz, $CDCl_3$) δ 10.43 (s, 1H), 8.52 (s, 1H), 8.26 (d, J = 8.4 Hz, 1H), 8.08 (d, J = 2.2 Hz, 1H), 7.77 (dd, J = 8.4, 2.3 Hz, 1H), 7.66 (d, J = 2.5 Hz, 1H), 7.64−7.60 (m, 2H), 7.58−7.51 (m, 2H), 7.41 (d, J = 8.4 Hz, 1H), 7.26−7.20 (m, 2H), 7.19−7.08 (m, 4H), 7.06 (dd, J = 8.7, 2.5 Hz, 1H), 6.98 (t, J = 5.3 Hz, 1H), 6.90 (t, J = 5.3 Hz, 1H), 6.69 (d, J = 8.7 Hz, 1H), 6.58−6.44 (m, 2H), 4.76 (dd, J = 8.7, 1.3 Hz, 1H), 4.59 (t, J = 9.0 Hz, 1H), 4.15−4.05 (m, 1H), 3.93 (s, 3H), 3.65 (d, J = 7.0 Hz, 10H), 3.63−3.59 (m, 4H), 3.59−3.49 (m, 2H), 2.87−2.80 (m, 1H), 1.60 (dd, J = 14.5, 9.7 Hz, 1H), 1.40 (dd, J = 14.4, 1.4 Hz, 1H), 1.02 (s, 9H). ^{13}C NMR (101 MHz, $CDCl_3$) δ 170.8, 166.9, 166.5, 161.0, 158.5, 157.8, 155.3, 148.4, 145.7, 138.6, 137.4, 136.3, 136.2, 132.2, 131.4, 131.3, 131.3, 130.3, 130.1, 129.9, 129.8, 129.8, 129.0, 128.8, 127.5, 126.6, 126.5, 125.3, 125.3, 124.7, 124.6, 124.2, 123.2, 121.4, 121.2, 120.4, 118.8, 118.1, 117.9, 117.0, 109.9, 70.5, 70.4, 70.2, 70.1, 69.8, 69.7, 65.0, 64.9, 64.3, 63.1, 63.1, 55.7, 50.1, 44.9, 39.9, 39.8, 30.4, 29.8. LC-MS (ESI) m/z $[M + H]^+$ Calcd for $C_{59}H_{57}Cl_4F_5N_6O_{10}S$: 1277.25; found: 1277.25.

*4-Fluoro-2-(1-methyl-2,6-dioxopiperidin-3-yl)isoindoline-1,3-dione (**56**).* Iodomethane (0.181 mL, 2.896 mmol) was added dropwise to 2-(2,6-dioxopiperidin-3-yl)-4-fluoroisoindoline-1,3-dione (200 mg, 0.724 mmol) and potassium carbonate (200 mg, 1.448 mmol) in DMF (7 mL). The reaction mixture was stirred at room temperature for 2 h. Upon reaction completion, H_2O (50 mL) was added, and the reaction mixture was extracted with EtOAc (2 × 100 mL). The organic phase was dried over magnesium sulfate, and the organic layers were evaporated under reduced pressure. The crude mixture was purified by flash column chromatography using a gradient of 1−7% MeOH/DCM to obtain 4-fluoro-2-(1-methyl-2,6-dioxopiperidin-3-yl)isoindoline-1,3-dione (125 mg, 0.431 mmol, yield: 60%) as a white solid. ^{1}H NMR (400 MHz, $CDCl_3$) δ 7.79 (ddd, J = 8.3, 7.4, 4.3 Hz, 1H), 7.74−7.68 (m, 1H), 7.44 (td, J = 8.5, 0.9 Hz, 1H), 5.11−4.92 (m, 1H), 3.20 (s, 3H), 3.05−2.93 (m, 2H), 2.83−2.72 (m, 1H), 2.22−2.09 (m, 1H). LC-MS (ESI) m/z $[M + H]^+$ Calcd for $C_{14}H_{11}FN_2O_4$: 291.07; found: 291.05.

*tert-Butyl (4-((2-(1-Methyl-2,6-dioxopiperidin-3-yl)-1,3-dioxoisoindolin-4-yl)amino)butyl)carbamate (**57**).* In a 10 mL flask, **56** (60.0 mg, 0.207 mmol) and *tert*-butyl (4-aminobutyl)carbamate (0.047 mL, 0.248 mmol) were dissolved in DMF (2 mL) followed by addition of DIPEA (0.036 mL, 0.207 mmol). The reaction mixture was stirred at 90 °C overnight. Upon reaction completion, H_2O (20 mL) was added, and the reaction mixture was extracted with EtOAc (2 × 30 mL). The organic phase was dried over magnesium sulfate, and the organic layers were evaporated under reduced pressure. The crude product was used further in the next step without purification.

*tert-Butyl (6-((2-(1-Methyl-2,6-dioxopiperidin-3-yl)-1,3-dioxoisoindolin-4-yl)amino)hexyl)carbamate (**58**).* In a 10 mL flask, **56** (60.0 mg, 0.207 mmol) and *tert*-butyl (6-aminohexyl)carbamate (0.051 mL, 0.227 mmol) were dissolved in DMF (2 mL) followed by addition of DIPEA (0.036 mL, 0.207 mmol). The reaction mixture was stirred at 90 °C overnight. Upon reaction completion, H_2O (20 mL) was added, and the reaction mixture was extracted with EtOAc (2 × 30 mL). The organic phase was dried over magnesium sulfate, and the organic layers were evaporated under reduced pressure. The crude product was used further in the next step without purification.

*4-((4-Aminobutyl)amino)-2-(1-methyl-2,6-dioxopiperidin-3-yl)-isoindoline-1,3-dione (**59**).* In a 10 mL flask, **57** (35.0 mg, 0.076 mmol) was dissolved in TFA (3 mL) and the mixture was stirred at rt for 1 h. Upon reaction completion, DCM (5 ML) was added, and the mixture was concentrated under reduced pressure to obtain 4-((4-aminobutyl)-

https://doi.org/10.1021/acs.jmedchem.5c02920
J. Med. Chem. 2025, 68, 26525−26546

amino)-2-(1-methyl-2,6-dioxopiperidin-3-yl)isoindoline-1,3-dione as a TFA salt. The crude product was used further in the next step without further purification.

*4-((6-Aminohexyl)amino)-2-(1-methyl-2,6-dioxopiperidin-3-yl)-isoindoline-1,3-dione (**60**).* In a 10 mL flask, **58** (18.00 mg, 0.037 mmol) was dissolved in TFA (2 mL) and the mixture was stirred at rt for 1 h. Upon reaction completion, DCM (5 mL) was added, and the mixture was concentrated under reduced pressure to obtain 4-((6-aminohexyl)amino)-2-(1-methyl-2,6-dioxopiperidin-3-yl)isoindoline-1,3-dione as a TFA salt. The crude product was used further in the next step without further purification.

*4-(4-Chloro-2-((4-chloro-3-(trifluoromethyl)phenyl)-sulfonamido)phenoxy)-N-(4-((2-(1-methyl-2,6-dioxopiperidin-3-yl)-1,3-dioxoisoindolin-4-yl)amino)butyl)benzamide (**18**).* In a 25 mL flask, **1** (37.3 mg, 0.074 mmol) was dissolved in DMF (5 mL) followed by addition of HATU (38.2 mg, 0.100 mmol) and DIPEA (0.035 mL, 0.201 mmol). **59** (24.00 mg, 0.067 mmol) dissolved in DMF (5 mL) was added to the benzoic acid mixture and stirred at rt for 2 h. Upon reaction completion, the reaction mixture was diluted with H_2O (100 mL) and extracted with EtOAc (3 × 120 mL). The combined organic layers were washed with brine (100 mL). The organic layers were dried over magnesium sulfate and evaporated under reduced pressure. The crude mixture was purified by reverse-phase automated flash column chromatography using a gradient of 30−90% ACN/H_2O to obtain 4-(4-chloro-2-((4-chloro-3-(trifluoromethyl)phenyl)sulfonamido)-phenoxy)-*N*-(4-((2-(1-methyl-2,6-dioxopiperidin-3-yl)-1,3-dioxoisoindolin-4-yl)amino)butyl)benzamide (7 mg, 0.008 mmol, yield: 4% over three steps) as a yellow solid. ^{1}H NMR (400 MHz, $CDCl_3$) δ 8.07 (d, J = 2.2 Hz, 1H), 7.82 (dd, J = 8.4, 2.3 Hz, 1H), 7.73 (d, J = 2.5 Hz, 1H), 7.65 (d, J = 8.8 Hz, 2H), 7.57−7.43 (m, 2H), 7.21 (s, 1H), 7.14−7.07 (m, 2H), 6.90 (dd, J = 8.6, 0.7 Hz, 1H), 6.73 (d, J = 8.7 Hz, 1H), 6.64 (d, J = 8.8 Hz, 2H), 6.21 (t, J = 5.9 Hz, 1H), 4.96−4.86 (m, 1H), 3.53 (d, J = 4.9 Hz, 2H), 3.34 (d, J = 6.1 Hz, 2H), 3.20 (s, 3H), 3.04−2.91 (m, 1H), 2.83−2.74 (m, 2H), 2.15−2.05 (m, 1H), 1.82−1.73 (m, 4H). ^{13}C NMR (151 MHz, $CDCl_3$) δ 171.4, 169.9, 169.2, 167.9, 166.9, 158.4, 146.9, 145.4, 138.2, 138.0, 136.3, 132.6, 132.6, 131.5, 130.5, 130.4, 129.8, 129.6, 129.3, 128.5, 126.9, 126.7, 123.5, 122.8, 121.0, 120.2, 117.4, 116.8, 111.8, 110.3, 49.8, 42.3, 39.8, 32.0, 27.4, 27.3, 26.7, 22.3. LC-MS (ESI) m/z [M + H]$^+$ Calcd for $C_{38}H_{32}Cl_2F_3N_5O_8S$: 845.13; found: 845.90.

*4-(4-Chloro-2-((4-chloro-3-(trifluoromethyl)phenyl)-sulfonamido)phenoxy)-N-(6-((2-(1-methyl-2,6-dioxopiperidin-3-yl)-1,3-dioxoisoindolin-4-yl)amino)hexyl)benzamide (**19**).* In a 25 mL flask, **1** (39.2 mg, 0.077 mmol) was dissolved in DMF (5.00 mL) followed by addition of HATU (33.9 mg, 0.089 mmol) and DIPEA (0.031 mL, 0.179 mmol). **60** (23.00 mg, 0.060 mmol) was dissolved in DMF (5.00 mL), added to the benzoic acid mixture, and stirred at rt for 2 h. Upon reaction completion, the reaction mixture was diluted with H_2O (100 mL) and extracted with EtOAc (3 × 120 mL). The combined organic layers were washed with brine (100 mL). The organic layers were dried over magnesium sulfate and evaporated under reduced pressure. The crude mixture was purified by reverse-phase automated flash column chromatography using a gradient of 30−90% ACN/H_2O to obtain 4-(4-chloro-2-((4-chloro-3-(trifluoromethyl)-phenyl)sulfonamido)phenoxy)-*N*-(6-((2-(1-methyl-2,6-dioxopiperidin-3-yl)-1,3-dioxoisoindolin-4-yl)amino)hexyl)benzamide (16 mg, 0.018 mmol, yield: 9% over three steps) as a yellow solid. ^{1}H NMR (400 MHz, $CDCl_3$) δ 8.07 (s, 1H), 7.82 (d, J = 8.4 Hz, 1H), 7.72 (d, J = 2.5 Hz, 1H), 7.64 (d, J = 8.3 Hz, 2H), 7.56−7.45 (m, 2H), 7.35 (s, 1H), 7.20−7.05 (m, 2H), 6.88 (d, J = 8.5 Hz, 1H), 6.74 (d, J = 8.7 Hz, 1H), 6.63 (d, J = 8.3 Hz, 2H), 6.31 (d, J = 6.2 Hz, 1H), 4.90 (q, J = 5.6 Hz, 1H), 3.47 (q, J = 6.8 Hz, 2H), 3.28 (t, J = 6.8 Hz, 2H), 3.18 (s, 3H), 3.00−2.92 (m, 1H), 2.79−2.69 (m, 2H), 2.08 (s, 1H), 1.79−1.61 (m, 4H), 1.59−1.32 (m, 4H). ^{13}C NMR (101 MHz, $CDCl_3$) δ 171.5, 169.9, 169.2, 167.9, 166.6, 158.3, 147.1, 145.4, 138.2, 138.0, 136.3, 132.6, 132.6, 131.5, 130.7, 130.4, 129.8, 129.5, 128.5, 126.9, 126.7, 123.6, 123.3, 120.5, 120.2, 117.3, 116.7, 111.6, 110.1, 49.7, 42.6, 40.1, 32.0, 29.1, 27.4, 26.7, 22.3. LC-MS (ESI) m/z [M + H]$^+$ Calcd for $C_{40}H_{36}Cl_2F_3N_5O_8S$: 874.16; found: 874.05.

Materials. [^{3}H]CCR2-RA-[*R*] (specific activity of 60.6 Ci/mmol) was custom-labeled by Vitrax (Placentia, CA, USA). Bortezomib (PS-341), MG-132, bafilomycin-A1 (Baf-A1), and chloroquine diphosphate were purchased from Selleck Chemicals (Bio-Connect, Huissen, The Netherlands); CRBN-6-5-5-VHL from MedChem Express (Bio-Connect, Huissen, The Netherlands); cycloheximide from LKT Laboratories (St. Paul, MN, USA); and chemokine ligand CCL2 from PeproTech (Cranbury, NJ, USA). NanoGlo Endurazine, CellTiter-Glo, and FuGENE6 were obtained from Promega (Madison, WI, USA). Dulbecco's modified Eagles medium (DMEM) was purchased from Capricorn Scientific (Ebsdorfergrund, Germany) or Gibco (ThermoFisher Scientific, Waltham, MA, USA). RPMI-1640 medium, Opti-MEM I reduced serum medium, CO2-independent medium, GlutaMAX, and penicillin/streptomycin were all purchased from Gibco (ThermoFisher Scientific, Waltham, MA, USA). Zeocin and hygromycin B gold were purchased from InvivoGen (Toulouse, France); fetal calf serum from PAN-biotech (Aidenbach, Germany); Hoechst 33342 and propidium iodide dyes were from Invitrogen (Waltham, MA, USA). Pierce bicinchoninic acid (BCA) protein assay kit was purchased from ThermoFisher Scientific (Waltham, MA, USA). 24-well Thincerts with 8.0 μm pore diameter were bought from Greiner Bio-One (Kremsmünster, Austria). Tango CCR2-bla osteosarcoma (U2OS) cells stably expressing the human CCR2B (U2OS-CCR2) were obtained from Invitrogen (Waltham, MA, USA); HEK293 cells stably expressing the Large BiT protein (HEK293-LgBiT) from Promega (Madison, WI, USA); HEK293T and THP-1 cells from the American Type Culture Collection (ATCC, Manassas, VA, USA). The previously described CCR2-HiBiT fusion protein[36] was generated by Promega by cloning human CCR2b (NP_001116868.1, UniProt accession number P41597-2) into a pFC37K HiBiT CMV-neo Flexi Vector (Promega, Madison, WI, USA). A HaloTag-Ubiquitin fusion vector (N2721) was obtained from Promega (Madison, WI, USA). Before use, DNA sequence was verified using Sanger sequencing at the Leiden Genome Technology Center (Leiden, The Netherlands).

Cell Culture. U2OS-CCR2 cells were cultured in 10 or 15 cm ϕ plates, using McCoy's 5A medium supplemented with 10% dialyzed fetal calf serum (FCS), 2 mM glutamine, 0.1 mM nonessential amino acids, 25 mM HEPES, 1 mM sodium pyruvate, 100 IU/mL penicillin, 100 μg/mL streptomycin, 100 μg/mL G418, 40 μg/mL hygromycin B gold, and 125 μg/mL zeocin. HEK293T was cultured in 10 cm ϕ plates using DMEM high-glucose medium supplemented with 10% FCS, 2 mM glutamine, 100 IU/mL penicillin, and 100 μg/mL streptomycin. HEK293-LgBiT cells were cultured in T75 flasks or 10 cm ϕ plates using DMEM high-glucose medium supplemented with 10% FCS, 2 mM glutamine, 100 IU/mL penicillin, 100 μg/mL streptomycin, and 160 μg/mL hygromycin B gold. The leukemia monocytic cell line THP-1 was cultured and maintained in a complete RPMI-1640 medium supplemented with 10% fetal calf serum (FCS), 20 U/mL penicillin, 20 U/mL streptomycin, and 0.5X GlutaMAX. All cells were kept in a humidified incubator at 37 °C with 5% CO_2.

Membrane Preparation. Membranes from U2OS-CCR2 cells were prepared as previously described.[48] Briefly, cells were scraped from confluent plates into 5 mL of phosphate buffered saline (PBS) and centrifuged for 5 min at 3000 rpm. Cell pellets were then resuspended in ice-cold Tris buffer (50 mM of Tris-HCl, 5 mM of MgCl2, pH 7.4) and homogenized using an Ultra Turrax homogenizer (IKA-Werke GmbH & Co. KG, Staufen, Germany). Separation of membranes from the cytosolic fractions was achieved by centrifugation at 31,000 rpm for 20 min at 4 °C, using an Optima LE-80 K ultracentrifuge (Beckman Coulter, Inc., Fullerton, CA). After two cycles of homogenization and centrifugation, the remaining pellets were resuspended in ice-cold Tris buffer and stored at −80 °C in aliquots of 100 or 250 μL. Protein concentrations were determined using a standard Pierce BCA protein assay kit.

Transfection. HEK293T and HEK293-LgBiT cells were transfected with the CCR2-HiBiT construct using FuGENE6 as a transfection reagent, as previously described.[36] Twenty-four hours before transfection, cells were seeded in 10 cm ϕ plates (2 × 10^6 cells/plate) to reach ∼50% confluence on the next day. Before transfection, a mix of 2 μg of CCR2-HibiT and FuGENE6 transfection reagent was

https://doi.org/10.1021/acs.jmedchem.5c02920
J. Med. Chem. 2025, 68, 26525−26546

diluted in an Opti-MEM I reduced serum medium using a 3:1 ratio of FuGENE6 to DNA. The transfection mix was incubated for 15 min a room temperature before adding it to the cells. For NanoBRET ubiquitination assays, HEK293-LgBiT cells were transfected with 1 μg of CCR2-HiBiT and 8 μg of HaloTag-ubiquitin (Promega, N2721). Transfected cells were further incubated for 24 h at 37 °C with 5% CO_2 before use in real-time assays or cell viability assays.

[^{3}H]CCR2-RA-[*R*] Binding Assays in U2OS-CCR2 Membranes. [^{3}H]CCR2-RA-[*R*] binding assays were performed using membranes from U2OS-CCR2 as previously described.[35] Briefly, U2OS-CCR2 homogenized membranes (10−15 μg of total protein per well) were incubated with ∼6 nM [^{3}H]CCR2-RA-[*R*] and competing compound (putative CCR2 degraders) in a final volume of 100 μL assay buffer (50 mM of Tris-HCl, 5 mM of MgCl2, 0.1% CHAPS, at pH 7.4). Competing compounds were diluted in assay buffer to a single concentration (10 μM) or multiple concentrations ranging from 1 nM to 10 μM. In all cases, total binding was determined in the absence of competing ligand while nonspecific binding was determined by addition of 10 μM JNJ-27141491. To prevent radioligand depletion, total binding did not exceed 10% of the total radioactivity added. After 2 h at 25 °C while shaking, incubations were terminated by rapid vacuum filtration through prewetted 96-well GF/C filter plates (Revvity, Groningen, The Netherlands) using a Filtermate harvester (Revvity, Groningen, The Netherlands). Filter plates were then washed 10 times with ice-cold wash buffer (50 mM Tris-HCl, 5 mM $MgCl_2$, 0.01% CHAPS, at pH 7.4) and dried at 55 °C for at least 30 min. After final addition of 25 μL Microscint scintillation cocktail (Revvity, Groningen, The Netherlands) per well, filter-bound radioactivity was measured in a P-E 2450 MicroBeta^2 scintillation plate counter (Revvity, Groningen, The Netherlands).

[^{3}H]CCR2-RA-[*R*] Binding Assays in THP-1 Cells. THP-1 cells were centrifuged, resuspended in a culture medium (RPMI-1640 medium supplemented with 10% fetal calf serum (FCS), 2 nM glutamine, 100 IU/mL penicillin, and 100 μg/mL streptomycin), and plated in 6 cm dishes, each containing 5×10^6 cells in 5 mL. Plates were treated with 5 μL of selected compounds (LUF8064 and LUF7996) or DMSO control at the desired concentrations. In all cases, the final DMSO concentration was 0.1%. After 24 h incubation at 37 °C, 5% CO_2, cells were centrifuged at 400×*g* for 5 min, resuspended in 5 mL PBS, and incubated at room temperature for 30 min before a final cycle of centrifugation. Next, cells were resuspended in assay buffer (50 mM of Tris-HCl, 5 mM of MgCl2, 0.1% CHAPS, at pH 7.4) to a final concentration of 7×10^6 cells/mL and plated in a round-bottom 96-well at a density of 350,000 cells/well in a volume of 50 μL. Treated THP-1 cells were incubated with ∼6 nM [^{3}H]CCR2-RA-[*R*] in a final volume of 100 μL assay buffer. In all cases, total binding and nonspecific binding were determined by the addition of DMSO control or 10 μM JNJ-27141491, respectively. To prevent radioligand depletion, total binding did not exceed 10% of the total radioactivity added. After 2 h at 25 °C while shaking, incubations were terminated by harvesting with ice-cold wash buffer (50 mM Tris-HCl, 5 mM $MgCl_2$, 0.01% CHAPS, at pH 7.4), and radioactivity was measured as described in the section of [3H]CCR2-RA-[R] Binding Assays in U2OS-CCR2 Membranes.

Label-Free Phenotypic Whole-Cell Assay (xCELLigence). Label-free whole-cell assays were performed with the xCELLigence Real-Time Cell Analyzer (RTCA) SP system (Agilent, Santa Clara, CA, USA), as previously described.[48] This assay can measure CCR2 activation or inhibition by measuring CCL2-induced changes in electrical impedance. First, baseline impedance was measured after addition of 40 μL per well of U2OS-CCR2 culture medium to 96-well E-plates PET (Agilent, Santa Clara, CA, USA). Next, 50 μL of U2OS-CCR2 cells was seeded at a density of 20,000 cells per well, and plate was left at room temperature for 30 min. Next, the E-plate was placed in the xCELLigence SP station at 37 °C and 5% CO_2, and cell growth was monitored every 15 min for 18−20 h. Afterward, cells were pretreated for 1 h with 5 μL of CCR2 compounds at a final concentration of 10 μM or vehicle control (PBS with 0.25% DMSO) before stimulation with 5 μL of 10 nM CCL2. In all cases, compounds were added using a VIAFLO 96 hand-held electronic 96-channel pipet (Integra Bioscience, Tokyo, Japan). Immediately after CCL2 stimulation, changes in electrical impedance were monitored in 15 s intervals for 20 min, followed by 1 min intervals for 10 min and 5 min intervals for 50 min.

Real-Time, Live Cell HiBiT Detection. Real-time, live cell HiBiT detection assays were performed with HEK293-LgBiT cells transiently transfected with 2 μg CCR2-HiBiT, as previously described.[36] Twenty-four hours after transfection, HEK293-LgBiT cells were plated in a clear-bottom, white 96-well tissue culture plate (Greiner Bio-One, Kremsmünster, Austria), at a density of 40,000 cells/well in a volume of 40 μL CO_2-independent medium. Next, 50 μL of extended live cell substrate NanoGlo Endurazine was added to each well, using a 50-fold dilution of the substrate in a CO_2-independent medium. After 2.5 h incubation at 37 °C, the selected compounds were added at the desired concentrations, ranging from 0.1 nM to 31.6 μM, in a final volume of 10 μL. In experiments with inhibitors, 5 uL of inhibitor (pomalidomide, CRBN-6-5-5-VHL, MLN-4924, bortezomib, MG-132, bafilomycin-A1 or chloroquine) was added to the cells at the indicated final concentration, and the plate was incubated for 2 h at 37 °C before addition of 5 μL of compound **14** at a final concentration of 10 μM. After compound addition, plates were immediately sealed with a breathable rayon film (VWR) and placed on a Flexstation 3 Multimode microplate reader (Molecular Devices, Workingham, UK) set at 37 °C, with their lids on. Luminescence was read every 10 min for 24 h from the bottom of the plate using an integration time of 1 s.

Homogeneous Time-Resolved Fluorescence (HTRF) Assay to Measure CRBN Binding. The assay is a HTRF competition assay where active compounds replace a Cy5-labeled CRBN binding compound. Streptavidin that is labeled with Terbium binds via Biotin to CRBN-DDB1. When Terbium and Cy5 are within proximity to each other, the donor is excited by an energy source and triggers energy transfer toward the acceptor, which emits specific fluorescence at given wavelength. If a compound binds to CRBN and thus competes with the Cy5-labeled probe, the donor (Tb) is excited but no energy transfer occurs and no acceptor (Cy5) emission occurs. Dual-wavelength detection reduces buffer and media interference, and the final signal is proportional to the extent of product formation. The result is measured in a form of ratio between donor and acceptor emission signal ratio = (channel A 665 nm/channel B 620 nm) × 10,000.

NanoBRET Ubiquitination Assay. NanoBRET Ubiquitination assays were performed with HEK293-LgBiT cells transiently transfected with 1 μg of CCR2-HiBiT and 8 μg of HaloTag-Ubiquitin using FuGENE6 as previously described. Twenty-four hours after transfection, HEK293-LgBiT cells were plated in solid, white 96-well tissue culture plates (Corning, #3917), at a density of 20,000 cells/well in a volume of 100 μL of assay medium (Opti-MEM I reduced serum medium, no phenol red supplemented with 4% FCS). Cells were seeded in the presence of 100 nM HaloTag NanoBRET 618 Ligand (Promega) or DMSO control and incubated for 24 h at 37 °C, 5% CO_2. In the following day, the medium was replaced with 90 μL of extended live cell substrate NanoGlo Vivazine, using a 100-fold dilution of the substrate in the assay medium. After 1 h incubation at 37 °C, 5% CO_2, and before compound addition, plates were placed in an EnVision Nexus Multimode Microplate reader (Revvity, Groningen, The Netherlands) and dual filtered luminescence signals were collected every 3 min for 9 min using a 460/80 nm filter (donor) and a 610 nm long pass filter (acceptor), with an integration time of 0.1 s. After collecting baseline measurements, the selected compounds (LUF8064 and LUF7996) or vehicle control were added at a final concentration of 10 μM, in a final volume of 10 μL, and plates were immediately placed on the EnVision Nexus to further collect kinetic measurements every 3 min for 3 h at 37 °C. Samples without HaloTag NanoBRET 618 Ligand (no ligand) were used to obtain background-corrected NanoBRET ratios according to the equation below, before calculations of the area under the curve.

$$\text{nano BRET ratio} = \left(\frac{\text{acceptor channel}}{\text{donor channel}} - \frac{\text{acceptor channel(no ligand)}}{\text{donor channel(no ligand)}} \right)$$

https://doi.org/10.1021/acs.jmedchem.5c02920
J. Med. Chem. 2025, 68, 26525−26546

Cell Viability. To determine if the CCR2 compounds affect cell viability at high concentrations, we used the CellTiter-Glo Luminescent cell viability assay (Promega, Madison, WI, USA). HEK293T cells were seeded on white 96-well tissue culture plates at a density of 40,000 cells per well, in a volume of 90 μL. Control wells containing the culture medium without cells were used to obtain background luminescence. Next, 10 μL of CCR2 compounds or vehicle control were added to the cells at a final concentration of 10 or 31.6 μM. After 24 h incubation, 100 μL of previously prepared CellTiter-Glo reagent (CellTiter-Glo substrate reconstituted in CellTiter-Glo buffer) was added to each well and plate was incubated for 10 min at room temperature in the dark to stabilize luminescent signal. Finally, luminescence was measured in an EnVision multilable plate reader (Revvity, Groningen, The Netherlands) using an integration time of 500 ms. To assess the effect of the CCR2 antagonists and CCR2 degrader 8 on the viability and morphology of THP-1 cells, the cells were incubated for 5 h with either 10 μM antagonist in the presence of 10 nM CCL2 or an equivalent volume of DMSO as a control. Cells were stained with Hoechst dye (1 μg/mL) and the fluorescent viability dye PI (0.2 μg/mL). Images were captured using a Nikon Ti2 confocal fluorescent microscope with a Plan Apo VC 20× objective (Nikon, Tokyo, Japan) at 405 and 561 nm excitation lasers. Cell viability was quantified by counting the number of PI-positive cells relative to the total number of cells using the particle analysis function within the Fiji image analysis software.

Migration Assay. The ability of THP-1 cells to migrate toward CCL2 was assessed using 24-well transwell inserts with 8 μm pores. Cells were starved with 1% FBS in RPMI-1640 for 24 h prior to the migration assay and maintained at low serum levels throughout the assay. Cells were collected, stained with Hoechst 33342 (1 μg/mL), and preincubated for 3 h with either 10 μM CCR2 compounds (or 126 nM compound 1) or an equivalent volume of DMSO as a control. The inserts were then placed in a 24-well plate filled with 600 μL DMEM containing either 10 nM CCL2 or an equivalent volume of 50 mM Tris-HCl buffer (pH 7.4) containing 0.1% BSA as vehicle control. THP-1 cells were centrifuged at 1000 rpm for 5 min and washed with DPBS. Then, cells were resuspended in DMEM at a concentration of 2×10^6 cells/mL in the presence of CCR2 compounds, and 100 μL of the cell suspension was slowly seeded into each insert. In all cases, CCR2 compounds were added to both the well and cell suspension. Cells were incubated for 1.5 h at 37 °C with 5% CO_2. Cells that migrated to the bottom of the well were imaged using the ZOE fluorescent imager (Bio-Rad Laboratories, CA, USA). The number of migrated cells was quantified by analyzing 10 representative images from two wells using the nuclei particle analysis function in Fiji image analysis software. The cell count was then normalized by dividing it by the surface area of each image.

Data Analysis. All data were analyzed using GraphPad Prism 9.0 or 10.0 (GraphPad Software Inc., San Diego, CA, USA). Unless stated otherwise, all data are presented as mean ± standard error of the mean (SEM) of at least three independent experiments performed in duplicate or triplicate. (p)IC_{50}/DC50 values from radioligand binding or CRBN engagement assays were obtained by nonlinear regression curve-fitting. pK_i values from radioligand binding assays were derived from IC_{50} values using the Cheng−Prusoff equation.[71] For xCELLigence experiments, the RTCA software v2.0 (Agilent, Santa Clara, CA, USA) was used to obtain cell index (CI) values normalized to the last time point prior to CCL2 stimulation. Vehicle response was then subtracted, and peak values were obtained within 7 min of CCL2 stimulation. In the case of real-time degradation assays, fractional RLU values were obtained by normalizing all RLU values after degrader treatment to the vehicle-control value at any given time point. Statistical differences in HiBiT assays after cotreatment with proteasomal or lysosomal inhibitors were analyzed using a two-way ANOVA with Dunnett's posthoc test; statistical differences in radioligand binding, ubiquitination, or migration assays were analyzed using a (paired) one-way ANOVA with Tukey's posthoc test. Significant differences were noted as *$p < 0.05$, **$p < 0.01$, ***$p < 0.001$, or ****$p < 0.0001$. ** $p <$ 0.01, and **** $p < 0.0001$.

■ ASSOCIATED CONTENT

Supporting Information

The Supporting Information is available free of charge at https://pubs.acs.org/doi/10.1021/acs.jmedchem.5c02920.

Molecular formula strings of compounds with some in vitro data (CSV)

Kinetic degradation profiles, CCR2 degraders, binding affinity, kinetic profiles, cell viability, synthetic schemes, HPLC-MS, and NMR spectra (PDF)

■ AUTHOR INFORMATION

Corresponding Authors

Daan van der Es − *Division of Medicinal Chemistry, Leiden Academic Centre for Drug Research (LACDR), Leiden University, Leiden 2333 CC, The Netherlands;* orcid.org/0000-0003-3662-8177; Email: d.van.der.es@lacdr.leidenuniv.nl

Laura H. Heitman − *Division of Medicinal Chemistry, Leiden Academic Centre for Drug Research (LACDR), Leiden University, Leiden 2333 CC, The Netherlands; Oncode Institute, Leiden 2333 CC, The Netherlands;* orcid.org/0000-0002-1381-8464; Email: l.h.heitman@lacdr.leidenuniv.nl

Authors

Khaled Essa − *Division of Medicinal Chemistry, Leiden Academic Centre for Drug Research (LACDR), Leiden University, Leiden 2333 CC, The Netherlands*

Natalia V. Ortiz Zacarías − *Division of Medicinal Chemistry, Leiden Academic Centre for Drug Research (LACDR), Leiden University, Leiden 2333 CC, The Netherlands*

Sascha Roth − *Safety Innovation and PROTAC Safety, Clinical Pharmacology & Safety Sciences, R&D, AstraZeneca, Cambridge CB2 0SL, United Kingdom*

Bo-Tao Xin − *Department of Cell and Chemical Biology, Chemical Immunology, Leiden University Medical Centre, Leiden 2333 ZC, The Netherlands*

Sabine de Winter − *Division of Cell Systems and Drug Safety, Leiden Academic Centre for Drug Research (LACDR), Leiden University, Leiden 2333 CC, The Netherlands;* orcid.org/0009-0002-1152-7994

Cas van der Horst − *Division of Medicinal Chemistry, Leiden Academic Centre for Drug Research (LACDR), Leiden University, Leiden 2333 CC, The Netherlands*

Bente Bleijs − *Division of Medicinal Chemistry, Leiden Academic Centre for Drug Research (LACDR), Leiden University, Leiden 2333 CC, The Netherlands*

Richard A. de Heiden − *Division of Medicinal Chemistry, Leiden Academic Centre for Drug Research (LACDR), Leiden University, Leiden 2333 CC, The Netherlands*

Rodanthi Voulgaraki − *Division of Medicinal Chemistry, Leiden Academic Centre for Drug Research (LACDR), Leiden University, Leiden 2333 CC, The Netherlands*

Elsa Neubert − *Division of Cell Systems and Drug Safety, Leiden Academic Centre for Drug Research (LACDR), Leiden University, Leiden 2333 CC, The Netherlands;* orcid.org/0000-0003-4642-9112

†**Huib Ovaa** − *Department of Cell and Chemical Biology, Chemical Immunology, Leiden University Medical Centre, Leiden 2333 ZC, The Netherlands*

https://doi.org/10.1021/acs.jmedchem.5c02920
J. Med. Chem. 2025, 68, 26525−26546

Erik H. J. Danen − *Division of Cell Systems and Drug Safety, Leiden Academic Centre for Drug Research (LACDR), Leiden University, Leiden 2333 CC, The Netherlands*

Monique P. C. Mulder − *Department of Cell and Chemical Biology, Chemical Immunology, Leiden University Medical Centre, Leiden 2333 ZC, The Netherlands;* orcid.org/0000-0001-5386-7132

Kevin Moreau − *Safety Innovation and PROTAC Safety, Clinical Pharmacology & Safety Sciences, R&D, AstraZeneca, Cambridge CB2 0SL, United Kingdom;* orcid.org/0000-0002-3688-3998

Complete contact information is available at: https://pubs.acs.org/10.1021/acs.jmedchem.5c02920

Author Contributions

[#]K.E. and N.V.O.Z. contributed equally. K.E., N.V.O.Z., S.R., B.-T.X., S.d.W., C.v.d.H., B.B., R.A.d.H., and R.V. contributed to the design and execution of the experiments. All the authors contributed to the discussion and evaluation of the obtained results and the manuscript preparation.

Notes

The authors declare the following competing financial interest(s): S.R. and K.M. are AstraZeneca employees. The funders had no role in the design of the study; in the collection, analyses, or interpretation of data; in the writing of the manuscript; or in the decision to publish the results.

[†]Deceased on May 19, 2020.

■ ACKNOWLEDGMENTS

This research was partly funded by the Dutch Research Council (N.V.O.Z., NWO Veni #13688). In addition, some of the materials used in this study were obtained through the Promega Benelux Oncology Research Grant (N.V.O.Z). The work done by B.-T.X. was funded by CHDI Foundation, Inc., a nonprofit biomedical research organization.

■ REFERENCES

(1) Schneekloth, A. R.; Pucheault, M.; Tae, H. S.; Crews, C. M. Targeted Intracellular Protein Degradation Induced by a Small Molecule: En Route to Chemical Proteomics. *Bioorg. Med. Chem. Lett.* **2008**, *18* (22), 5904−5908.

(2) Sievers, Q. L.; Petzold, G.; Bunker, R. D.; Renneville, A.; Słabicki, M.; Liddicoat, B. J.; Abdulrahman, W.; Mikkelsen, T.; Ebert, B. L.; Thomä, N. H. Defining the Human C2H2 Zinc Finger Degrome Targeted by Thalidomide Analogs through CRBN. *Science (1979)* **2018**, *362* (6414), No. eaat0572.

(3) Ma, Z.; Ji, Y.; Yu, Y.; Liang, D. Specific Non-Genetic IAP-Based Protein Erasers (SNIPERs) as a Potential Therapeutic Strategy. *Eur. J. Med. Chem.* **2021**, *216*, No. 113247.

(4) Banik, S. M.; Pedram, K.; Wisnovsky, S.; Ahn, G.; Riley, N. M.; Bertozzi, C. R. Lysosome-Targeting Chimaeras for Degradation of Extracellular Proteins. *Nature 2020 584:7820* **2020**, *584* (7820), 291−297.

(5) Caianiello, D. F.; Zhang, M.; Ray, J. D.; Howell, R. A.; Swartzel, J. C.; Branham, E. M. J.; Chirkin, E.; Sabbasani, V. R.; Gong, A. Z.; McDonald, D. M.; Muthusamy, V.; Spiegel, D. A. Bifunctional Small Molecules That Mediate the Degradation of Extracellular Proteins. *Nature Chemical Biology 2021 17:9* **2021**, *17* (9), 947−953.

(6) Ji, C. H.; Kim, H. Y.; Lee, M. J.; Heo, A. J.; Park, D. Y.; Lim, S.; Shin, S.; Ganipisetti, S.; Yang, W. S.; Jung, C. A.; Kim, K. Y.; Jeong, E. H.; Park, S. H.; Bin Kim, S.; Lee, S. J.; Na, J. E.; Kang, J. I.; Chi, H. M.; Kim, H. T.; Kim, Y. K.; Kim, B. Y.; Kwon, Y. T. The AUTOTAC Chemical Biology Platform for Targeted Protein Degradation via the Autophagy-Lysosome System. *Nat. Commun.* **2022**, *13* (1), 1−14.

(7) Teng, M.; Gray, N. S. The Rise of Degrader Drugs. *Cell Chem. Biol.* **2023**, *30* (8), 864−878.

(8) Ruffilli, C.; Roth, S.; Rodrigo, M.; Boyd, H.; Zelcer, N.; Moreau, K. Proteolysis Targeting Chimeras (PROTACs): A Perspective on Integral Membrane Protein Degradation. *ACS Pharmacology and Translational Science.*; American Chemical Society October 14, 2022; pp 849−858. .

(9) Ciulli, A.; Trainor, N. A Beginner's Guide to PROTACs and Targeted Protein Degradation. *Biochem (Lond)* **2021**, *43* (5), 74−79.

(10) Ge, J.; Li, S.; Weng, G.; Wang, H.; Fang, M.; Sun, H.; Deng, Y.; Hsieh, C.-Y.; Li, D.; Hou, T. PROTAC-DB 3.0: An Updated Database of PROTACs with Extended Pharmacokinetic Parameters. *Nucleic Acids Res.* **2013**, *1*, 13−14.

(11) Sriram, K.; Insel, P. A. G Protein-Coupled Receptors as Targets for Approved Drugs: How Many Targets and How Many Drugs? *Mol. Pharmacol.* **2018**, *93* (4), 251−258.

(12) Saca, V. R.; Huber, T.; Sakmar, T. P. G Protein-Coupled Receptor−Targeted Proteolysis-Targeting Chimeras in Cancer Therapeutics. *Mol. Pharmacol.* **2025**, *107* (2), No. 100013.

(13) Huber, M. E.; Toy, L.; Schmidt, M. F.; Vogt, H.; Budzinski, J.; Wiefhoff, M. F. J.; Merten, N.; Kostenis, E.; Weikert, D.; Schiedel, M. A Chemical Biology Toolbox Targeting the Intracellular Binding Site of CCR9: Fluorescent Ligands, New Drug Leads and PROTACs. *Angewandte Chemie - International Edition* **2022**, *61* (12), No. e202116782.

(14) Lu, A. S.; Rouhimoghadam, M.; Arnatt, C. K.; Filardo, E. J.; Salem, A. K. Proteolytic Targeting Chimeras with Specificity for Plasma Membrane and Intracellular Estrogen Receptors. *Mol. Pharmaceutics* **2021**, *18* (3), 1455−1469.

(15) Li, Z.; Lin, Y.; Song, H.; Qin, X.; Yu, Z.; Zhang, Z.; Dong, G.; Li, X.; Shi, X.; Du, L.; Zhao, W.; Li, M. First Small-Molecule PROTACs for G Protein-Coupled Receptors: Inducing A1A-Adrenergic Receptor Degradation. *Acta Pharm. Sin B* **2020**, *10* (9), 1669.

(16) Zheng, Y.; Qin, L.; Zacarías, N. V. O.; De Vries, H.; Han, G. W.; Gustavsson, M.; Dabros, M.; Zhao, C.; Cherney, R. J.; Carter, P.; Stamos, D.; Abagyan, R.; Cherezov, V.; Stevens, R. C.; IJzerman, A. P.; Heitman, L. H.; Tebben, A.; Kufareva, I.; Handel, T. M. Structure of CC Chemokine Receptor 2 with Orthosteric and Allosteric Antagonists. *Nature* **2016**, *540* (7633), 458−461.

(17) Yamasaki, R.; Liu, L.; Lin, J.; Ransohoff, R. M. Role of CCR2 in Immunobiology and Neurobiology. *Clin Exp Neuroimmunol* **2012**, *3* (1), 16−29.

(18) Connor, S. J.; Paraskevopoulos, N.; Newman, R.; Cuan, N.; Hampartzoumian, T.; Lloyd, A. R.; Grimm, M. C. CCR2 Expressing CD4+ T Lymphocytes Are Preferentially Recruited to the Ileum in Crohn's Disease. *Gut* **2004**, *53* (9), 1287.

(19) Geissmann, F.; Jung, S.; Littman, D. R. Blood Monocytes Consist of Two Principal Subsets with Distinct Migratory Properties. *Immunity* **2003**, *19* (1), 71−82.

(20) Yerra, V. G.; Advani, A. Role of CCR2-Positive Macrophages in Pathological Ventricular Remodelling. *Biomedicines* **2022**, *10* (3), 661.

(21) Chemokine, C. Chemokine/Chemokine Receptor Nomenclature. *Cytokine* **2003**, *21* (1), 48−49.

(22) Shao, Z.; Tan, Y.; Shen, Q.; Hou, L.; Yao, B.; Qin, J.; Xu, P.; Mao, C.; Chen, L. N.; Zhang, H.; Shen, D. D.; Zhang, C.; Li, W.; Du, X.; Li, F.; Chen, Z. H.; Jiang, Y.; Xu, H. E.; Ying, S.; Ma, H.; Zhang, Y.; Shen, H. Molecular Insights into Ligand Recognition and Activation of Chemokine Receptors CCR2 and CCR3. *Cell Discovery 2022 8:1* **2022**, *8* (1), 1−11.

(23) O'Connor, T.; Borsig, L.; Heikenwalder, M. CCL2-CCR2 Signaling in Disease Pathogenesis. *Endocrine, Metabolic & Immune Disorders-Drug Targets* **2015**, *15* (2), 105−118.

(24) Hao, Q.; Vadgama, J. V.; Wang, P. CCL2/CCR2 Signaling in Cancer Pathogenesis. *Cell Communication and Signaling 2020 18:1* **2020**, *18* (1), 1−13.

(25) Nahrendorf, M.; Swirski, F. K. Cholesterol, CCR2, and Monocyte Phenotypes in Atherosclerosis. *Eur. Heart J.* **2017**, *38* (20), 1594−1596.

(26) Wu, X. B.; Jing, P. B.; Zhang, Z. J.; Cao, D. L.; Gao, M. H.; Jiang, B. C.; Gao, Y. J. Chemokine Receptor CCR2 Contributes to Neuropathic Pain and the Associated Depression via Increasing NR2B-Mediated Currents in Both D1 and D2 Dopamine Receptor-Containing Medium Spiny Neurons in the Nucleus Accumbens Shell. *Neuropsychopharmacology* **2018**, *43* (11), 2320−2330.
(27) She, S.; Wu, X.; Zheng, D.; Pei, X.; Ma, J.; Sun, Y.; Zhou, J.; Nong, L.; Guo, C.; Lv, P.; Song, Q.; Zheng, C.; Liang, W.; Huang, S.; Li, Q.; Liu, Z.; Song, Z.; Li, Y.; Zhang, Y.; Kong, W.; You, H.; Xi, J.; Wang, Y. PSMP/MSMP Promotes Hepatic Fibrosis through CCR2 and Represents a Novel Therapeutic Target. *J. Hepatol* **2020**, *72* (3), 506−518.
(28) Rana, A. K.; Li, Y.; Dang, Q.; Yang, F. Monocytes in Rheumatoid Arthritis: Circulating Precursors of Macrophages and Osteoclasts and, Their Heterogeneity and Plasticity Role in RA Pathogenesis. *Int. Immunopharmacol* **2018**, *65*, 348−359.
(29) *Search for: ccr2, Interventional studies | List Results | ClinicalTrials.gov*.https://clinicaltrials.gov/search?cond=ccr2&aggFilters=studyType:int (accessed 2023−11−22).
(30) Anstee, Q. M.; Neuschwander-Tetri, B. A.; Wai-Sun Wong, V.; Abdelmalek, M. F.; Rodriguez-Araujo, G.; Landgren, H.; Park, G. S.; Bedossa, P.; Alkhouri, N.; Tacke, F.; Sanyal, A. J. Cenicriviroc Lacked Efficacy to Treat Liver Fibrosis in Nonalcoholic Steatohepatitis: AURORA Phase III Randomized Study. *Clin Gastroenterol Hepatol* **2024**, *22*, 124.
(31) Horuk, R. Chemokine Receptor Antagonists: Overcoming Developmental Hurdles. *Nature Reviews Drug Discovery 2009 8:1* **2009**, *8* (1), 23−33.
(32) Pienta, K. J.; Machiels, J. P.; Schrijvers, D.; Alekseev, B.; Shkolnik, M.; Crabb, S. J.; Li, S.; Seetharam, S.; Puchalski, T. A.; Takimoto, C.; Elsayed, Y.; Dawkins, F.; De Bono, J. S. Phase 2 Study of Carlumab (CNTO 888), a Human Monoclonal Antibody against CC-Chemokine Ligand 2 (CCL2), in Metastatic Castration-Resistant Prostate Cancer. *Invest New Drugs* **2013**, *31* (3), 760−768.
(33) Dromey, J. R.; Pfleger, K. D. G. G Protein Coupled Receptors as Drug Targets: The Role of *β*-Arrestins. *Endocr Metab Immune Disord Drug Targets* **2008**, *8* (1), 51−61.
(34) Liggett, S. B. Phosphorylation Barcoding as a Mechanism of Directing GPCR Signaling. *Sci. Signal* **2011**, *4* (185), pe36.
(35) Ortiz Zacarías, N. V.; Chahal, K. K.; Šimková, T.; Van Der Horst, C.; Zheng, Y.; Inoue, A.; Theunissen, E.; Mallee, L.; Van Der Es, D.; Louvel, J.; IJzerman, A. P.; Handel, T. M.; Kufareva, I.; Heitman, L. H. Design and Characterization of an Intracellular Covalent Ligand for CC Chemokine Receptor 2. *J. Med. Chem.* **2021**, *64* (5), 2608−2621.
(36) Ortiz Zacarías, N. V.; Röth, S.; Broekhuis, J. D.; van der Es, D.; Moreau, K.; Heitman, L. H. Inducing Receptor Degradation as a Novel Approach to Target CC Chemokine Receptor 2 (CCR2). *International Journal of Molecular Sciences 2024, Vol. 25, Page 8984* **2024**, *25* (16), 8984.
(37) Peace, S.; Philp, J.; Brooks, C.; Piercy, V.; Moores, K.; Smethurst, C.; Watson, S.; Gaines, S.; Zippoli, M.; Mookherjee, C.; Ife, R. Identification of a Sulfonamide Series of CCR2 Antagonists. *Bioorg. Med. Chem. Lett.* **2010**, *20* (13), 3961−3964.
(38) Cieślak, M.; Słowianek, M. Cereblon-Recruiting PROTACs: Will New Drugs Have to Face Old Challenges? *Pharmaceutics* **2023**, *15* (3), 812.
(39) Diehl, C. J.; Ciulli, A. Discovery of Small Molecule Ligands for the von Hippel-Lindau (VHL) E3 Ligase and Their Use as Inhibitors and PROTAC Degraders. *Chem. Soc. Rev.* **2022**, *51* (19), 8216.
(40) Ding, Q.; Zhang, Z.; Liu, J. J.; Jiang, N.; Zhang, J.; Ross, T. M.; Chu, X. J.; Bartkovitz, D.; Podlaski, F.; Janson, C.; Tovar, C.; Filipovic, Z. M.; Higgins, B.; Glenn, K.; Packman, K.; Vassilev, L. T.; Graves, B. Discovery of RG7388, a Potent and Selective P53-MDM2 Inhibitor in Clinical Development. *J. Med. Chem.* **2013**, *56* (14), 5979−5983.
(41) Ishida, T.; Ciulli, A. E3 Ligase Ligands for PROTACs: How They Were Found and How to Discover New Ones. *SLAS Discovery* **2021**, *26* (4), 484−502.
(42) Smith, B. E.; Wang, S. L.; Jaime-Figueroa, S.; Harbin, A.; Wang, J.; Hamman, B. D.; Crews, C. M. Differential PROTAC Substrate Specificity Dictated by Orientation of Recruited E3 Ligase. *Nat. Commun.* **2019**, *10* (1), 131.
(43) Ortiz Zacarías, N. V.; Van Veldhoven, J. P. D.; Portner, L.; Van Spronsen, E.; Ullo, S.; Veenhuizen, M.; Van Der Velden, W. J. C.; Zweemer, A. J. M.; Kreekel, R. M.; Oenema, K.; Lenselink, E. B.; Heitman, L. H.; IJzerman, A. P. Pyrrolone Derivatives as Intracellular Allosteric Modulators for Chemokine Receptors: Selective and Dual-Targeting Inhibitors of CC Chemokine Receptors 1 and 2. *J. Med. Chem.* **2018**, *61* (20), 9146−9161.
(44) Mares, A.; Miah, A. H.; Smith, I. E. D.; Rackham, M.; Thawani, A. R.; Cryan, J.; Haile, P. A.; Votta, B. J.; Beal, A. M.; Capriotti, C.; Reilly, M. A.; Fisher, D. T.; Zinn, N.; Bantscheff, M.; MacDonald, T. T.; Vossenkamper, A.; Dace, P.; Churcher, I.; Benowitz, A. B.; Watt, G.; Denyer, J.; Scott-Stevens, P.; Harling, J. D. Extended Pharmacodynamic Responses Observed upon PROTAC-Mediated Degradation of RIPK2. *Communications Biology 2020 3:1* **2020**, *3* (1), 1−13.
(45) Atilaw, Y.; Poongavanam, V.; Svensson Nilsson, C.; Nguyen, D.; Giese, A.; Meibom, D.; Erdelyi, M.; Kihlberg, J. Solution Conformations Shed Light on PROTAC Cell Permeability. *ACS Med. Chem. Lett.* **2021**, *12* (1), 107−114.
(46) Troup, R. I.; Fallan, C.; Baud, M. G. J. Current Strategies for the Design of PROTAC Linkers: A Critical Review. *Open Exploration 2019 1:5* **2020**, *1* (5), 273−312.
(47) Doornbos, M. L. J.; Heitman, L. H. Label-Free Impedance-Based Whole Cell Assay to Study GPCR Pharmacology. *Methods Cell Biol.* **2019**, *149*, 179−194.
(48) Zweemer, A. J. M.; Nederpelt, I.; Vrieling, H.; Hafith, S.; Doornbos, M. L. J.; De Vries, H.; Abt, J.; Gross, R.; Stamos, D.; Saunders, J.; Smit, M. J.; IJzerman, A. P.; Heitman, L. H. Multiple Binding Sites for Small-Molecule Antagonists at the CC Chemokine Receptor 2. *Mol. Pharmacol.* **2013**, *84* (4), 551−561.
(49) Riching, K. M.; Mahan, S.; Corona, C. R.; McDougall, M.; Vasta, J. D.; Robers, M. B.; Urh, M.; Daniels, D. L. Quantitative Live-Cell Kinetic Degradation and Mechanistic Profiling of PROTAC Mode of Action. *ACS Chem. Biol.* **2018**, *13* (9), 2758−2770.
(50) Tao, Y. X.; Conn, P. M. Chaperoning G Protein-Coupled Receptors: From Cell Biology to Therapeutics. *Endocr Rev.* **2014**, *35* (4), 602.
(51) Shroka, T. M.; Kufareva, I.; Salanga, C. L.; Handel, T. M. The Dual Function Chemokine Receptor CCR2 Drives Migration and Chemokine Scavenging through Distinct Pathways. *Sci. Signal* **2023**, *16* (770), No. eabo4314.
(52) Wu, H.; Yang, K.; Zhang, Z.; Leisten, E. D.; Li, Z.; Xie, H.; Liu, J.; Smith, K. A.; Novakova, Z.; Barinka, C.; Tang, W. Development of Multifunctional Histone Deacetylase 6 Degraders with Potent Antimyeloma Activity. *J. Med. Chem.* **2019**, *62* (15), 7042−7057.
(53) Wang, Z.; He, N.; Guo, Z.; Niu, C.; Song, T.; Guo, Y.; Cao, K.; Wang, A.; Zhu, J.; Zhang, X.; Zhang, Z. Proteolysis Targeting Chimeras for the Selective Degradation of Mcl-1/Bcl-2 Derived from Non-selective Target Binding Ligands. *J. Med. Chem.* **2019**, *62* (17), 8152−8163.
(54) Zhang, C.; Han, X. R.; Yang, X.; Jiang, B.; Liu, J.; Xiong, Y.; Jin, J. Proteolysis Targeting Chimeras (PROTACs) of Anaplastic Lymphoma Kinase (ALK). *Eur. J. Med. Chem.* **2018**, *151*, 304−314.
(55) Bricelj, A.; Steinebach, C.; Kuchta, R.; Gütschow, M.; Sosič, I. E3 Ligase Ligands in Successful PROTACs: An Overview of Syntheses and Linker Attachment Points. *Front Chem.* **2021**, *9*, No. 707317.
(56) Buhimschi, A. D.; Armstrong, H. A.; Toure, M.; Jaime-Figueroa, S.; Chen, T. L.; Lehman, A. M.; Woyach, J. A.; Johnson, A. J.; Byrd, J. C.; Crews, C. M. Targeting the C481S Ibrutinib-Resistance Mutation in Bruton's Tyrosine Kinase Using PROTAC-Mediated Degradation. *Biochemistry* **2018**, *57* (26), 3564−3575.
(57) Steinebach, C.; Kehm, H.; Lindner, S.; Vu, L. P.; Köpff, S.; López Mármol, Á.; Weiler, C.; Wagner, K. G.; Reichenzeller, M.; Krönke, J.; Gütschow, M. PROTAC-Mediated Crosstalk between E3 Ligases. *Chem. Commun.* **2019**, *55* (12), 1821−1824.
(58) Schwalm, M. P.; Menge, A.; Elson, L.; Greco, F. A.; Robers, M. B.; Müller, S.; Knapp, S. Functional Characterization of Pathway Inhibitors for the Ubiquitin-Proteasome System (UPS) as Tool

Compounds for CRBN and VHL-Mediated Targeted Protein Degradation. *ACS Chem. Biol.* **2025**, 94.
(59) Shenoy, S. K.; Xiao, K.; Venkataramanan, V.; Snyder, P. M.; Freedman, N. J.; Weissman, A. M. Nedd4Mediates Agonist-Dependent Ubiquitination, Lysosomal Targeting, and Degradation of the B2-Adrenergic Receptor. *J. Biol. Chem.* **2008**, *283* (32), 22166−22176.
(60) Dores, M. R.; Trejo, J. A. Endo-Lysosomal Sorting of G-Protein-Coupled Receptors by Ubiquitin: Diverse Pathways for G-Protein-Coupled Receptor Destruction and Beyond. *Traffic* **2019**, *20* (2), 101−109.
(61) Marchese, A.; Benovic, J. L. Agonist-Promoted Ubiquitination of the G Protein-Coupled Receptor CXCR4Mediates Lysosomal Sorting. *J. Biol. Chem.* **2001**, *276* (49), 45509−45512.
(62) Burton, J. C.; Grimsey, N. J. Ubiquitination as a Key Regulator of Endosomal Signaling by GPCRs. *Front Cell Dev Biol.* **2019**, *7* (MAR), 43.
(63) Skieterska, K.; Rondou, P.; Van Craenenbroeck, K. Regulation of G Protein-Coupled Receptors by Ubiquitination. *Int. J. Mol. Sci.* **2017**, *18* (5), 923.
(64) Wang, R.; Wang, J.; Hassan, A.; Lee, C. H.; Xie, X. S.; Li, X. Molecular Basis of V-ATPase Inhibition by Bafilomycin A1. *Nature Communications 2021 12:1* **2021**, *12* (1), 1−8.
(65) Qu, X.; Liu, H.; Song, X.; Sun, N.; Zhong, H.; Qiu, X.; Yang, X.; Jiang, B. Effective Degradation of EGFRL858R+T790M Mutant Proteins by CRBN-Based PROTACs through Both Proteosome and Autophagy/Lysosome Degradation Systems. *Eur. J. Med. Chem.* **2021**, *218*, No. 113328.
(66) Zhang, H.; Xie, R.; Ai-Furas, H.; Li, Y.; Wu, Q.; Li, J.; Xu, F.; Xu, T. Design, Synthesis, and Biological Evaluation of Novel EGFR PROTACs Targeting Del19/T790M/C797S Mutation. *ACS Med. Chem. Lett.* **2022**, *13* (2), 278−283.
(67) Zhao, H. Y.; Yang, X. Y.; Lei, H.; Xi, X. X.; Lu, S. M.; Zhang, J. J.; Xin, M.; Zhang, S. Q. Discovery of Potent Small Molecule PROTACs Targeting Mutant EGFR. *Eur. J. Med. Chem.* **2020**, *208*, No. 112781.
(68) Martinelli, R.; Sabroe, I.; LaRosa, G.; Williams, T. J.; Pease, J. E. The CC Chemokine Eotaxin (CCL11) Is a Partial Agonist of CC Chemokine Receptor 2b. *J. Biol. Chem.* **2001**, *276* (46), 42957−42964.
(69) Wain, J. H.; Kirby, J. A.; Ali, S. Leucocyte Chemotaxis: Examination of Mitogen-Activated Protein Kinase and Phosphoinositide 3-Kinase Activation by Monocyte Chemoattractant Proteins-1, −2, −3 and −4. *Clin. Exp. Immunol.* **2002**, *127* (3), 436−444.
(70) Macanas-Pirard, P.; Quezada, T.; Navarrete, L.; Broekhuizen, R.; Leisewitz, A.; Nervi, B.; Ramírez, P. A. The CCL2/CCR2 Axis Affects Transmigration and Proliferation but Not Resistance to Chemotherapy of Acute Myeloid Leukemia Cells. *PLoS One* **2017**, *12* (1), No. e0168888.
(71) Yung-Chi, C.; Prusoff, W. H. Relationship between the Inhibition Constant (KI) and the Concentration of Inhibitor Which Causes 50 per Cent Inhibition (I50) of an Enzymatic Reaction. *Biochem. Pharmacol.* **1973**, *22* (23), 3099−3108.

https://doi.org/10.1021/acs.jmedchem.5c02920
J. Med. Chem. 2025, 68, 26525−26546